Centriolar satellites are required for efficient ciliogenesis and ciliary content regulation

by

Ezgi Odabaşı Kurtuluş

A Dissertation Submitted to the
Graduate School of Sciences and Engineering
in Partial Fulfillment of the Requirements for
the Degrees of
Doctor of Philosophy
In
Molecular Biology and Genetics

August 2021

Centriolar satellites are required for efficient ciliogenesis and ciliary content regulation

Koç University

Graduate School of Sciences and Engineering

This is to certify that I have examined this copy of a doctoral dissertation by

Ezgi Odabaşı Kurtuluş

and have found that it is complete and satisfactory in all respects,

and that any and all revisions required by the final

examining committee have been made.

Committee Members:

_____

Assoc. Prof. Elif Nur Fırat Karalar (Advisor, Koç University)

_____

Assoc. Prof. Nurhan Özlü (Koç University)

_____

Prof. Nesrin Özören (Boğaziçi University)

_____

Asst. Prof. Onur Çizmecioğlu (İhsan Doğramacı Bilkent University)

_____

Asst. Prof. Oktay İsmal Kaplan (Abdullah Gül University)

Date: _____09.08.2021_____

“Gülemiyorsun ya, gülmek

Bir halk gülüyorsa gülmektir

Ne kadar benziyoruz Türkiye'ye Ahmet Abi.”

Edip Cansever

To my dearest family, my dear friends

and my only love

ABSTRACT

Centrosome is the main microtubule organizing center of the cell. It has the role in cell division, cell shape and migration. Other than these roles, centrosome has an important function which is forming primary cilium. Primary cilium is a microtubule-based organelle serving as signaling hub for the cell. Structural or functional defects associated with centrosome/cilium complex lead to genetic diseases called ciliopathies. In order to understand molecular mechanism under ciliopathies, it is important to understand how centrosome/cilium complex is regulated in time and space. Centriolar satellites are the third component of the centrosome/cilium complex

In the second chapter of my thesis, I characterized the cells without centriolar satellites in terms of ciliogenesis and ciliary function. I established the satellite-less cells by knocking-out PCM1 gene in inner medullary collecting duct (IMCD3) cells. PCM1 is the scaffolding protein of the centriolar satellites. Satellite-less IMCD3 cells do not ciliate efficiently as much as control cells. Content and function of cilia formed by satellite-less cells are also different. To understand how cellular process are affected in PCM1 knock-out cells, I applied tandem mass tag (TMT) labeling-based quantitative analysis to compare the global proteome control and satellite-less cells. This analysis revealed that many processes such as actin cytoskeleton, cell migration and adhesion, endocytosis, neuronal processes are affected in the absence of PCM1 protein. With these observations, I showed that centriolar satellites are important to regulate ciliogenesis, ciliary content and function. However, the mechanism behind this regulation is poorly understood.

In the third chapter of my thesis, I applied the miniTurbo labeling method to compare interaction partners of PCM1 in asynchronous and ciliated cells. The aim of this chapter to find interaction partners of PCM1 specific to ciliated cells to explain mechanism of regulation by centriolar satellites during ciliogenesis. After miniTurbo experiments and mass spectrometry analysis, we determined a set of protein which interact with PCM1 in ciliated cells. Among these proteins, we checked the localization and function of the TBC1D31 protein by loss of function experiments. In this chapter, we determined the set of protein might have a role in regulation of ciliogenesis with centriolar satellites. The interactions between these proteins with PCM1 and their relationship in the regulation of ciliogenesis are going to be explored in our future studies.

ÖZET

Sentrozom, hücrenin ana mikrotübül organize edici bölgesidir. Hücre bölünmesi, hücrenin şeklinin oluşturulmasında ve hücre hareketinde rolü vardır. Bu rollerin dışında sentrozom, primer silyum oluşturan önemli bir işleve sahiptir. Primer silyum, hücre için sinyal merkezi olarak görev alan mikrotübül bazlı bir organeldir. Sentrozom/silyum kompleksi ile ilişkili yapısal veya işlevsel kusurlar, silyopati adı verilen genetik hastalıklara yol açar. Silyopatilere neden olan bozuklukların moleküler mekanizmasını anlamak için, sentrozom/silyum kompleksinin zaman ve uzayda nasıl düzenlendiğini anlamak önemlidir. Sentriyolar satelitler sentrozom/silyum kompleksinin üçüncü bileşenidir.

Tezimin ikinci bölümünde, sentriyolar satelitleri olmayan hücreleri primer silyum oluşumu ve silyum fonksiyonları açısından karakterize ettim. İç medüller toplama kanalı (IMCD3) hücrelerinde PCM1 genini knock-out ederek satelliti olamayan hücreler oluşturdum. PCM1, sentriyolar satelitlerin iskelet proteinidir. Satelitleri olmayan IMCD3 hücreleri, kontrol hücreleri kadar verimli bir şekilde primer silyum oluşturamadı. Satelitsiz hücrelerin oluşturduğu primer silyaların içeriği ve işlevi de kontrol hücrelerine göre farklıydı. PCM1 knock-out hücrelerinde diğer hücresel süreçlerin nasıl etkilendiğini anlamak için, kontrol ve satelitsiz hücrelerin küresel proteomunu ikili kütle etiketi (TMT) etiketleme tabanlı kantitatif analizi kullanarak karşılaştırdım. Bu analiz, aktin hücre iskeleti, hücre hareketi ve adezyonu, endositoz, nöronal süreçler gibi birçok sürecin PCM1 proteininin yokluğunda etkilendiğini ortaya koydu. Bu gözlemlerle, sentriyolar satelitlerin primer silyum oluşumu, silyum içeriğini ve işlevini düzenlemek için önemli olduğunu gösterdim. Ancak, bu düzenlemenin arkasındaki mekanizmayı hala tam olarak bilememekteyiz.

Tezimin üçüncü bölümünde, primer silyum oluşturmayan ve oluşturan hücrelerdeki PCM1'nın etkileştiği proteinleri karşılaştırmak için miniTurbo etiketleme yöntemini uyguladım. Bu bölümün amacı, sentriyolar satelitlerin primer silyum olumunu sırasındaki rolünün altında yatan mekanizmaya ışık tutabilmek için primer silyum oluşturmuş hücrelerde PCM1'nın etkileştiği proteinleri bulmaktı. miniTurbo deneyleri ve kütle spektrometrisi analizi ile primer silyum oluşturan hücrelerde PCM1 ile etkileşime giren bir proteinlerin listesini çıkardık. Bu proteinler arasında, TBC1D31 proteininin lokalizasyonunu ve fonksiyon kaybı deneyleri ile primer silyum oluşumundaki rolüne baktık. TBC1D31 proteini dışında belirlediğimiz diğer primer silyum oluşumundaki rolleri ve PCM1 ile etkileşimleri sentriolar satelitler ile primer silyum oluşumu arasındaki ilişkinin anlaşılması için ileriki çalışmalarımızda daha detaylı çalışılacaktır.

Work presented in this thesis has been published in the following books/journals:

Chapter 1:

Unraveling the mysteries of centriolar satellites: time to rewrite the textbooks about the centrosome/cilium complex. *Molecular Biology of the Cell*. (2020)

Chapter 2:

Centriolar satellites are required for efficient ciliogenesis and ciliary content regulation. *EMBO Reports*. (2019)

ACKNOWLEDGEMENTS

First of all, I would like to express my deepest gratitude to my supervisor Dr. Elif Nur Fırat-Karalar. It has been hard but great journey of growth as a scientist under her supervision. She has been a wonderful scientist model to me with her enthusiasm, resilience and ambition for science.

I would like to next thank to my thesis monitoring committee members, Dr. Nurhan Özlü and Prof. Dr. Nesrin Özören for their valuable comments and contributions during the formation of my thesis work and to the other members of my thesis committee, Dr. Oktay İsmail Kaplan and Dr. Onur Çizmecioğlu for their critical reading of my thesis and their comments.

I would like to acknowledge the financial support from European Research Council (679140 to Elif Nur Fırat Karalar), Scientific and Technological Research Council of Turkey (TÜBİTAK) (115Z521 to Elif Nur Fırat Karalar and 120Z759 to Ezgi Odabaşı), EMBO Installation Grant (to Elif Nur Fırat Karalar), Newton Advanced Fellowship (RG84475 to Elif Nur Fırat Karalar) and Koç University during my doctoral studies.

I would also like to thank to KUPAM (Koç Universitesi Proteomikk Analiz Merkezi) and Büşra Akarlar to analyze mass spectrometry samples. Their contribution to chapter 3 of my thesis is very valuable.

Next, I would like to express my gratitude to my dearest labmates Deniz Çonkar, Efraim Culfa, Özge Zelal Aydın, Kübra Hazal Gürkaşlar, Melis Dilara Arslanhan, Onur Taflan, Dila Gülensoy, Umut Batman, Fatmanur Tiryaki, Ebru Topçu, Jovana Deretic, Erdem Ercan, Fatma Başak Turan and Efe Begar. I am very grateful to work with such brilliant people. Especially, with Deniz and Efraim, we shared a lot of hard days and joyful days starting from the very first day of Ph.D. I will always keep the laughers with Deniz, Özge and Melis in my heart. I also thank all of my labmates for their valuable discussions and contributions to my thesis work during our lab meetings

Lastly, I would like to thank my family, my mother Serpil, my father Erol and my sister Sıla, for always being there for me, and supporting me no matter what happens in life. I would also like to thank my husband Onur for his friendship and love.

TABLE OF CONTENT

ACKNOWLEDGEMENTS v

TABLE OF CONTENT vi

LIST OF FIGURES viii

ABBREVIATIONS xi

CHAPTER 1: INTRODUCTION 1

1.1 Structural and Cellular Complexities of Centriolar Satellites 16

1.2 Composition and Assembly Mechanisim of Centriolar Satellites 168

1.3 Functional Complexities of Centriolar Satellites 19

1.4 Mechanistic Underpinnigs of Centriolar Satellite Functions 16

1.5 Future Perspectivies 19

1.5.1 What criteria should we use to define proteins as "centriolar satellite" component? 194

1.5.2 Does "centriolar satellite" terminology need reevalutation? 15

CHAPTER 2: CENTRIOLAR SATELLITES ARE REQUIRED FOR EFFICENT CILIOGENESIS AND CILIARY CONTENT REGULATION 16

2.1 Introduction 16

2.2 Literature Review 16

2.3 Materials and Methods 19

2.3.1 Cell Culture and Transfection 19

2.3.2 3D spheroid assay 20

2.3.3 Lentivirus production and cell transduction 20

2.3.4 Cloning and genome editing 21

2.3.5 Flow cytometry and proliferation assays 21

2.3.6 Cell lysis and immunoblotting 21

2.3.7 RNA isolation, cDNA Synthesis, and qPCR 22

2.3.8 Antibodies 22

2.3.9 Immunofluorescence, microscopy, and quantitation 23

2.3.10 Fluorescence recovery after photobleaching analysis 24

2.3.11 Transcriptome analysis 25

2.3.12 Mass spectrometry 25

2.3.13 Mass spectrometry data analysis 27

2.3.14 Statistical analysis 27

2.4 Results 28

2.4.1 Disruption of PCM1 causes loss of centriolar satellites in kidney epithelial cells 28

2.4.2 Satellites are required for efficient ciliogenesis, but not for cell proliferation, cell cycle progression, and centriole duplication 35

2.4.3 Satellites have variable effects on regulating centrosomal and cellular abundance of key ciliogenesis factors 44

2.4.4 Satellites regulate ciliary protein content 21

2.4.5 Satellites are required for epithelial cell organization in 3D cultures 2159

2.4.6 Loss of satellites leads to a rearrangement of the global proteome profile, but not the global transcriptome profile 2162

2.5 Discussion 68

CHAPTER 3: COMPARASION OF PCM1 INTERACTOME IN CYCLING AND CILIATED CELLS BY MINITURBO LABELING METHOD 72

3.1 Introduction 72

3.2 Literature Review 73

3.2.1 Structures and Functions of Centrosome / Cilium Complex 73

3.2.2 miniTurbo Proximity Labeling Method 74

3.3 Materials and Methods 76

3.3.1 Cell Culture and Transfection 76

3.3.2 Immunofluorescence and microscopy 76

3.3.3 miniTurbo Labeling, Cell Lysis, Streptavidin Pulldown and Immunoblotting 77

3.3.4 Mass Spectrometry 77

3.3.5 Analysis of Mass Spectrometry 78

3.3 Results 78

3.3.1 miniTurbo-PCM1 forms satellites in satelliteless cells and induces biotinylation 78

3.3.2 Identification and validation of the PCM1 proximity interactome in asynchronous and ciliated cells. 82

3.3.3 Comparison of PCM1 interactome in asynronous and ciliated cells. 86

3.3.4 TBC1D31 is a novel TBC1D31 centriolar satellite protein 88

3.3.5 TBC1D31 has role in ciliogenesis 89

3.4 Discussion and Future Directions 90

BIBLIOGRAPHY 92

APPENDIX 92

VITA 104

LIST OF FIGURES

Figure 1.1 Centriolar satellite structure

Figure 1.2 Centriolar satellite distribution in a variety of different cell types

Figure 1.3 Centriolar satellite distribution during cell cycle

Figure 1.4 Comparative analysis of the centrosome, primary cilium and centriolar satellite proteomes

Figure 2.1 Mutations analysis for PCM1 KO colonies

Figure 2.2 IMCD3 PCM1 KO cells do not express PCM1

Figure 2.3 Immunofluorescence analysis of control and IMCD3 PCM1 KO1 cells.

Figure 2.4 Localization of satellite proteins Cep72 and Cep131 is restricted to the centrosome in IMCD3 PCM1 KO cells

Figure 2.5 Satellites are required for efficient ciliogenesis.

Figure 2.6 Effects of satellite loss on cell proliferation

Figure 2.7 Effect of satellite loss on percentage of cells in different cell cycle phases.

Figure 2.8 Effect of satellites loss on mitotic times.

Figure 2.9 Effect of satellite loss on centriole duplication

Figure 2.10 Validation of RPE1 PCM1 KO cells

Figure 2.11 Characterization of RPE1 PCM1 KO cells

Figure 2.12 Effect of satellite loss on centrosomal abundance of Cep164 and Cep290 in serum-starved cells and asynchronous cells

Figure 2.13 Effect of satellite loss on centrosomal abundance of Cp110 in serum-starved cells and asynchronous cells

Figure 2.14 Effect of satellite loss on centrosomal abundance of Ift88 in serum-starved cells and asynchronous cells

Figure 2.15 Effect of satellite loss on centrosomal abundance of Mib1 and Talpid3 in serum-starved cells and asynchronous cells

Figure 2.16 Effects of satellite loss on cellular abundance of centrosome proteins

Figure 2.17 Satellites are required for regulating the ciliary content

Figure 2.18 FRAP experiments in IMCD3 control and PCM1 KO cells expressing SSTR3-LAP and HTR6-LAP

Figure 2.19 Effect of satellite loss on ciliary recruitment of Smo

Figure 2.20 Effect of satellite loss on ciliary SMO levels

Figure 2.21 Effect of satellite loss on Gli1 transcriptional activation

Figure 2.22 Satellites are required for epithelial cell organization in 3D spheroid cultures

Figure 2.23 Expression of myc-PCM1 in IMCD3 PCM1 KO cells

Figure 2.24 Quantitative proteomics profiling of IMCD3 PCM1 KO cells

Figure 2.25 Interaction network and GO analysis of the upregulated and downregulated proteins in IMCD3 PCM1 KO cells

Figure 2.26 Comparison of the centrosome proteome with the IMCD3 PCM1 KO global proteome

Figure 3.1 Localization of miniTurbo and miniTurbo-PCM1 in presence and absence of biotin.

Figure 3.2 Localization of miniTurbo and miniTurbo-PCM1 in IMCD3 PCM1 KO cells

Figure 3.3 Expression and biotinylation of Flag-miniTurbo and Flag-miniTurbo-PCM1 in stable cells lines in IMCD3 PCM1 KO cells.

Figure 3.4 Pulldown of biotiylated proteins in IMCD3 PCM1 KO cells stably expressing Flag-miniTurbo and Flag-miniTurbo PCM1.

Figure 3.5 Interactome of PCM1 in asynchronous IMCD3 cells

Figure 3.6 Interactome of PCM1 in ciliated IMCD3 cells

Figure 3.7 Comparison of PCM1 interactome in asynronous and ciliated cells

Figure 3.8 Localization of TBC1D31

Figure 3.9 Depletion of TBC1D31 results in ciliogenesis defect.

Table 2.1 Genes significantly up- or down-regulated in IMCD3 PCM1 KO cells compared to WT controls

ABBREVIATIONS

ALI	air liquid interface
ANOVA	Analysis of variance
APEX	ascorbate peroxidase
ARL13B	ADP-ribosylation factor-like protein 13B
ATCC	American Type Culture Collection
AZI	5-azacytidine-induced protein 1
BBS4	Bardet Biedl Syndrome 4
BBSome	Bardet Biedl Syndrome Complex
BioID	Biotin Identification
BirA	Bifunctional ligase
BSA	Bovine Serum Albumin
Cas9	CRISPR associated protein 9
CCDC66	Coiled-coil domain-containing protein 66
CEP131	Centrosomal protein of 131 kDa
CEP152	Centrosomal protein of 152 kDa
CEP164	Centrosomal protein of 164 kDa
CEP290	Centrosomal protein of 290 kDa
CP110	Centriolar coiled-coil protein of 110 kDa
CRISPR	clustered regularly interspaced short palindromic repeats
DAPI	4′,6-diamidino-2-phenylindole
DMEM	Dulbecco's Modified Eagle Medium
DMEMF12	DMEM/Nutrient Mixture-12
DMSO	Dimethyl sulfoxide
DNA	Deoxyribonucleic acid
DYRK3	Dual specificity tyrosine-phosphorylation-regulated kinase 3
FACS	Fluorescence-activated Cell Sorting
FBS	Fetal Bovine Serum
GABARAP	Gamma-aminobutyric acid receptor-associated protein
GFP	Green Fluorescent Protein
H2B	Histone 2B

HAUS	augmin-like complex
HEK293T	Human Embryonic Kidney
HeLa	Henrietta Lacks
hTERT	Human Telomerase reverse transcriptase
HTR6	Serotonin receptor 6
IFT	Intraflagellar transport
IFT88	Intraflagellar transport protein 88
IMCD3	inner medullary collecting duct cells
KIAA0586	Protein TALPID3
LAP	The localization and affinity purification
MIB1	E3 ubiquitin-protein ligase MIB1
MTEC	mouse tracheal epithelial cells
MTOC	microtubule organizing center
NPHP3	Nephrocystin-3
NSAF	Normalized Spectral Abundance Factor
OFD1	Oral-facial-digital syndrome 1 protein
p38	mitogen-activated protein kinases
PBS	Phosphate-buffered saline
PCM1	Pericentriolar Material 1
PEI	Polyethylenimine
PFA	Paraformaldehyde
PLK4	Polo-like kinase 4
RPE1	Retinal Pigment Epithelium 1
SAS6	Spindle assembly abnormal protein 6 homolog
SAINT	Significance Analysis of INTeractome
SLAIN2	SLAIN motif-containing protein 2
SMO	Smoothened homolog
SSTR3	Somatostatin receptor 3
SSX2IP	Afadin- and alpha-actinin-binding protein
STIL	SCL-interrupting locus protein
TBST	Tris-Buffered Saline, 0.1% Tween®
ZO1	Tight junction protein ZO-1

CHAPTER 1: INTRODUCTION

1.1 Structural and Cellular Complexities of Centriolar Satellites

Centriolar satellites are membraneless granules that localize and move around centrosomes and cilia. Once referred to as structures with no obvious function, research in the past decade has identified satellites as key regulators of a wide range of cellular and organismal processes. Importantly, these studies have revealed a substantial overlap between functions, proteomes, and disease links of satellites with centrosomes and cilia. Therefore, satellites are now accepted as the "third component" of the vertebrate centrosome/cilium complex, which profoundly changes the way we think about the assembly, maintenance, and remodeling of the complex at the cellular and organismal levels. In this perspective, we first provide an overview of the cellular and structural complexities of centriolar satellites. We then describe the progress in the identification of the satellite interactome, which have paved the way to a molecular understanding of their mechanism of action and assembly mechanisms. After exploring current insights into their functions as recently described by loss-of-function studies and comparative evolutionary approaches, we discuss major unanswered questions regarding their functional and compositional diversity and their functions outside centrosomes and cilia.

We will first highlight the complexity of centriolar satellites (hereafter satellites) by showcasing their structural and cellular properties as the third component of the vertebrate centrosome/cilium complex and as a member of the emerging class of membraneless organelles. Satellites were first described by electron microscopy as an array of 70–100-nm electron dense membraneless spherical granules that localize around the centrosome (Figure 1, A–B) (Bernhard W 1960, deThé 1964, Kubo, Sasaki et al. 1999).

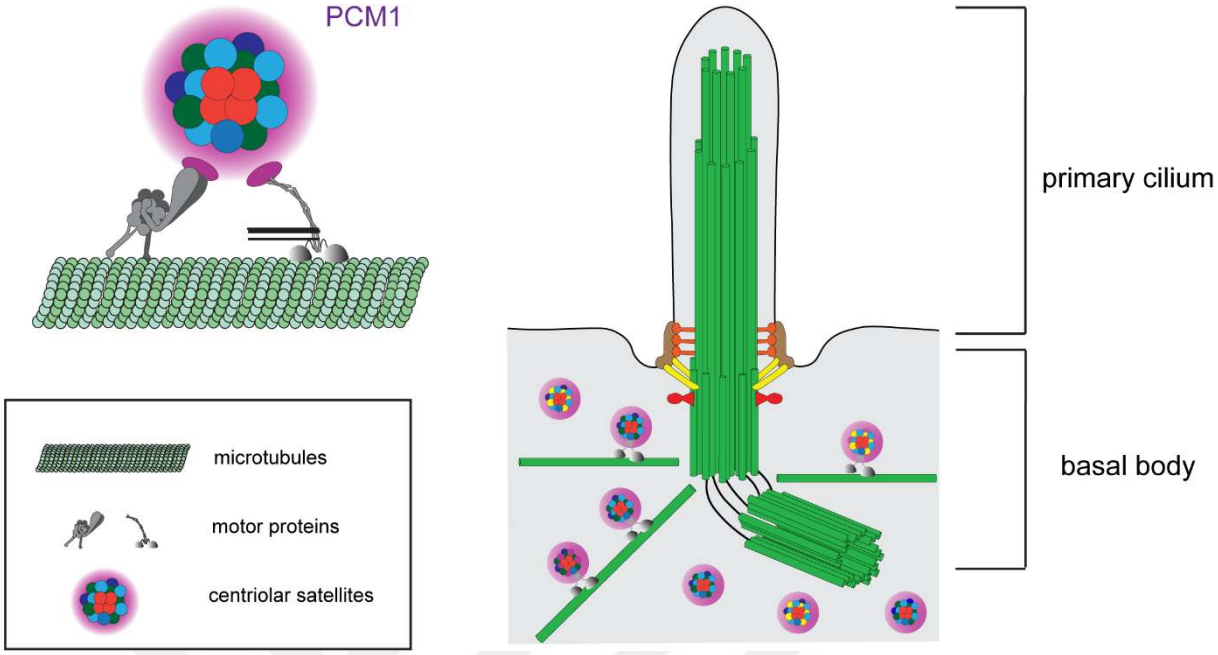

Figure 1.1 Centriolar satellite structure. (A) Satellites are membrane-less macromolecular protein complexes. They have extensive interactions with centrosome proteins, microtubule-associated proteins and enzymes such as kinases and ubiquitin ligases. They interact with the dynein/dynactin-complex and multiple kinesin motors, which engage in "tug-of-war". Adaptor proteins mediate the interaction between motors and satellites. The residents of satellites are represented as circles within each satellite granule. (B) The vertebrate centrosome/cilium complex is composed of centrosomes, cilia and centriolar satellites. At the core of centrosomes are two centrioles, which recruit pericentriolar material and nucleate formation of the primary cilium. Satellites are an array of membrane-less structures that localize and move around centrosomes and cilia in a microtubule and molecular motor-dependent manner. There is compositional heterogeneity among different satellite granules.

In different cell types and tissues, their cellular distribution ranges from clustering at the centrosomes, nucleus, or basal bodies, to scattering throughout cytoplasm (Figure 2, A–E) (Kubo and Tsukita 2003, Vladar and Stearns 2007, Srsen, Fant et al. 2009). Notably, the location of the major microtubule organizing center (MTOC) dictates satellite positioning in most cells, which is nicely exemplified in specialized cell types with noncentrosomal MTOCs (Kubo and Tsukita 2003, Srsen, Gnadt et al. 2006, Vladar and Stearns 2007, Sanchez and Feldman 2017). While satellites cluster around the nuclear envelope in myotubes, they are concentrated at the apical side in polarized epithelial cells of the intestine and kidney (Figure 2, B, D and E). The variation in their cellular distribution suggests cell type and tissue-specific functions for satellites, which remains mostly unexplored.

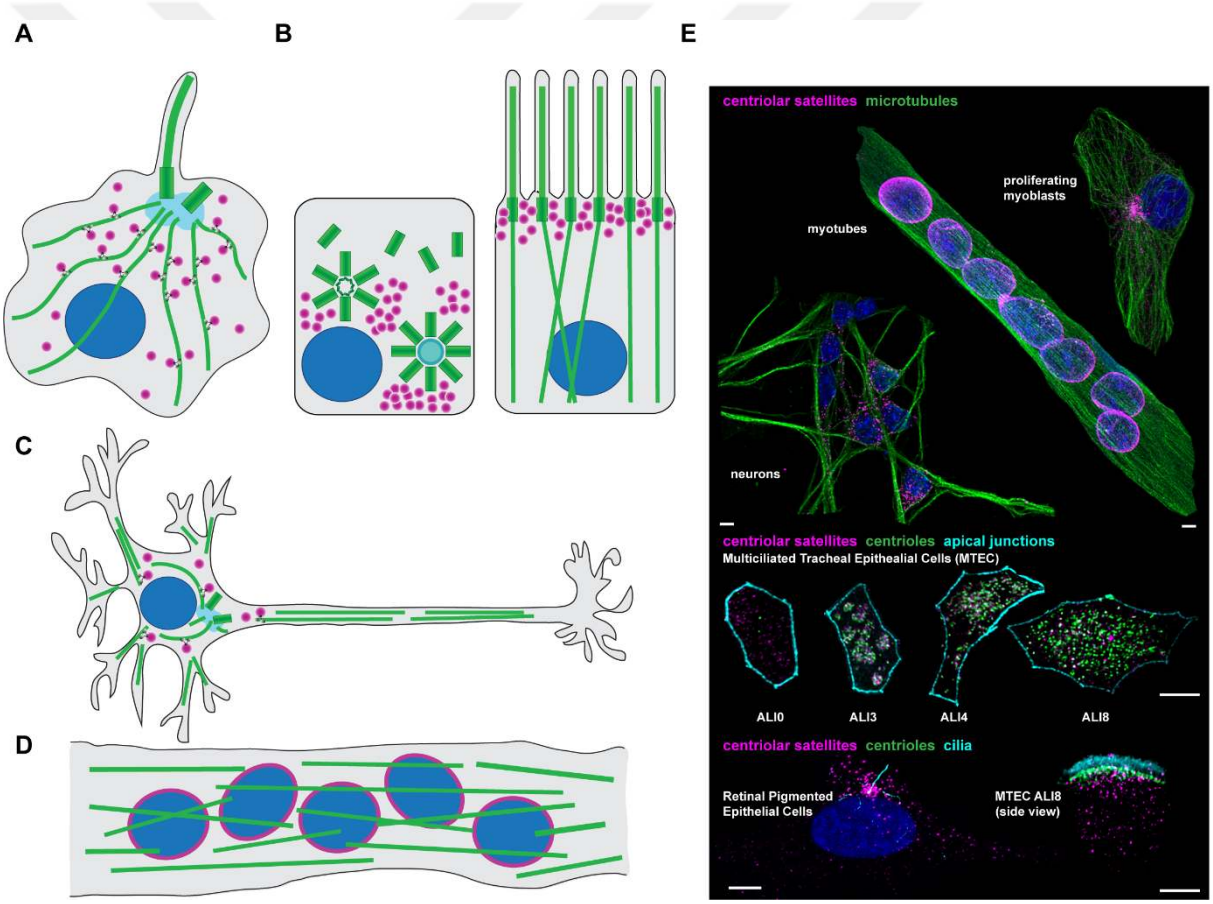

Figure 1.2 Centriolar satellite distribution in a variety of different cell types (A) Drawings are not to scale. (A) Majority of satellites concentrate around the basal body in epithelial cells that form primary cilia. (B) Satellites are remodeled during differentiation of in vitro mouse tracheal epithelial cells (MTEC) after induction with air liquid interface (ALI). At the centriole amplification stage, satellites form fibrous granules in close proximity to nascent centrioles generated by parental centriole and

deuterosome-mediated duplication pathways. In mature ciliated cells, a small pool of satellites is scattered below the basal bodies at the apical surface. (C) In neuronal cells, satellites are scattered throughout the cell body. (D) In muscle cells, satellites are concentrated around the nuclear envelope, the non-centrosomal MTOC. (E) Proliferating and differentiated mouse C2C12 cells, primary embryonic cortical neurons, in vitro MTEC cultures at different stages of differentiation and retinal pigmental epithelial cells were fixed and stained for satellites (anti-PCM1 antibody, magenta), microtubules (anti-alpha-tubulin antibody) or centrioles (anti-Centrin antibody, green), apical junction markers (anti-ZO1 antibody) or cilia (anti-acetylated-tubulin antibody, cyan) and DNA (DAPI, blue). Scale bar: 5 um

The number, distribution, and composition of satellites are dynamically altered in response to different stimuli and during differentiation. For example, their composition is remodeled during cilium assembly induced by serum starvation or environmental stress by releasing key ciliogenesis factors from satellites to centrosomes and cilia (Hori and Toda 2017). Activation of p38 MAPK pathway by cellular stresses such as UV radiation, heat shock, and transcription blocks displaces AZI1/CEP131 and CEP290 from satellites and promotes ciliogenesis (Villumsen, Danielsen et al. 2013, Tollenaere, Villumsen et al. 2015). Analogously, degradation of the satellite pool of OFD1 by autophagy promotes ciliogenesis (Tang, Lin et al. 2013). Regulated satellite remodeling is also nicely illustrated during the differentiation of multiciliated epithelial cells, which assemble hundreds of centrioles and cilia (Sorokin 1968, Kubo, Sasaki et al. 1999, Vladar and Stearns 2007). At the centriole amplification stage, satellites form fibrous granules in close proximity to nascent centrioles duplicated from preexisting centrioles and deuterosomes. As cells differentiate further to form motile cilia, size and abundance of satellite granules decrease to a level that there is only a small pool scattered around the basal bodies at the apical surface in mature ciliated cells. While the events associated with satellite remodeling have so far been described in multiple different contexts, their functional significance and mechanistic underpinnings remain as significant, unresolved questions that will keep cell biologists busy for many years to come.

One of the initial observations made about satellites was their molecular motor-dependent retrograde and anterograde motility along microtubules in vitro and in cells (Kubo, Sasaki et al. 1999). Recent systematic quantitation of the dynamic behavior of satellites by live imaging of their molecular marker PCM1 and one of their residents CCDC66 showed that a small fraction of satellites exhibits long-range bimodal motility, while the majority displays diffusive motility (Conkar, Bayraktar et al. 2019). Intriguingly, a subset of satellites also undergoes fission and fusion events, which is reminiscent of liquid-like behavior (Banani, Lee et al. 2017, Conkar, Bayraktar et al. 2019). Another line of evidence in support of this behavior is the regulation of satellite integrity during mitosis by the dual specificity kinase DYRK3, the recently identified mitotic dissolvase for multiple membraneless organelles such as stress granules (Rai, Chen et al. 2018). Satellites tightly cluster around duplicated centrosomes in prophase and spindle poles in early metaphase, dissolve as cells progress in mitosis when relative

DYRK3 levels and activity increase, and recondense back upon mitotic exit when DYRK3 is degraded by the anaphase promoting complex (Figure 3) (Rai, Chen et al. 2018). The discovery of DYRK3 during mitotic remodeling of satellites paves the way to addressing the longstanding questions that relate to how and why satellites dissolve during mitosis and how liquid–liquid phase transitions contribute to satellite assembly and maintenance.

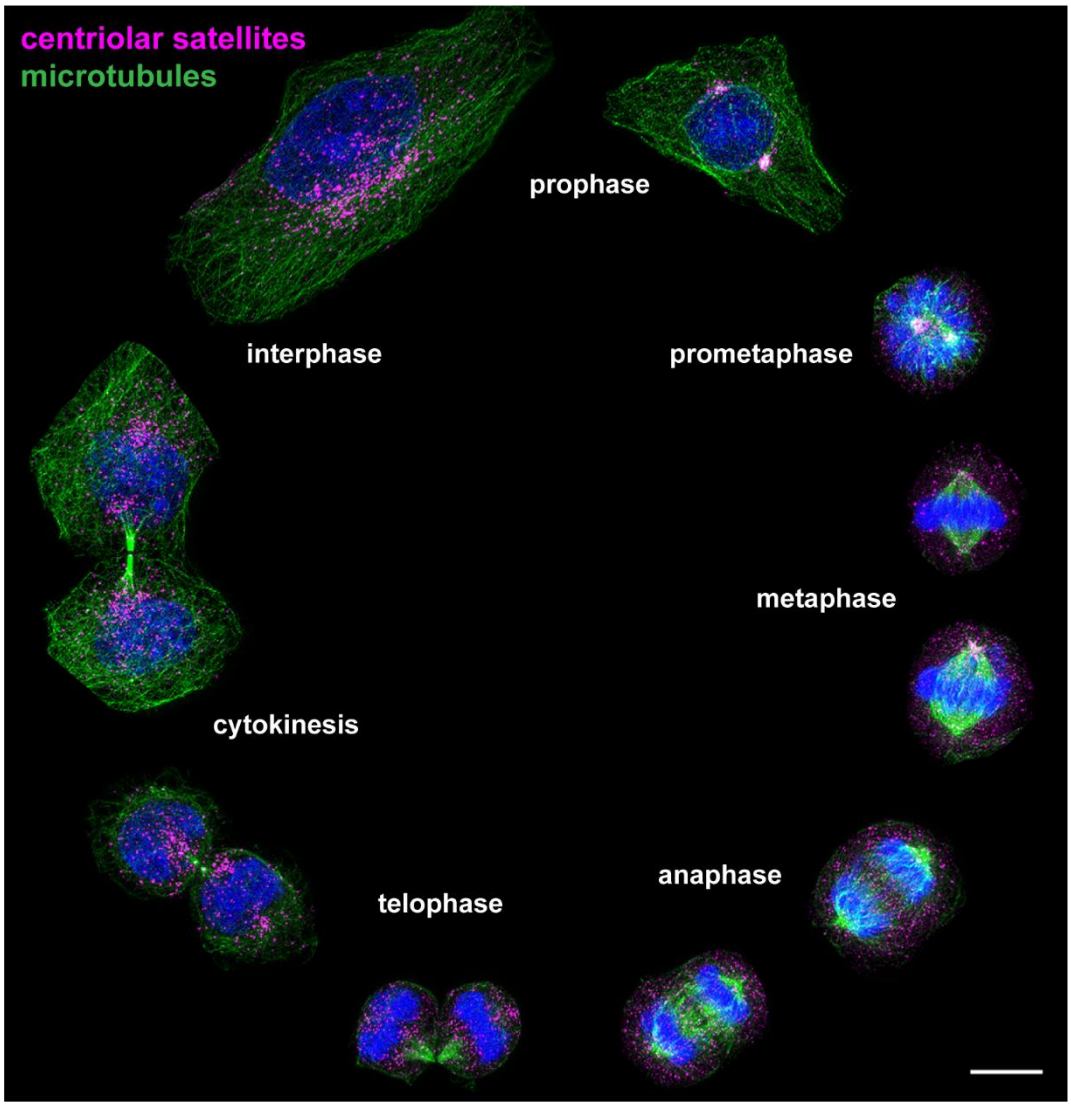

Figure 1.3 Centriolar satellite distribution during cell cycle. Satellites are dynamically regulated in mitosis. Human HeLa cells were fixed at different stages of mitosis and stained for satellites (anti-PCM1 antibody, magenta), microtubules (anti-alpha-tubulin antibody, green) and DNA (DAPI, blue). Satellites localize to duplicated centrosomes in prometaphase and spindle poles during early metaphase, dissolve as cells progress further in mitosis and recondense back upon mitotic exit. Mitotic satellite dissolution is reflected as an increase in their cytoplasmic pool and decrease in the number of granules. Scale bar: 10 um

1.2 Composition and Assembly Mechanisms of Centriolar Satellites

Analogous to centrosomes, satellites are macromolecular protein complex assemblies. The first satellite protein identified was PCM1 (pericentriolar material 1), which functions as the scaffold for their assembly and maintenance (Kubo, Sasaki et al. 1999, Wang, Lee et al. 2016, Odabasi, Gul et al. 2019). Although its terminology misleadingly suggests localization to the pericentriolar material, PCM1 exclusively localizes to satellites. Over the past two decades, identification of satellite components has been done in a piecemeal way by defining new proteins that interact or colocalize with PCM1, and thus there has not been a coherent picture of how satellites assemble and function. More recently, by taking advantage of mass spectrometry–based high-throughput proteomics and proximity labeling techniques, several studies profiled the larger proteome of satellites in different mammalian cell types (Firat-Karalar, Rauniyar et al. 2014, Gupta, Coyaud et al. 2015, Gheiratmand, Coyaud et al. 2019, Quarantotti, Chen et al. 2019). Affinity purification of satellites using PCM1 as the bait identified 223 proteins, which reflects the relatively stable interactions of satellite proteome (Quarantotti, Chen et al. 2019). Additionally, application of the proximity-dependent biotin identification (BioID) approach to 22 satellite proteins also identified weak, transient and insoluble interactions of satellites and generated an interactome composed of 660 proteins (Gheiratmand, Coyaud et al. 2019). We note that these two approaches generated largely different satellite interactomes that only had 9% overlap (Figure 4A). While proteins implicated in centrosome organization, cilium assembly, and cell division were shared, several distinct biological processes such as transcriptional regulation and centrosome duplication were highly enriched in only one proteomic dataset. In agreement with a previous study that directly compared chromatin-associated protein complexes by BioID and affinity purification, these two approaches complement each other in mapping the satellite interactome and their resulting maps must be considered together to study the full extent of satellite functions and mechanisms (Lambert, Tucholska et al. 2015).

A striking feature of the satellite interactome is its substantial overlap with the published centrosome proteome (Figure 4B) (Jakobsen, Vanselow et al. 2011, Gheiratmand, Coyaud et al. 2019, Quarantotti, Chen et al. 2019). The satellite-associated centrosome proteins function in a wide range of processes such as cilium assembly, microtubule nucleation and dynamics, mitosis, centriole duplication, and

pericentriolar material organization, and a subset of them is mutated in ciliopathies, primary microcephaly, and amyotrophic lateral sclerosis. Although 50% of centrosome proteins are found at the satellites, their presence does not assign satellites competence in microtubule nucleation, de novo centriole duplication, and other centrosome-associated functions. While lack of centriole duplication proteins such as PLK4, SASS6, CEP152, and STIL might explain why they do not initiate centriole duplication, why satellite-associated γ-tubulin and HAUS complex do not nucleate microtubules is not known. One possibility is that the folding, modifications, or complex partners of these proteins are different than the ones at the centrosomes and that this inhibits their ectopic functions. In contrast to the striking enrichment of centrosome proteins, only about 14% of the ciliary proteome mapped by proximity labeling approaches was found in the satellite interactome (Figure 4B) (Mick, Rodrigues et al. 2015, Kohli P 2017). There are two likely explanations for the low coverage of cilium proteins. First, these proteins might not transit through satellites. Second, given that the proximity interaction landscape of the centrosome changes in ciliated cells, the satellite interactome generated from asynchronous cells might not reflect that of ciliated cells (Gupta, Coyaud et al. 2015). Future proteomic profiling studies aimed at characterizing the satellite interactome in response to different stimuli and across different cell types and tissues is required to determine whether satellites adapt by dynamically changing their composition and to catalogue a more comprehensive inventory for satellites.

In addition to corroborating the intimate molecular and functional relationship between centrosomes and satellites, there are two important findings revealed by the satellite interactome that open up new avenues about their biology as membraneless organelles. First, prey–prey clustering analysis of satellites identified core and peripheral interaction models, suggesting that satellite granules might be spatially organized like the pericentriolar material or stress granules (Luders 2012, Jain, Wheeler et al. 2016, Gheiratmand, Coyaud et al. 2019). Second, comparative analysis of the proteomic profiles of satellite residents with that of PCM1 revealed compositional heterogeneity among satellite granules (Gheiratmand, Coyaud et al. 2019). Proteomic profiling of different satellite subpopulations together with probing satellite assembly and disassembly mechanisms with biochemical and imaging assays will be essential in gaining insight into these emerging satellite properties.

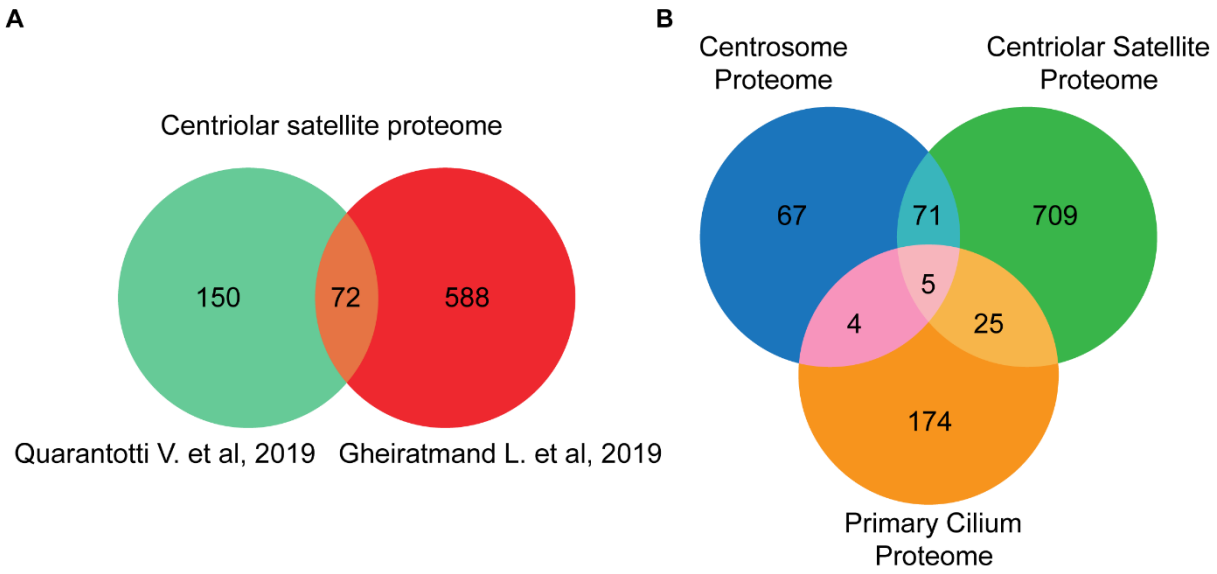

Figure 1.4 Comparative analysis of the centrosome, primary cilium and centriolar satellite proteomes. (A) Comparison of shared and distinct protein numbers between satellite proteomes generated by different approaches. Venn diagram of the satellite proteome identified by affinity purification of PCM1 from sucrose gradient fractions enriched for satellites (Quarantotti, Chen et al. 2019) and by BioID proximity mapping of 22 satellite proteins (Gheiratmand, Coyaud et al. 2019) (B) Comparison of shared and distinct protein numbers between satellite, centrosome and primary cilium proteomes. Venn diagram of the satellite proteome identified by affinity purifications (Quarantotti, Chen et al. 2019) and BioID-based proximity mapping (Gheiratmand, Coyaud et al. 2019), centrosome proteome identified by enrichment of centrosomes using sucrose gradients followed by protein correlation profiling (Jakobsen, Vanselow et al. 2011) and primary cilium proteome identified by APEX-based proximity mapping of the ciliary targeting domains of NPHP3 (Mick, Rodrigues et al. 2015) and HTR6 (Kohli, Hohne et al. 2017).

1.3 Functional Complexities of Centriolar Satellites

The functions of satellites have so far been ascribed to the cellular processes associated with their residents, or more specifically, by phenotypic changes that occur upon their acute or chronic cellular loss (Hori and Toda 2017). These studies collectively identified satellites as multifunctional organelles with regulatory functions during centriole duplication, cilium assembly, microtubule nucleation and organization, mitotic progression, autophagy, stress response, neurogenesis, and nuclear alignment (Hori and Toda 2017, Prosser and Pelletier 2020). A major limitation of studying satellite functions through their residents arises from the fact that these proteins not only localize to satellites, but also to other cellular structures such as centrosomes, cilia, and/or microtubules. For this reason, loss-of-function experiments cannot distinguish between functions associated with different cellular pools of these proteins, which also explains the discrepancy between phenotypes described upon depletion of PCM1 or its associated satellite interactors. Currently, identification of functions specific to satellites as discrete protein complexes can only be derived from characterization of satelliteless cells generated by cellular depletion or deletion of PCM1. Future experiments that make use of localized degradation of satellite pools of proteins or phenotypic rescue experiments with their satellite- or centrosome-localization mutants in null backgrounds will be essential in identifying the full repertoire of satellite-specific functions.

There are discrepancies between phenotypes associated with acute and chronic depletion of satellites from cells, which might be due to functional compensation mechanisms as previously described by a loss-of-function study of another satellite resident CEP131 (Hall, Keighren et al. 2013). Although CEP131 depletion in mouse fibroblasts by siRNA caused defective ciliogenesis, the fibroblasts from CEP131 null mutant mouse did not exhibit ciligonesis defects (Hall, Keighren et al. 2013). Shared phenotypes between acute and chronic depletion of satellites in epithelial cells are the ones associated with the primary cilium, which include defective cilium assembly, ciliary recruitment of signaling receptors, and epithelial cell organization (Wang, Lee et al. 2016, Hori and Toda 2017, Odabasi, Gul et al. 2019). Of note, loss of satellites in zebrafish caused pronephric kidney cysts, hydrocephaly, and inverted heart looping reported, which corroborates key regulatory functions of satellites at the cilia (Stowe, Wilkinson et al. 2012). In addition to epithelial cells, satellite functions have also been described in various specialized cell types and tissues. In myotubes, satellites assemble

into an insoluble matrix around the nuclear envelope and regulate nuclear positioning during their differentiation through recruitment of molecular motor–associated proteins to the nuclear envelope (Srsen, Gnadt et al. 2006, Espigat-Georger, Dyachuk et al. 2016, Gimpel P 2017). Despite the unique localization of PCM1 to fibrous granules around nascent centrioles in differentiating in vitro multiciliated tracheal cultures, PCM1 loss did not compromise centriole and cilia assembly in these cells (Vladar and Stearns 2007). Finally, loss of satellites during embryonic neurogenesis revealed satellite functions in the maintenance of the neuronal progenitor pool and interkinetic nuclear migration of neuronal progenitors (Ge, Frank et al. 2010, Zhang, Kim et al. 2016). Despite the significant progress in unraveling the functional complexities of satellites in recent years, we note that the complete spectrum of satellite functions at the cellular, tissue, and organismal levels remains to be established.

Research on satellites has so far been undertaken with a biased view from a centrosome/cilium-centered perspective. However, there are several lines of data that suggest functions for satellites outside centrioles and cilia. First, satellites are present in cell types with noncentrosomal MTOCs where centrosomes are inactivated or centrioles are lost, and their composition remains mostly unaltered in mammalian cell lines ablated for centrioles (Kubo, Sasaki et al. 1999, Gheiratmand, Coyaud et al. 2019, Quarantotti, Chen et al. 2019). Moreover, systems level characterization of the global proteome of satelliteless cells and the satellite interactome suggested links to actin-mediated processes, neurogenesis, and RNA granules (Gheiratmand, Coyaud et al. 2019, Odabasi, Gul et al. 2019, Quarantotti, Chen et al. 2019). The centriole and cilia-independent functions of satellites should be investigated through defining interactions and dynamic behavior of satellites in different contexts and utilizing unbiased approaches like functional screens.

1.4 Mechanistic Underpinnings of Centriolar Satellite Functions

The prevalent model for satellite mechanisms defines them as regulators of dynamic protein localization at the centrosome (Prosser and Pelletier 2020). However, the mechanistic underpinnings of their targeting function remain enigmatic. Is it as simple as a classical trafficking model where satellites deliver or remove proteins from or to centrosomes by active transport along microtubules? Alternatively, do satellites function as sequestration sites to limit incorporation of proteins to the centrosome and to

enhance biochemical reactions such as the ones that mediate posttranslational modifications? Here, we discuss the recent data that supports and challenges these models.

The idea that satellites act as trafficking machines was proposed based on their directed long-range motility to and away from centrosomes and defective centrosomal targeting of multiple proteins in satelliteless cells (Kubo, Sasaki et al. 1999, Dammermann and Merdes 2002, Conkar, Bayraktar et al. 2019). These lines of data are not sufficient as direct evidence for such function, and future studies utilizing photoactivation and pulse labeling–based time-lapse imaging of satellite residents are required to test it. This model also falls short in explaining how organisms that lack satellites maintain proper centrosome biogenesis and function. Taking into account the function of satellites as sites for regulated sequestration and release of proteins during ciliogenesis and autophagy, an alternative and/or complementary "proximity-dependent sequestration" model is proposed for satellites (Stowe, Wilkinson et al. 2012, Wang, Lee et al. 2016, Joachim and Tooze 2018). This model suggests that microtubule-mediated motility of satellites is required for maintaining their proximity to the centrosome and this proximity mediates timely and efficient exchange of the satellite proteins with the centrosome. While the exchange can be mediated simply by diffusion, a compelling mechanism can also be the fusion and splitting events between centrosomes and satellites (Banani, Lee et al. 2017, Conkar, Bayraktar et al. 2019).

Finally, it is noteworthy to emphasize that various enzymes such as kinases, ubiquitin ligases, and deacetylases were also identified as part of the satellite interactome (Gheiratmand, Coyaud et al. 2019, Quarantotti, Chen et al. 2019). Functional characterization of the satellite pool of the E3 ubiquitin ligase MIB1 showed that satellites sequester MIB1 and prevent untimely centrosomal ubiquitination and degradation of KIAA0586/Talpid3 during initiation of ciliogenesis and GABARAP during autophagosome formation (Wang, Lee et al. 2016, Joachim and Tooze 2018). Corroborating the link between satellites and proteostatic regulation, PCM1 binds to ATG8 family members such as GABARAP and LC3 by an LC3-interacting region domain at its carboxy terminus and regulates degradation of satellite residents such as OFD1 by targeting them to the autophagosome–lysosome pathway (Tang, Lin et al. 2013, Joachim, Razi et al. 2017, Holdgaard, Cianfanelli et al. 2019).

In addition to sequestering their resident enzymes to inhibit their activity at other cellular locations, satellites might also regulate their centrosomal and ciliary residents at the posttranslational level by concentrating them with relevant enzymes or by mediating their protein–protein interactions. The latter possibility was addressed by comparing the proximity interaction profile of five centrosome proteins in wild-type and satellite-less cells (Gheiratmand, Coyaud et al. 2019). Although several functional modules were altered in satelliteless cells, most interaction modules were maintained suggesting that their assembly is independent of satellites. Analogous to these studies, future studies that compare the posttranslational modification profiles of satellite residents such as phosphorylation and ubiquitination in wild-type and satelliteless cells are required to test satellite functions as transit sites where proteins are modified and/or degraded.

1.5 Future Perspectives

The functions and mechanisms of satellites are proving to be more complex than once thought. Our knowledge on the biology of satellites has advanced significantly in the last decade and we described the progress in understanding their molecular composition, mechanism of action, and numerous functions along with the new emerging questions that remain open. These recent discoveries have put the field in a position where there is a clear need to adopt a more appropriate and consistent terminology about satellites and their resident proteins and to study satellite functions outside centrosomes and cilia, which we will discuss here as two major questions.

1.5.1 What criteria should we use to define proteins as "centriolar satellite" components?

Recent studies showed that about 50% of the centrosome proteome overlaps with the satellite proteome, which challenges the current classification of proteins into "centrosome" or "satellite" categories. Once the proteomes of satellites in different contexts are identified in the future, we might even realize that all centrosome proteins at some point during their lifetime reside at satellites. If satellites are ubiquitous paths for centrosome proteins, it will be even more essential to develop methodologies that will distinguish between functions of centrosome- and satellite-associated pools of these proteins.

1.5.2 Does "centriolar satellite" terminology need reevaluation?

"Centiolar satellite" and "Pericentrosomal satellite" terminologies were based on the scattered localization of satellite granules around the centrosome in most cell types. With the realization that satellites are present in cells that lack centrioles and concentrate around noncentrosomal MTOCs in specialized cell types, the term "centriolar satellites" is clearly not inclusive enough to reflect changes in their distribution in a context-dependent way. Another terminology problem relates to the way their core scaffolding protein PCM1 was named. Even though PCM1 does not localize to the pericentriolar material and is exclusive to satellites, "pericentriolar material 1" nomenclature is misleading in terms of its cellular localization, especially for the newcomers into the field. Whether these issues are addressed by adopting new terminology or not, it is essential to identify and tease apart centriolar and noncentriolar functions and mechanisms of satellites.

CHAPTER 2: CENTRIOLAR SATELLITES ARE REQUIRED FOR EFFICIENT CILIOGENESIS AND CILIARY CONTENT REGULATION.

2.1 Introduction

Centriolar satellites are ubiquitous in vertebrate cells. They have recently emerged as key regulators of centrosome/cilium biogenesis, and their mutations are linked to ciliopathies. However, their precise functions and mechanisms of action remain poorly understood. Here, we generated a kidney epithelial cell line (IMCD3) lacking satellites by CRISPR/Cas9-mediated PCM1 deletion and investigated the cellular and molecular consequences of satellite loss. Cells lacking satellites still formed full-length cilia but at significantly lower numbers, with changes in the centrosomal and cellular levels of key ciliogenesis factors. Using these cells, we identified new ciliary functions of satellites such as regulation of ciliary content, Hedgehog signaling, and epithelial cell organization in three-dimensional cultures. However, other functions of satellites, namely proliferation, cell cycle progression, and centriole duplication, were unaffected in these cells. Quantitative transcriptomic and proteomic profiling revealed that loss of satellites affects transcription scarcely, but significantly alters the proteome. Importantly, the centrosome proteome mostly remains unaltered in the cells lacking satellites. Together, our findings identify centriolar satellites as regulators of efficient cilium assembly and function and provide insight into disease mechanisms of ciliopathies.

2.2 Literature Review

The vertebrate centrosome/cilium complex is composed of centrosomes, cilia, and centriolar satellites. The evolutionarily conserved microtubule-based cylindrical structures, centrioles, recruit the pericentriolar material to form the centrosome (Hodges, Scheumann et al. 2010, Carvalho-Santos, Azimzadeh et al. 2011). In quiescent and differentiated cells, the older mother centriole functions as a basal body to nucleate the formation of flagella and cilia, microtubule-based structures projecting out from the apical surface of cells. In addition to these conserved structures, specific to vertebrate cells is the array of 70- to 100-nm membraneless granules termed centriolar satellites, which localize to and move around the centrosome/cilium complex in a microtubule-

and dynein-/dynactin-dependent manner and are implicated in active transport or sequestration of centrosome and cilium proteins (Kubo, Sasaki et al. 1999, Tollenaere, Mailand et al. 2015, Hori and Toda 2017).

The assembly and function of the centrosome/cilium complex are regulated in response to cell cycle cues and environmental factors. In interphase cells, the centrosome nucleates and organizes the microtubule array, which functions in vesicular trafficking, cell motility, and maintaining cell shape and polarity (Luders and Stearns 2007, Paz and Luders 2018). Centrosomes duplicate in S phase and form the bipolar mitotic spindle during mitosis (Nigg, Cajanek et al. 2014, Nigg and Holland 2018). In quiescent cells, centrioles dock to the plasma membrane to form the primary cilia, which function as a nexus for developmentally important signaling pathways like Hedgehog and Wnt signaling (Nachury 2014). Primary cilium formation is a highly complex and regulated process that is mediated through intracellular pathway in the majority of cells and extracellular pathway in polarized epithelial cells (Sorokin 1962, Sorokin 1968). Given that centrosomes and cilia are indispensable for key cellular processes, their structural and functional defects are associated with a variety of human diseases including cancer and ciliopathies (Bettencourt-Dias, Hildebrandt et al. 2011, Nigg, Cajanek et al. 2014). Elucidating the mechanisms that regulate the assembly and function of the centrosome/cilium complex in time and space is required to define the molecular defects underlying these diseases.

Centriolar satellites have recently emerged as key regulators of centrosome/cilium complex biogenesis (Barenz, Mayilo et al. 2011, Tollenaere, Mailand et al. 2015, Hori and Toda 2017). Consistently, mutations affecting satellites components are linked to diseases associated with defects in the centrosome/cilium complex such as ciliopathies, primary microcephaly, and schizophrenia (Tabares-Seisdedos and Rubenstein 2009, Bradshaw and Porteous 2012, Kodani, Yu et al. 2015, Hori and Toda 2017). Ciliopathies are genetic diseases characterized by a multitude of symptoms including retinal degeneration and polycystic kidney disease (Braun and Hildebrandt 2017, Reiter and Leroux 2017). Why defects of the broadly expressed centrosome/cilium complex components are reflected as clinically restricted and heterogeneous phenotypes among different tissue types is unknown. Corroborating the link between satellites and ciliopathies, loss of satellites in zebrafish caused characteristics of cilium dysfunction, analogous to those observed in human ciliopathies (Stowe, Wilkinson et al. 2012).

Although centriolar satellites are ubiquitous in vertebrate cells, their size and number vary among different cell types, and change in response to signals including cell cycle cues and stress (Villumsen, Danielsen et al. 2013, Nielsen, Nordgaard et al. 2018, Rai, Chen et al. 2018). In different cell types and tissues, their cellular distribution ranges from clustering at the centrosomes, nuclear envelope, and/or basal bodies, to scattering throughout the cytoplasm (Kubo and Tsukita 2003, Vladar and Stearns 2007, Srsen, Fant et al. 2009). This variation suggests that satellites might have cell type- and tissue-specific functions. Elucidation of these functions could provide important insight into the mechanisms underlying the phenotypic heterogeneity of ciliopathies.

Over 100 proteins have been defined as satellite components through their co-localization with or proximity to PCM1 (pericentriolar material-1), the scaffolding protein of satellites that mediates their assembly and maintenance (Gupta, Coyaud et al. 2015, Hori and Toda 2017). Phenotypic characterization of various satellite proteins has defined functions in cilium formation, centrosome duplication, microtubule organization, mitotic spindle formation, chromosome segregation, actin filament nucleation and organization, stress response, and autophagy (K, K et al. 2012, Staples, Myers et al. 2012, Pampliega, Orhon et al. 2013, Tang, Lin et al. 2013, Villumsen, Danielsen et al. 2013, Firat-Karalar, Rauniyar et al. 2014, Silva, Betleja et al. 2016, Wang, Lee et al. 2016, Conkar, Culfa et al. 2017, Hori and Toda 2017, Joachim, Razi et al. 2017). However, these may not be satellite-specific functions per se, because all satellite proteins identified so far except for PCM1 localize to both satellites and centrosomes and/or cilia.

Satellite-specific functions have been identified through transient or constitutive depletion of PCM1 from cells, which causes satellite disassembly (Dammermann and Merdes 2002, Wang, Lee et al. 2016). Transient PCM1 depletion causes defects in protein targeting to the centrosome, interphase microtubule network organization, cell cycle progression, cell proliferation, and cilium formation, as well as neuronal progenitor cell proliferation and migration during cortical development (Dammermann and Merdes 2002, Nachury, Loktev et al. 2007, Ge, Frank et al. 2010, K, K et al. 2012, Zhang, Kim et al. 2016). A recent study generated human PCM1−/− retinal pigmental epithelial (RPE1) cells and showed that satellites are essential for cilium assembly, where they sequester the E3 ubiquitin ligase Mib1 and prevent degradation of the key ciliogenesis factor Talpid3, which is required for the recruitment of ciliary vesicles

(Wang, Lee et al. 2016). However, because RPE1::PCM1−/− cells did not ciliate, they did not allow assessment of satellite-specific functions in ciliary signaling and ciliary targeting of proteins, which are among the predominant phenotypic defects underlying ciliopathies. Therefore, a major unresolved question that pertains to our understanding of satellites and their relationship to specific ciliopathies is the identification of the full repertoire of satellite-specific functions.

In this study, we generated kidney epithelial cells that are null for centriolar satellites by ablating the core satellite component PCM1 using genome editing and studied the cellular and molecular consequences specifically of satellite loss on both centrosome- and cilium-related cellular processes. We chose mouse inner medullary collecting duct (IMCD3) cells to complement RPE1 cells because they are Hedgehog-responsive, they form epithelial spheroids that are dependent on cilia functions when grown in a three-dimensional matrix, and they ciliate using the extracellular ciliogenesis pathway, whereas RPE1 cells use the intracellular pathway. Together, our results identify satellites as key regulators of ciliogenesis, ciliary signaling, tissue architecture, protein targeting, and cellular proteostasis, and provide insight into the mechanisms underlying specific ciliopathies.

2.3 Materials and Methods

2.3.1 Cell Culture and Transfection

IMCD3::Flippin cells (gift from Max Nachury, UCSF, CA) and hTERT::RPE1 cells (ATCC® CRL-4000) were grown in DMEM/F12 50/50 (Life Technologies) supplemented with 10% fetal bovine serum (FBS; Life Technologies). HEK293T cells were grown in DMEM supplemented with 10% FBS. Media were supplemented with 100 U/ml penicillin and 100 µg/ml streptomycin (Life Technologies). All cells were cultured at 37°C and 5% CO_2. All cell lines were authenticated by Multiplex Cell line Authentication (MCA) and were tested for mycoplasma contamination by MycoAlert Mycoplasma Detection Kit (Lonza). RPE1 and IMCD3 cells were transfected with the plasmids using Lipofectamine LTX according to the manufacturer's instructions (Life Technologies). HEK293T cells were transfected with the plasmids using 1 µg/µl polyethylenimine, MW 25 kDa (PEI, Sigma-Aldrich, St. Louis, MO). IMCD3 cells stably expressing HTR6-LAP, SSTR3-LAP, LAP-PCM1, and LAP-PCM1 (1–3,600) were generated by cotransfecting IMCD3 Flip-in cells with pEF5.FRT.LAP expression vectors and pOG44 at a ratio of 1:7 using Lipofectamine LTX. After incubating cells

with the transfection mix for 6 h, medium was replaced with complete medium for 24 h, which was followed by selection with 200 μg/ml hygromycin B (Sigma-Aldrich) for 1 week. Colonies formed within 10–14 days, individual colonies were picked after selection and screened by immunofluorescence for expression of LAP-fusion proteins. For cilium-related experiments, cells were incubated in low-serum medium (0.5% serum) for 24 h or 48 h. For Smo relocalization experiments, cells were serum-starved for 24 h and incubated with 200 nm SAG (EMD Millipore) for 4, 8, 12, or 24 h.

2.3.2 3D spheroid assay

40 μl/well of 100% Matrigel (BD Biosciences) was solidified in Lab-Tek 8-well chamber slides (Thermo Fisher) through 15-min incubation at 37°C. Control and IMCD3 PCM1 KO cells were trypsinized, washed with PBS, and resuspended in DMEM/F12 50/50 supplemented with 2% fetal bovine serum and 2% Matrigel, and 5,000 cells/well were plated in Matrigel-coated 8-well chamber slides. Cells were grown at 37°C for 4 days, serum-starved for 1 day, fixed with paraformaldehyde (PFA) and stained with the indicated markers. Cell clusters with no hollow lumen, multiple lumens, disturbed organization of apical and basal markers, and/or misaligned nuclei were quantified as defective. Rescue experiments were performed by transient transfection of myc-BirA*-PCM1.

2.3.3 Lentivirus production and cell transduction

Lentivirus were generated as described, using pLentiCRISPRv2, pLentiCRISPRv2-mousePCM1, and pLentiCRISPRv2-humanPCM1 plasmids as transfer vectors (Mahjoub, Xie et al. 2010). For infection, 1 × 105 IMCD3 cells were seeded on 6-well tissue culture plates the day before infection, which were infected with 1 ml of viral supernatant the following day. 24 h post-infection, medium was replaced with complete medium. 48 h post-infection, cells were split and selected in the presence of 2 μg/ml puromycin for 5–7 days till all the control cells died. LentiCRISPRv2 empty vector-transfected and puromycin-selected cells were used as control. After the PCM1 knockout efficiency was determined in the heterogeneous pool using immunofluorescence experiments, cells were trypsinized and serial dilutions were performed into normal growth medium. Colonies formed within 10–14 days were then trypsinized and expanded for screening for knockouts by immunofluorescence and Western blotting. IMCD3 cells stably expressing mCherry-H2B were generated by

infection of cells with mCherry-H2B-expressing lentivirus. Lentivirus was generated using pLVPT2-mCherry-H2B plasmid as transfer vectors.

2.3.4 Cloning and genome editing

Full-length cDNAs for human PCM1 (NM_006197), HTR6 (NM_021358), and SSTR3 (BC120843) were amplified from the peGFP-N1-PCM1, peGFP-N1-SSTR3, and peGFP-N1-HTR6 plasmids. PCR-amplified open reading frames of full-length PCM1 and its deletion mutant (1–3,600), HTR6, BBS4, and SSTR3 were cloned into pDONR221 using the Invitrogen Gateway system. Subsequent Gateway recombination reactions using pMN444 pEF5-FRT-LAP DEST, provided by M. Nachury (UCSF, CA), were used to generate LAP-PCM1, LAP-PCM1(1–1,200), HTR6-LAP, SSTR3-LAP, and BBS4-LAP. Full-length PCM1 was PCR-amplified using forward primer flanked with XhoI Site and reverse primer flanked with KpnI Site and ligated into pcDNA3.1-mycBirA* plasmid digested with XhoI and KpnI using T4 DNA ligase. Guide RNAs targeting human and mouse PCM1 coding exon 2 were cloned into LentiCRISPRv2 (gift of Feng Zhang, Addgene plasmid #52961) using the following primers: mouseOligo forward: 5′-CACCGCTGCTGTGTGGAAACGTATG-3′, mouseOligo reverse: 5′- AAACCATACGTTTCCACACAGCAGC-3′, humanOligo forward: 5′-CACCGCTACTGTGTGGGAACGTATG-3′, humanOligo reverse: 5′-AAACCATACGTTCCCACACAGTAGC-3′, nontargeting forward: 5′-CGCTTCCGCGGCCCGTTCAA-3′, nontargeting reverse: 5′-TTGAACGGGCCGCGGAAGCG-3′. All plasmids were verified by DNA sequencing.

2.3.5 Flow cytometry and proliferation assays

Cells were harvested and fixed in 70% ethanol at −20°C overnight, followed by washes in phosphate-buffered saline (PBS) and staining with 40 μg/ml propidium iodide and 10 μg g/ml RNaseA at 37 for 30 min. Cell cycle analysis was performed using a Sony SH800S Cell Sorter for IMCD3 cells (Sony) and BD Accuri C6 Sorter for RPE1 cells (BD Biosciences). For proliferation assays, 2 × 105 cells were plated and cells were counted at 1, 2, 3, and 5 days. At each count, cells were split at 1:2.

2.3.6 Cell lysis and immunoblotting

For preparation of cell extracts, cells were trypsinized off the plate, washed in PBS, and lysed in lysis buffer (50 mM Tris (pH 7.6), 150 mM NaCI, 1% Triton X-100, and protease inhibitors) for 30 min at 4°C and centrifuged at 15,000 g for 15 min. The

protein concentration of the resulting supernatants was determined with the Bradford solution (Bio-Rad Laboratories, CA, USA). For immunoblotting, equivalent amount of total protein for each cell extract were first resolved on SDS–PAGE gels, transferred onto nitrocellulose membranes, blocked in TBS-T (Tris-buffered saline with 0.1% Tween-20) with 5% milk, blotted with primary antibodies overnight at 4°C and secondary antibodies for 1 h at room temperature. Visualization of the blots was carried out with the LI-COR Odyssey® Infrared Imaging System and software at 169 μm (LI-COR Biosciences).

2.3.7 RNA isolation, cDNA Synthesis, and qPCR

Total RNA was isolated from control and IMCD PCM1 KO cells before SAG treatment and 24 h after SAG treatment using NucleoSpin RNA kit (Macherey-Nagel) according to the manufacturer's protocol. Quantity and purity of RNA were determined by measuring the optical density at 260 and 280 nm. Single-strand cDNA synthesis was carried out with 1 mg of total RNA using iProof High-Fidelity DNA Polymerase) qPCR analysis of Gli1 was performed with primers 5′ GCATGGGAACAGAAGGACTTTC 3′ and 5′ CCTGGGACCCTGACATAAAGTT 3′ using GoTaq® qPCR Master Mix (Promega).

2.3.8 Antibodies

Anti-PCM1 antibody was generated and used for immunofluorescence as previously described (Firat-Karalar, Rauniyar et al. 2014). Other primary antibodies used for immunofluorescence in this study were rabbit anti-PCM1 (Proteintech—19856-1-AP) at 1:1,000, goat anti-PCM1 (E-5, Santa Cruz Biotechnology—sc50164) at 1:1,000, mouse anti-γ-tubulin (GTU-88; Sigma-Aldrich—T6557) at 1:4,000, mouse anti-GFP (3e6; Invitrogen—11120) at 1:750, mouse anti-acetylated tubulin (6-11-B; Sigma-Aldrich—T6793)) at 1:10,000, mouse anti-polyglutamylated tubulin (GT335, Adipogen—AG-20B-0020) at 1:500, mouse anti-Smo (Santa Cruz Biotechnology—sc166685) at 1:500, mouse anti-Arl13b (Neuromab—75-287) at 1:1,000, rabbit anti-IFT88 (Proteintech—13967-1-AP) at 1:200 81, mouse anti-MIB1 (Santa Cruz Biotechnology—sc-393811) at 1:500, rabbit anti-CP110 (Proteintech—12780-1-AP) at 1:200 82, rabbit anti-Talpid3 (Proteintech—24421-1-AP) at 1:500 83, rabbit anti-Cep290 (Abcam—ab84870) at 1:750 84, rat anti-ZO1 (Santa Cruz Biotechnology—sc33725) at 1:200, rabbit anti-beta-catenin (Proteintech—51062-2-AP) at 1:500, and mouse anti-Cep164 at 1:500 85.

Secondary antibodies used for immunofluorescence experiments were Alexa Fluor 488-, 568-, or 633-coupled (Life Technologies), and they were used at 1:2,000. Primary antibodies used for Western blotting were rabbit anti-PCM1 (ProteinTech—19856-1-AP) at 1:500, mouse anti-γ-tubulin (GTU-88; Sigma-Aldrich—T6557) at 1:4,000, mouse anti-acetylated tubulin (6-11-B; Sigma-Aldrich) at 1:10,000, mouse anti-polyglutamylated tubulin (GT335, Adipogen) at 1:500, mouse anti-Arl13b (Neuromab—75-287) at 1:500, mouse anti-Smo (D-19, Santa Cruz Biotechnology—sc166685) at 1:500, rabbit anti-IFT88 (Proteintech—13967-1-AP) at 1:500, mouse anti-MIB1 (Sigma-Aldrich—M5948) at 1:500 36, rabbit anti-CP110 (Proteintech—12780-1-AP) at 1:500 82 and rabbit anti-Cep164 (Proteintech—22227-1-AP) at 1:500, rabbit anti-Talpid3 (Proteintech—24421-1-AP) at 1:500, rabbit anti-Cep290 (Proteintech—22490-1-AP) at 1:500 rabbit, rabbit anti-BBS4 (Proteintech—12766-1-AP) at 1:500 86, and mouse anti-vinculin (H-10—Santa Cruz Biotechnology—sc-25336) at 1:1,000. Secondary antibodies used for Western blotting experiments were IRDye 680- and IRDye 800-coupled and were used at 1:15,000 (LI-COR Biosciences).

2.3.9 Immunofluorescence, microscopy, and quantitation

For immunofluorescence experiments, cells were grown on coverslips and fixed in either methanol for 5 min or 4% PFA for 15 min in PBS for indirect immunofluorescence. For CP110 staining, cells were pre-extracted in 0.01% Tx-100 in PBS for 1 min before fixation. After rehydration in PBS, cells were blocked in 3% BSA (Sigma-Aldrich) in PBS + 0.1% Triton X-100 for 30 min. Coverslips were incubated in primary antibodies diluted in blocking solution for 1 h at room temperature and Alexa Fluor 488-, 594-, or 680-conjugated secondary antibodies for 1 h at room temperature. Samples were mounted using Mowiol mounting medium containing N-propyl gallate (Sigma-Aldrich). Coverslips of cells were imaged using LAS X software (Premium; Leica) on a scanning confocal microscope (SP8; Leica Microsystems) with Plan Apofluar 63 × 1.4 NA objective or a fluorescent microscope (DMi8; Leica Microsystems) with Plan Apofluar 63 × 1.4 NA objective using a digital CMOS camera (Hamamatsu Orca Flash 4.0 V2 Camera). Images were processed using Photoshop (Adobe) or ImageJ (National Institutes of Health, Bethesda, MD).

Quantitative immunofluorescence of centrosomal and ciliary levels of proteins was performed on cells by acquiring a z-stack of control, knockout, and rescue cells using

identical gain and exposure settings, determined by adjusting settings based on the fluorescence signal in the control cells. The z-stacks were used to assemble maximum-intensity projections. The centrosome regions in these images were defined by γ-tubulin staining for each cell, and the total pixel intensity of a circular 3 μm^2 area centered on the centrosome in each cell was measured using ImageJ and defined as the centrosomal intensity. The ciliary regions in these images were defined by Arl13b or acetylated tubulin for each cell. Background subtraction was performed by quantifying fluorescence intensity of a region of equal dimensions in the area neighboring the centrosome or cilium. Ciliary protein concentrations were determined by dividing fluorescence signal of the protein to the cilium length, which was quantified using Arl13b or acetylated tubulin staining. Primary cilium formation was assessed by counting the total number of cells and the number of cells with primary cilia, as detected by Arl13b or acetylated tubulin staining and DAPI staining. All data acquisition was done in a blinded manner.

Quantitative analysis of ciliogenesis efficiency in 3D cultures was determined by acquiring a z-stack of control, knockout, and rescue cells and assembling maximum-intensity projections. The number of cilia counted by Arl13b staining was divided into the number of cells counted by DAPI staining to calculate ciliogenesis efficiency of each spheroid and cell cluster.

2.3.10 Fluorescence recovery after photobleaching analysis

Cells were cultured in coverglass-bottom dishes (Laboratory-Tek II Chamber) and serum-starved for 24 h. Photobleaching experiments were performed using Leica SP8 confocal laser scanner (Leica SP8) a Plan Apofluar 63 × 1.4 NA objective and a scan zoom of 5. Cells were kept at 37°C with 5% CO_2 during the imaging. A z-stack of 4 μm with 0.5 μm step size was taken during pre- and post-bleaching cilium FRAP experiments. One stack of images was captured before photobleaching, followed by photobleaching done in five iterations with 488-nm Argon laser with 100% power in the defined region of interest (ROI). Post-bleaching stacks were captured every 5 s for SSTR3-LAP and 6 s for HTR6-LAP for 2 min for half-cilium FRAP experiments and 5 min for full-cilium FRAP experiments. The relative fluorescence intensities were calculated from the maximum projection files using ImageJ and plotted against time. Recovery graph quantifications, t-half, and mobile pool quantifications were done using the equations as described (Sprague, Pego et al. 2004).

2.3.11 Transcriptome analysis

Transcriptome analysis was performed as described previously with the following modifications. Quality of reads of raw data was analyzed via FastQC program. We removed the sequencing reads with adaptor contamination and low-quality bases (quality score < Q30) via Trimmomatic (v0.35) to clean and advance the quality of the reads. All sequence data were 2 × 100 bp in length. The high-quality reads were saved in fastq files and deposited to NCBI's Gene Expression Omnibus under GEO Series accession number GSE123017. Clean and high-quality data were utilized for all downstream analysis. We used STAR aligner (v2.5.3) to generate genome indexes and mapping reads to the reference genomes that are hg38 for human cell line samples and GRCm38.p5 for mouse cell line samples. At the mapping step, reads having the non-canonical junctions were removed and only uniquely mapping reads were utilized. Following the alignment, Pearson's correlation analysis was conducted to obtain the transcript-level R^2 value between replicates. To determine the differentially expressed genes (DEGs), we utilized Cuffdiff with a minimum alignment count of 10, false discovery rate (FDR) < 0.05. The absolute value of |Fold change| ≥ 2 and q-value < 0.05 was used as the threshold to judge significant differences in gene expression. DAVID Bioinformatics Resources 6.8 was utilized to determine the statistical enrichment of the significantly (P < 0.05) differentially expressed genes in KEGG pathways and GO-enrichment analysis (Huang da, Sherman et al. 2009). Analysis of GO annotation pathways provides information based on the biological processes (BP), cellular components (CC), and molecular functions (MF).

2.3.12 Mass spectrometry

For the quantitative comparison of WT and knockout cells, snap-frozen cell pellets of 1×10^6 cells were resuspended in 50 µl PBS followed by the addition of 50 µl of 1% SDS in 100 mM HEPES, pH 8.4 and protease inhibitor cocktail (Roche, #11873580001). Samples were heated to 95°C for 5 min and then transferred on ice. Samples were treated with benzonase (EMD Millipore Corp., #71206-3) at 37°C for 1 h to degrade DNA. Protein concentrations were determined and adjusted to 1 µg/µl. 20 µg thereof were subjected to an in-solution tryptic digest using a modified version of the single-pot solid-phase-enhanced sample preparation (SP3) protocol (Hughes, Foehr et al. 2014, Moggridge, Sorensen et al. 2018). Here, lysates were added to Sera-Mag Beads (Thermo Scientific, #4515-2105-050250, 6515-2105-050250) in 10 µl 15%

formic acid and 30 µl of ethanol. Binding of proteins was achieved by shaking for 15 min at room temperature. SDS was removed by 4 subsequent washes with 200 µl of 70% ethanol. Proteins were digested with 0.4 µg of sequencing grade modified trypsin (Promega, #V5111) in 40 µl HEPES/NaOH, pH 8.4 in the presence of 1.25 mM TCEP and 5 mM chloroacetamide (Sigma-Aldrich, #C0267) overnight at room temperature. Beads were separated, washed with 10 µl of an aqueous solution of 2% DMSO, and the combined eluates were dried down. Peptides were reconstituted in 10 µl of H_2O and reacted with 80 µg of TMT10plex (Thermo Scientific, #90111) label reagent dissolved in 4 µl of acetonitrile for 1 h at room temperature (Werner, Sweetman et al. 2014). Excess TMT reagent was quenched by the addition of 4 µl of an aqueous solution of 5% hydroxylamine (Sigma, 438227). Peptides were mixed to achieve a 1:1 ratio across all TMT channels. Mixed peptides were subjected to a reverse phase clean-up step (OASIS HLB 96-well µElution Plate, Waters #186001828BA) and subjected to an off-line fractionation under high pH condition (Hughes, Foehr et al. 2014). The resulting 12 fractions were then analyzed by LC-MS/MS on a Q Exactive Plus (Thermo Scientific) as previously described (PMID: 29706546). Briefly, peptides were separated using an UltiMate 3000 RSLC (Thermo Scientific) equipped with a trapping cartridge (Precolumn; C18 PepMap 100, 5 lm, 300 lm i.d. × 5 mm, 100 A°) and an analytical column (Waters nanoEase HSS C18 T3, 75 lm × 25 cm, 1.8 lm, 100 A°). Solvent A: aqueous 0.1% formic acid; Solvent B: 0.1% formic acid in acetonitrile (all solvents were of LC-MS grade). Peptides were loaded on the trapping cartridge using solvent A for 3 min with a flow of 30 µl/min. Peptides were separated on the analytical column with a constant flow of 0.3 µl/min applying a 2-h gradient of 2–28% of solvent B in A, followed by an increase to 40% B. Peptides were directly analyzed in positive ion mode applying with a spray voltage of 2.3 kV and a capillary temperature of 320°C using a Nanospray-Flex ion source and a Pico-Tip Emitter 360 lm OD × 20 lm ID; 10 lm tip (New Objective). MS spectra with a mass range of 375–1,200 m/z were acquired in profile mode using a resolution of 70,000 [maximum fill time of 250 ms or a maximum of 3e6 ions (automatic gain control, AGC)]. Fragmentation was triggered for the top 10 peaks with charge 2–4 on the MS scan (data-dependent acquisition) with a 30-s dynamic exclusion window (normalized collision energy was 32). Precursors were isolated with a 0.7 m/z window, and MS/MS spectra were acquired in profile mode with a resolution of 35,000 (maximum fill time of 120 ms or an AGC target of 2e5 ions).

Acquired data were analyzed using IsobarQuant and Mascot V2.4 (Matrix Science) using a reverse UniProt FASTA Mus musculus database (UP000000589) including common contaminants (Franken, Mathieson et al. 2015). The following modifications were taken into account: Carbamidomethyl (C, fixed), TMT10plex (K, fixed), Acetyl (N-term, variable), Oxidation (M, variable), and TMT10plex (N-term, variable). The mass error tolerance for full-scan MS spectra was set to 10 ppm and for MS/MS spectra to 0.02 Da. A maximum of 2 missed cleavages were allowed. A minimum of 2 unique peptides with a peptide length of at least seven amino acids and a false discovery rate below 0.01 were required on the peptide and protein levels (Savitski, Wilhelm et al. 2015).

2.3.13 Mass spectrometry data analysis

The proteins.txt output file of IsobarQuant was analyzed using the R programming language. As a quality control filter, we only allowed proteins that were quantified with at least two different unique peptides. The "signal_sum" columns were used and annotated to the knockout (KO) and wild-type (WT) conditions. Batch effects were removed using the limma package, and the resulting data were normalized with the vsn package (variance stabilization) (Hughes, Foehr et al. 2014). Limma was employed again to look for differentially expressed proteins between KO and WT. We classified proteins as hits with a false discovery rate (FDR) smaller 5% and a fold change of at least twofold. Candidates were defined with an FDR smaller 20% and a fold change of at least 50%.

2.3.14 Statistical analysis

Statistical significance and *P*-values were assessed by analysis of variance and Student's *t*-tests using Prism software (GraphPad Software, La Jolla, CA). Error bars reflect SD. Following key is followed for asterisk placeholders for *P*-values in the figures: ****$P < 0.001$ ***$P < 0.001$, **$P < 0.01$, *$P < 0.05$.

2.4 Results

2.4.1 Disruption of PCM1 causes loss of centriolar satellites in kidney epithelial cells

To determine the cellular functions of centriolar satellites, we generated satellite-less cells by disrupting the PCM1 gene in mouse kidney epithelial IMCD3 cells. Homozygous null mutations in both alleles of the PCM1 locus were made using CRISPR/Cas9-mediated genome editing with guides designed to target exon 3 (protein-coding exon 2) in IMCD3 cells (Figure 2.1). We isolated three PCM1−/− IMCD3 clones (hereafter IMCD3 PCM1 KO) and one control colony (hereafter WT) that was transfected with the plasmid encoding the scrambled gRNA. Sequencing of the PCM1 alleles identified these clones as compound heterozygotes bearing premature stop codons that result from small deletions of < 20 base pairs and/or insertion of one or two base pairs around the cut site (Figure 2.1-A and B).

Figure 2.1 Mutations analysis for PCM1 KO colonies (A) IMCD3 PCM1 KO clones are all compound heterozygotes with mutations that lead to early stop codons. 1000 bp region around the gRNA-target site was PCR amplified and cloned. Sequencing of five different clones for each line identified one nucleotide (nt) deletion on one allele and one nt insertion on the other for line 1, 16 nt deletion on one allele and 2 nt insertion on the other for line 2 and 16 nt deletion for one allele and 4 nt deletion on the other for line 3 (B) Translation products on protein coding exon 2 of the gRNA-targeting exon in IMCD3 KO clones.

Immunoblot analysis of whole-cell lysates with two different polyclonal antibodies, one directed against the N-terminal 1–254 amino acids and the other against the C-terminal 630–726 amino acids of PCM1, showed that PCM1 was not expressed in the IMCD3 PCM1 KO clones and that LAP-PCM1 was expressed in the rescue line (Figure 2.2).

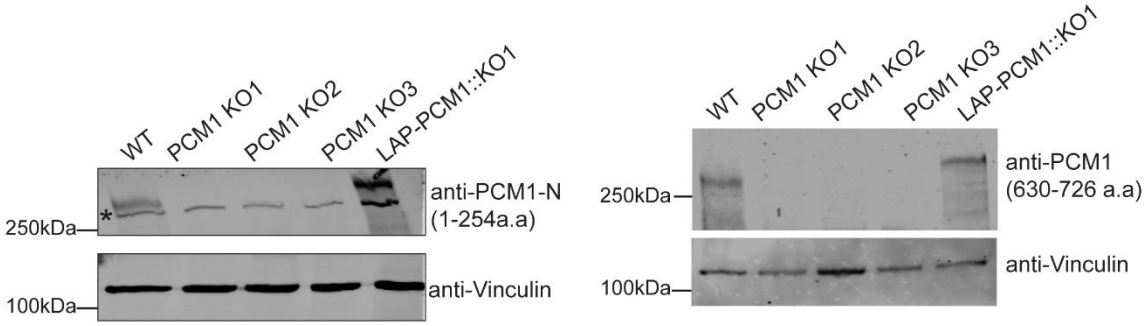

Figure 2.2 IMCD3 PCM1 KO cells do not express PCM1. (A) Immunoblot analysis of whole-cell lysates from control cells, three IMCD3 PCM1 KO lines, and one IMCD3 PCM1KO::LAP-PCM1 rescue line with two different PCM1 antibodies, one raised against the N-terminal amino acids 1 – 254 and the other against amino acids 630–726.

Immunofluorescence analysis of these clones with the N-terminal antibody and an antibody targeting the C-terminal 1,665–2,026 amino acids of PCM1 further validated lack of PCM1 expression (Figure 2.3-A and B). The absence of PCM1 signal in the PCM1 KO clones with the C-terminal PCM1 antibody eliminated the possibility that in-frame gene products downstream of the gRNA-target site were initiated, and showed that PCM1 alleles in these clones are likely to be null mutations, which was confirmed by mass spectrometry-based quantitative global proteome analysis described below.

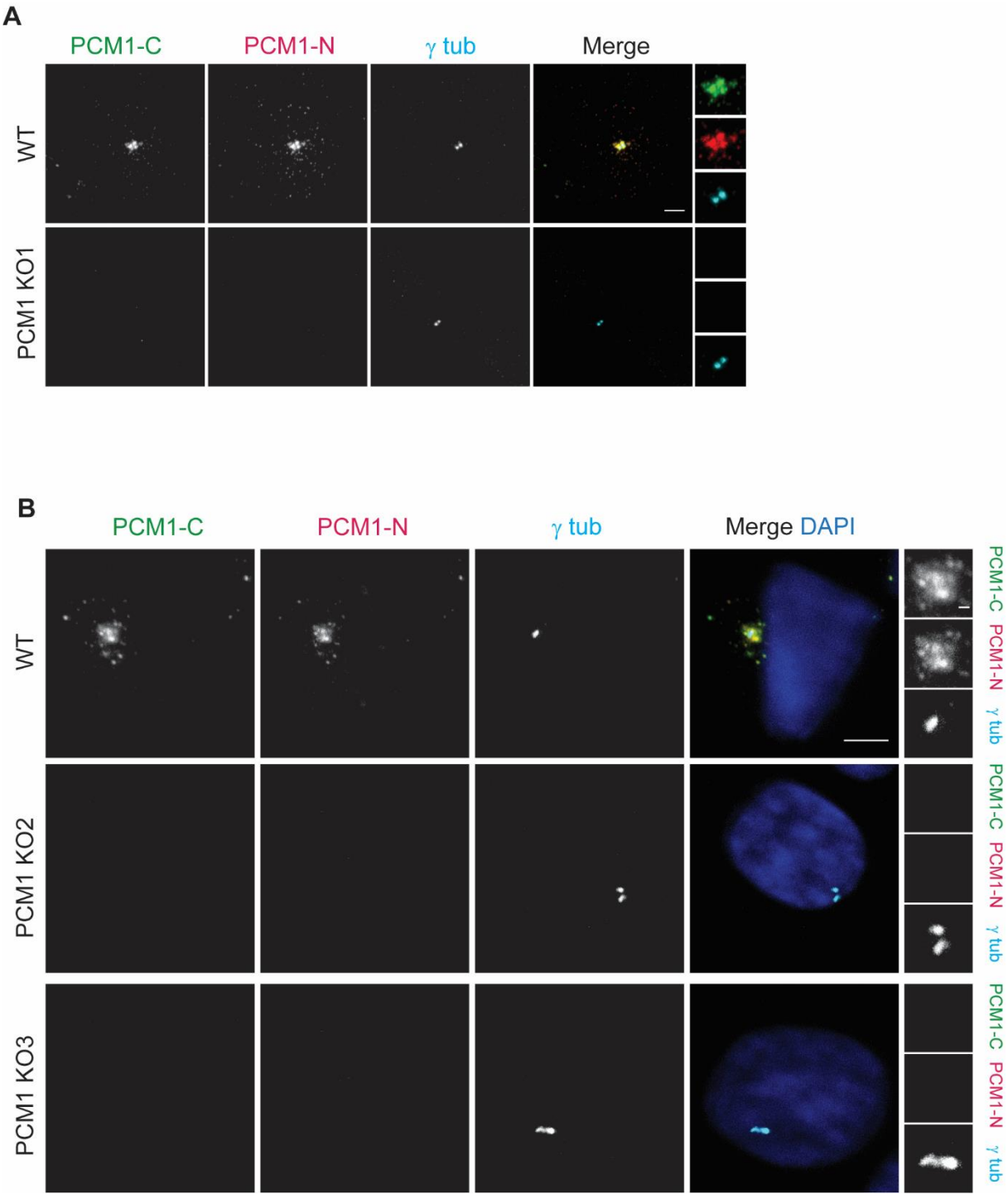

Figure 2.3 Immunofluorescence analysis of control and IMCD3 PCM1 KO1 cells. Cells were fixed and stained for centrosomes with anti-c-tubulin antibody and PCM1 withPCM1-N antibody raised against its N-terminal (amino acids 1–254) fragment and PCM1-C antibody raised against its C-terminal (amino acids 1,665–2,026) fragment. Scale bar, 4 μm, for colony 1 (A) and for colony 2 and 3 (B)

To confirm that PCM1 KO cells lack satellite structures, we determined the localization of other known satellite components in these cells. While Cep131 and Cep72 localized to both the centrosome and satellites in control cells, their localization was restricted to the centrosomes in IMCD3 PCM1 KO cells, and there were no granules around the centrosome that were positive for satellite markers in these cells (Figure 2.4-A). Stable expression of LAP-tagged human full-length PCM1 and PCM1 (1–1,200) in IMCD3 PCM1 KO clone#1 rescued satellite assembly and localization defects, confirming the specificity of these phenotypes (Figure 2.4-B). Of note, even though PCM1 (1–1,200) expression formed PCM1-positive granules that recruited other satellite components including Cep131, the size of the granules was larger than the ones formed through expression of full-length PCM1 (Figure 2.4-B), suggesting a regulatory role for the C-terminal part of PCM1 in satellite assembly. These results show that IMCD3 PCM1 KO clones are devoid of satellites and that PCM1 is essential for the assembly of satellites and sequestration of centrosome proteins to the satellites.

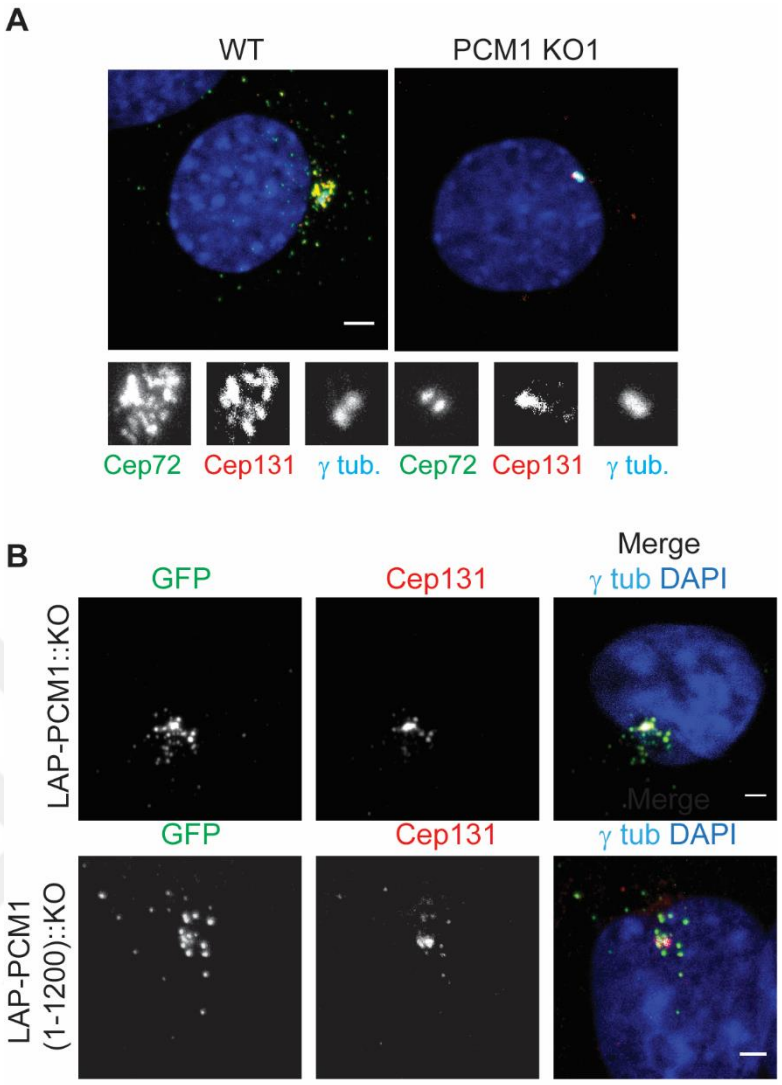

Figure 2.4 Localization of satellite proteins Cep72 and Cep131 is restricted to the centrosome in IMCD3 PCM1 KO cells. (A) Cells were fixed and stained for Cep72, Cep131, and gamma-tubulin. DNA was stained with DAPI. Scale bar, 5 μm. (B) Stable expression of LAP-PCM1 and LAP-PCM1 (1–1200) rescues the satellite assembly defects in IMCD3 PCM1 KO cells. Cells were fixed and stained with GFP, Cep131, and gamma-tubulin antibodies. DNA was stained with DAPI. Scale bar,4 μm

2.4.2 Satellites are required for efficient ciliogenesis, but not for cell proliferation, cell cycle progression, and centriole duplication

Many satellite proteins, including PCM1, have previously been implicated in ciliogenesis-related functions (Nachury, Loktev et al. 2007, Kim, Krishnaswami et al. 2008, Hoang-Minh, Deleyrolle et al. 2016, Wang, Lee et al. 2016). While a recent PCM1 knockout study in RPE1 cells and our characterization of RPE1 PCM1 KO cells generated by genome editing identified essential roles for satellites in cilium assembly 36, the function of satellites in a wide range of centrosome-/cilium-related cellular processes has not been studied in clean genetic backgrounds. To address this, IMCD3 PCM1 KO cells were serum-starved for 24 h and 48 h and the percentage of ciliated cells were quantified by staining cells for Arl13b, a marker for the ciliary membrane, and acetylated tubulin, a marker for the ciliary axoneme. Lack of satellites resulted in a significant decrease in the fraction of ciliated cells in serum-starved IMCD3 cells relative to control cells serum-starved for 24 and 48 h (Figure 2.5-A and B). This is in contrast to RPE1 PCM1 KO cells, which did not ciliate 36. All three IMCD3 PCM1 KO clones had similar ciliogenesis defects (Figure 2.5-B), and we used clone # 1 for subsequent rescue and phenotypic characterization experiments (hereafter IMCD3 PCM1 KO). The ciliogenesis phenotype in IMCD3 PCM1 KO cells was rescued by stable expression of LAP-tagged full-length human PCM1, confirming that the ciliogenesis phenotype is a specific consequence of satellite loss (Figure 2.5-A and B). Despite the reduction in the ciliating population in IMCD3 PCM1 KO cells, the cilia that formed in these cells were normal in length (wt: 3.14 μm ± 0.8, KO: 3.38 μm ± 1.18), which suggests that PCM1 acts during cilia initiation (Figure 2.5-C).

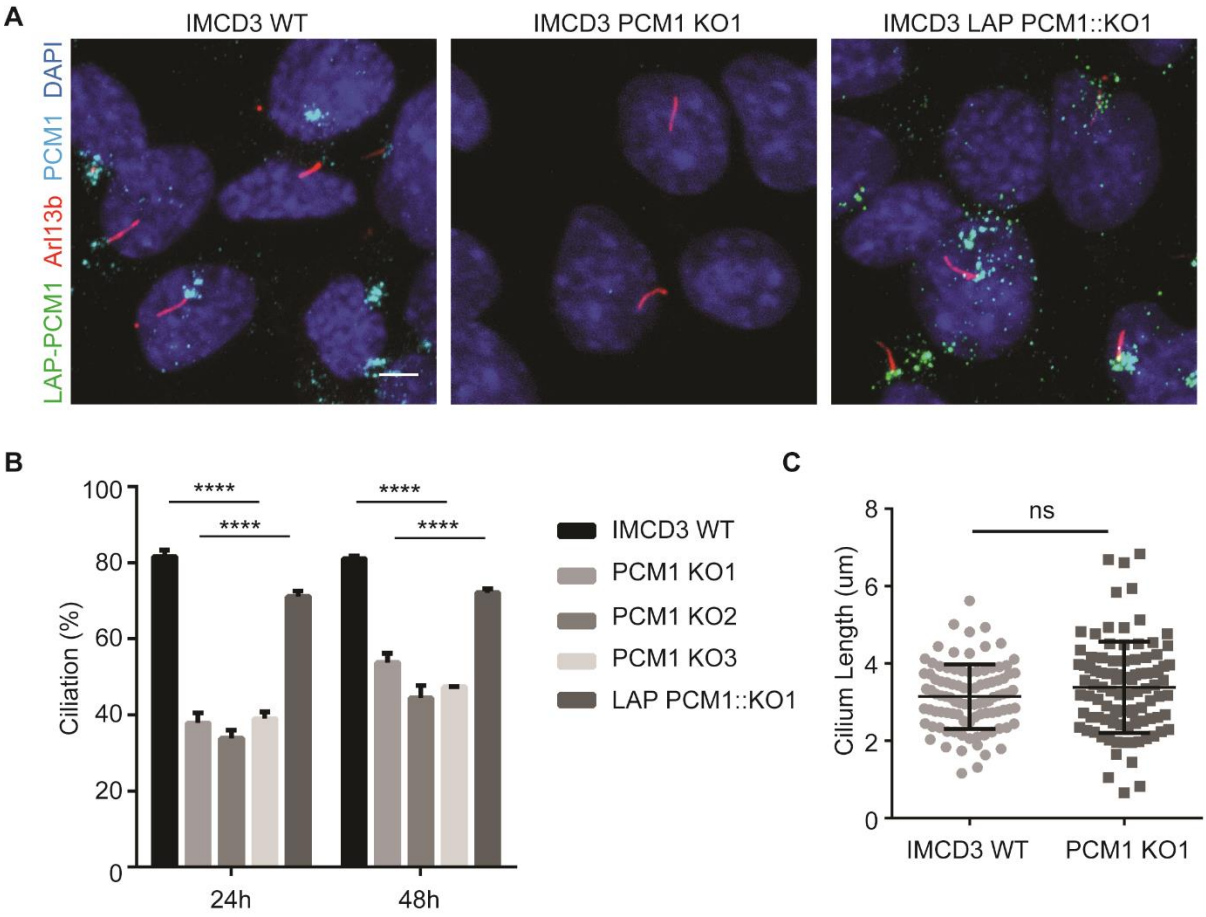

Figure 2.5 Satellites are required for efficient ciliogenesis. (A) Effect of satellite loss on cilium formation. Control cells, IMCD3 PCM1 KO cells and LAP-PCM1-expressing IMCD3 PCM1 KO cells serum-starved for the indicated times,and percentage of ciliated cells was determined by staining for acetylated tubulin, Arl13b, and DAPI. Scale bar, 4 μm. (B) Quantification of ciliogenesis and rescue experiments. Results shown are the mean of three independent experiments ±SD (500 cells/experiment, ****P < 0.0001, t-test). (C) Effect of satellite loss on cilium length. IMCD3 cells serum-starved for 24 h, and cilium length was determined by staining for acetylated tubulin and DAPI.Quantification of cilium length was done from three independent experiments with an average of 90 cilia measured per experiment. Error bars represent SD.Horizontal line represents the mean value of each group. There is no significant difference between control and IMCD3 PCM1 KO cells (t-test).

We next asked whether the ciliogenesis defects of IMCD3 PCM1 KO cells are an indirect consequence of defects in cell cycle progression or centriole duplication. We tested the cell cycle-related phenotypes using a combination of assays. First, we performed proliferation assays with control and IMCD3 PCM1 KO cells by plating equal number of cells and counting them at indicated time intervals, which showed that loss of satellites did not have a significant impact on cell doubling times (Figure 2.6).

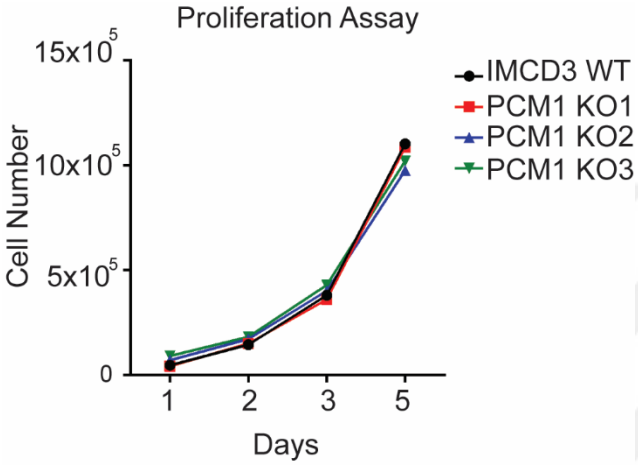

Figure 2.6 Effects of satellite loss on cell proliferation. 2×10^5 cells were plated and counted at 1, 2, 3, and 5 days. Data points show mean ±SD of three independentexperiments. There was no significant difference between control and IMCD3 PCM1 KO cells at any time point

Second, we analyzed the fraction of control and IMCD3 PCM1 KO cells in different phases of the cell cycle using flow cytometry and showed that both had similar cell cycle profiles (Figure 2.7).

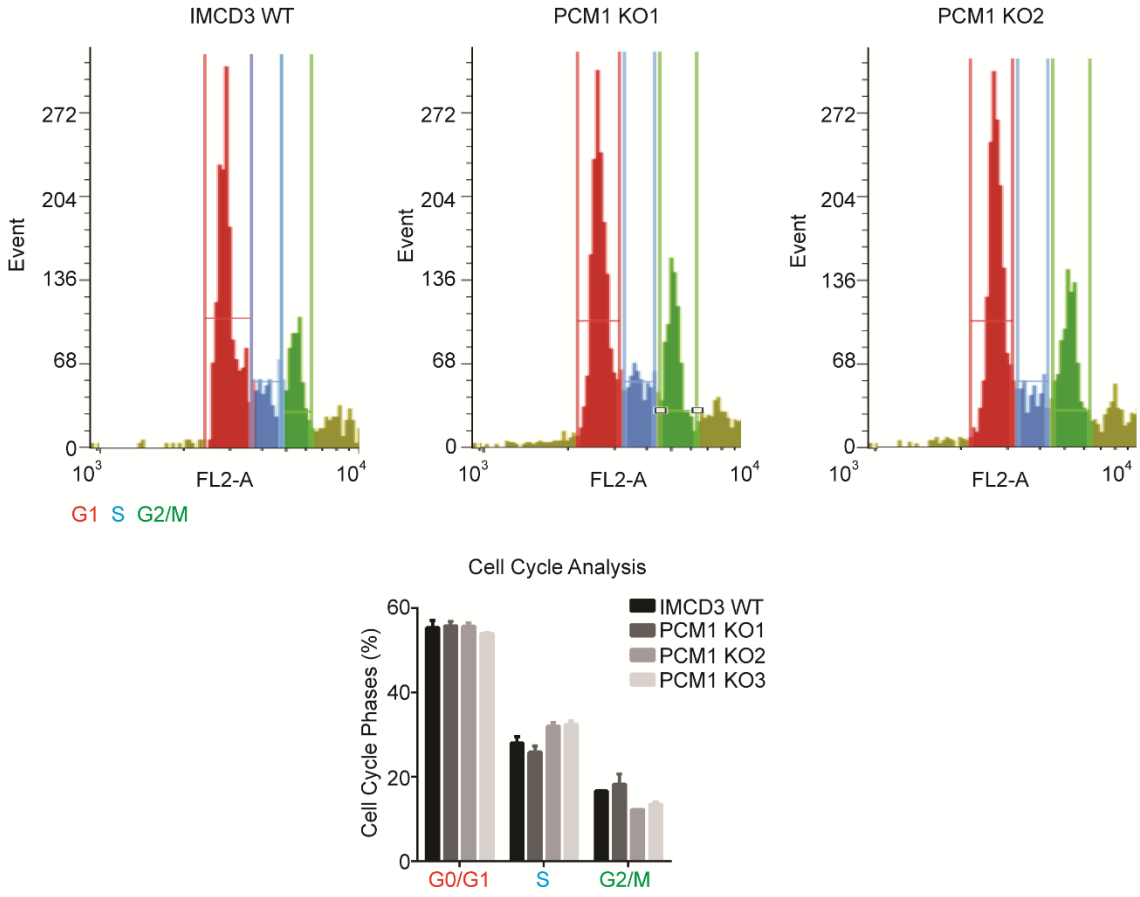

Figure 2.7 Effect of satellite loss on percentage of cells in different cell cycle phases. Flow cytometry analysis of control or IMCD3 PCM1 KO cells. Data points show mean ±SD of three independent experiments FACS sorting of propidium iodide stained IMCD3 control and PCM1 KO cells. Graphs are prepared with the cell number on y-axis and PI fluorescence reflecting the DNA content on x-axis.

Moreover, we performed live imaging of control and IMCD3 PCM1 KO cells stably expressing mCherry-H2B to assay for cell cycle progression defects. Both control and PCM1 KO cells had similar mitotic times (WT: 29 ± 7.7 min, KO: 28.1 ± 6.7 min; Figure 2.8).

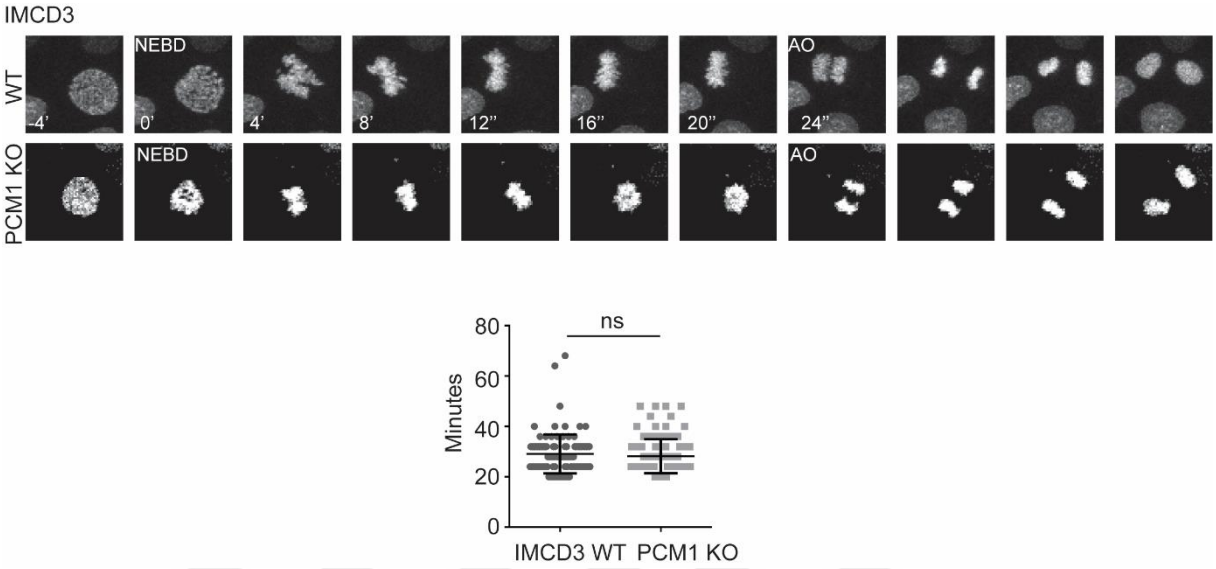

Figure 2.8 Effect of satellites loss on mitotic times. Control and IMCD3 PCM1 KO cell stably expressing mCherry-H2B were imaged every 4 min for 24 h. Representative still frames from time-lapse experiments are shown.

Finally, we quantified centriole number in asynchronous control and IMCD3 PCM1 KO cells by centrin2 and centrin3 labeling and showed that PCM1 KO cells had similar centriole counts relative to control cells (Figure 2.9).

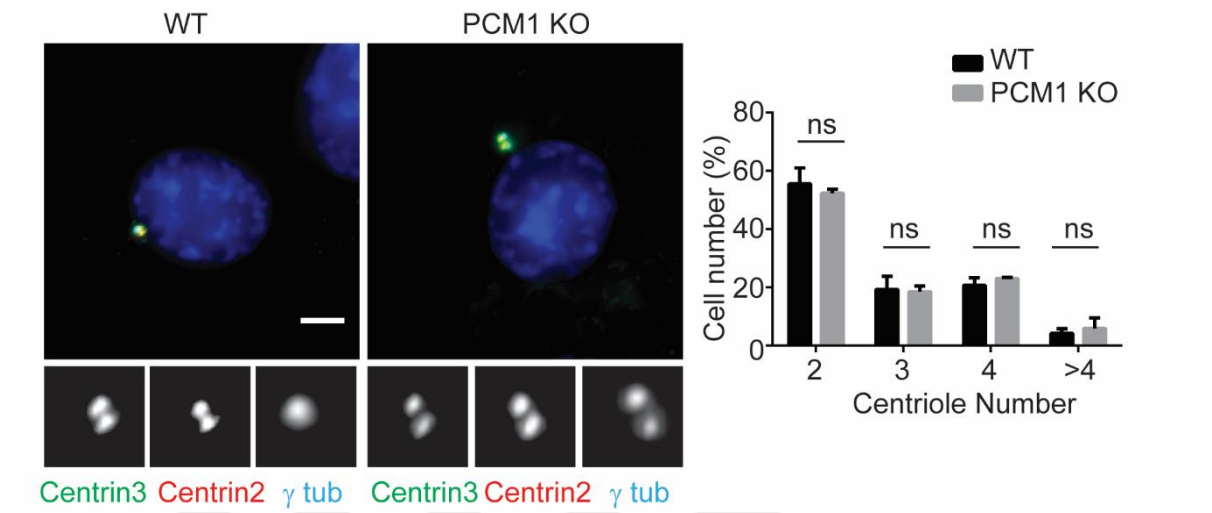

Figure 2.9 Effect of satellite loss on centriole duplication. Asynchronous control and IMCD3 PCM1 KO cells were stained for centrioles using centrin2 and centrin3 antibodies, centrosomes using gamma-tubulin antibody, and DNA with DAPI stain. Quantification results shown are the mean of two independent experiments ± SD (100 cells/experiment, t-test, ns: non-significant). Scale bar, 4 μm.

To investigate the generality of these phenotypes, we generated two RPE1 PCM1 KO clones using genome editing and confirmed their satellite null state by sequencing, immunoblotting, and immunofluorescence (Figure 2.10).

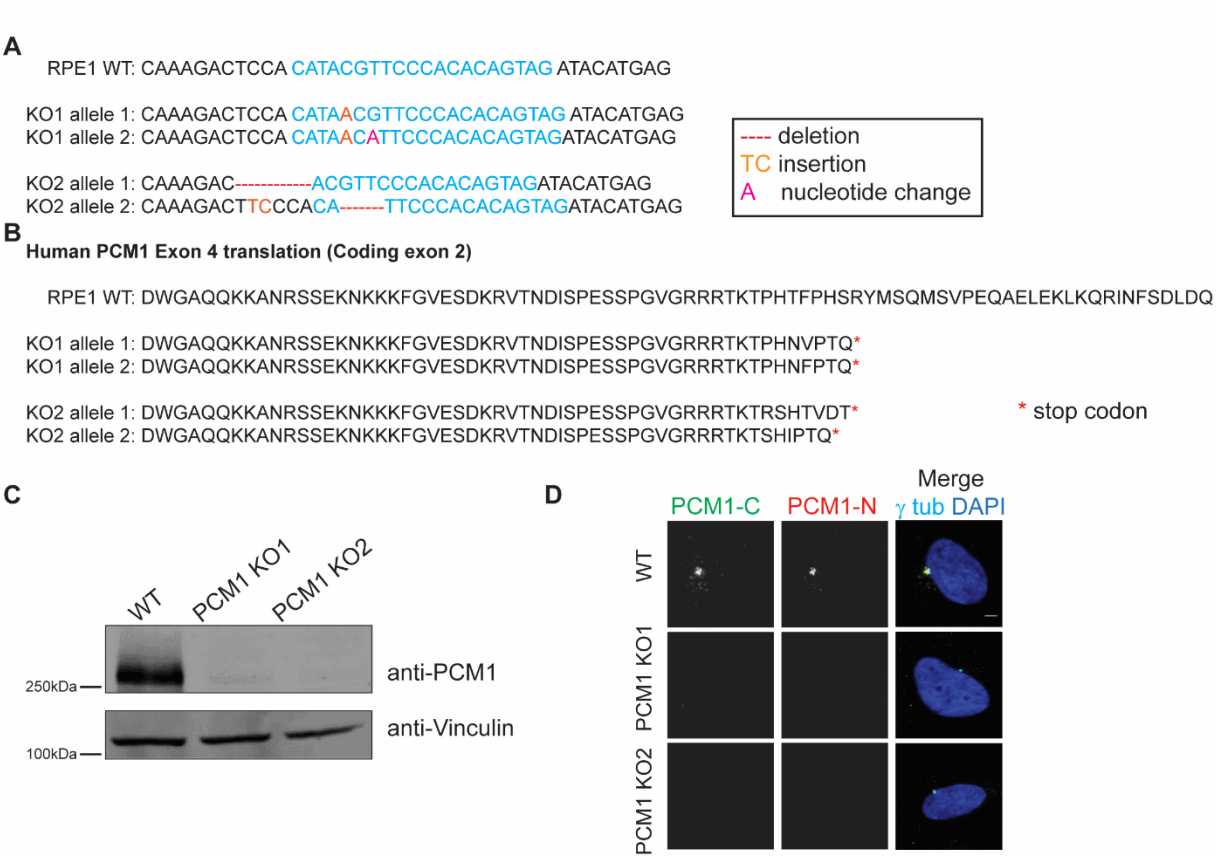

Figure 2.10 Validation of RPE1 PCM1 KO cells (A) RPE1 PCM1 KO clones are all compound heterozygotes with mutations that lead to early stop codons. 1000 bp region around the gRNA-target site was PCR amplified and cloned. Sequencing of five different clones for each line identified one 1nt insertion on one allele and one nt insertion and one nucleotide change on the other for line 1, 7 nt deletion on one allele and 4 nt deletion and and 2 nt insertion on the other for line 2. (B) Translation products of the gRNA-tareting exon (protein coding exon 2) in RPE1 PCM1 KO clones. (C) Immunoblot analysis of whole-cell lysates from control cells and two RPE1 PCM1 KO clones with PCM1 antibody targeting N-terminal 1-254 amino acids. (D) Immunofluorescence analysis of control and RPE1 PCM1 KO clones. Cells were fixed and stained for centrosomes with anti-g-tubulin antibody and PCM1 with PCM1-N antibody and PCM1-C antibody. Scale bar, 3 μm.

Like IMCD3 PCM1 KO cells, RPE1 PCM1 KO cells did not have defects in cell proliferation, distribution of cell cycle phases, and centriole duplication (Figure 2.11). Collectively, these data indicate that satellites are not required for cell cycle progression and centriole duplication, and that the reduced ciliogenesis phenotype of PCM1 KO cells is not caused by defects in these processes.

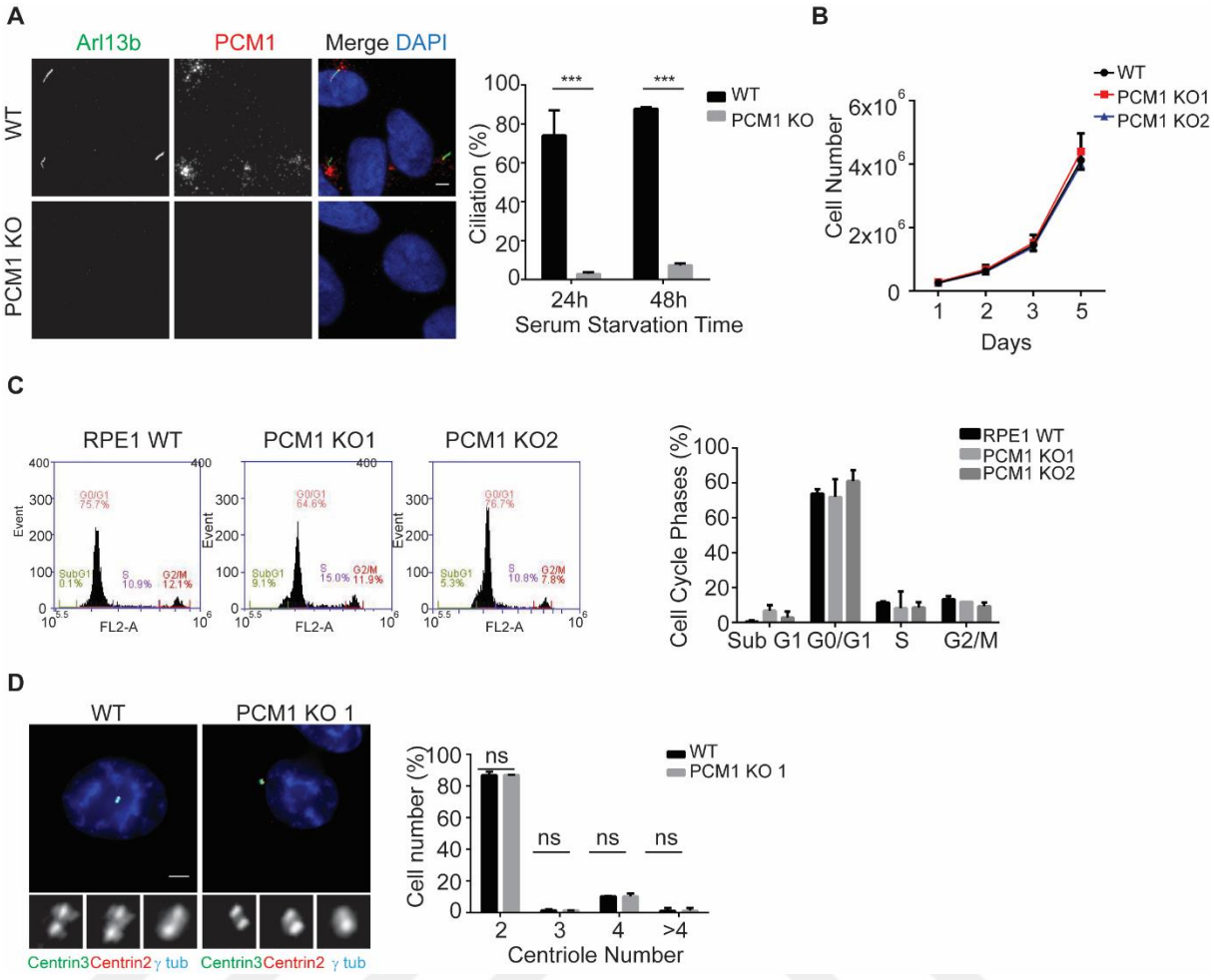

Figure 2.11 Characterization of RPE1 PCM1 KO cells. (A) Effect of satellite loss on cilium formation. Control and RPE1 PCM1 KO cells were serum-starved for the indicated times and percentage of ciliated cells was determined by staining for acetylated-tubulin, Arl13b and DAPI. Results shown are the mean of three independent experiments±SD (500 cells/experiment, ***p<0.001, t-test) (B) Effects of satellite loss on cell proliferation. 105 cells were plated and counted at 1,2, 3 and 5 days. Data points show mean±SD of three independent experiments. There was no significant difference between control and RPE1 PCM1 KO cells at any time point. (C) Effect of satellite loss on percentage of cells in different cell cycle phases. Flow cytometry analysis of control or RPE1 PCM1 KO cells. Data points show mean ± SD of three independent experiments. (D) Effect of satellite loss on centriole duplication. Asynchronous control and RPE1 PCM1 KO cells were stained with staining for centrin2, centrin3 and gamma-tubulin and DAPI. Quantification results shown are the mean of two independent experiments ±SD (100 cells/experiment, t test). Scale bar, 4 μm

2.4.3 Satellites have variable effects on regulating centrosomal and cellular abundance of key ciliogenesis factors

Satellites regulate centrosomal recruitment of proteins including centrin, pericentrin, and ninein among others (Dammermann and Merdes 2002). We hypothesized that the ciliogenesis defects of IMCD3 cells might be due to inefficient targeting of key ciliogenesis factors to the centrosome. To test this, we used quantitative immunofluorescence to determine the centrosomal levels of proteins that are components of distal appendages, transition zone proteins, IFT machinery as well as activators and suppressors of ciliogenesis in asynchronous and serum-starved control cells, IMCD3 PCM1 KO cells, and the LAP-PCM1 rescue clone.

Distal appendages function in docking of the mother centriole to the membrane during ciliogenesis, and transition zone regulates the entry and exit of ciliary cargo (Mirvis, Stearns et al. 2018, Wang and Dynlacht 2018). The defects in ciliogenesis were not because of mislocalization of distal appendage or the transition zone proteins since Cep164 and Cep290 localized correctly to the centrosomes in both control and IMCD3 PCM1 KO cells (Figure 2.12). Of note, the centrosomal levels of Cep164 were higher in PCM1 KO cells, which were rescued by stable LAP-PCM1 expression (Figure 2.12-A and C). This increase might be due to the increased abundance of Cep164 in total cell lysates in PCM1 KO cells (Figure 2.16-A).

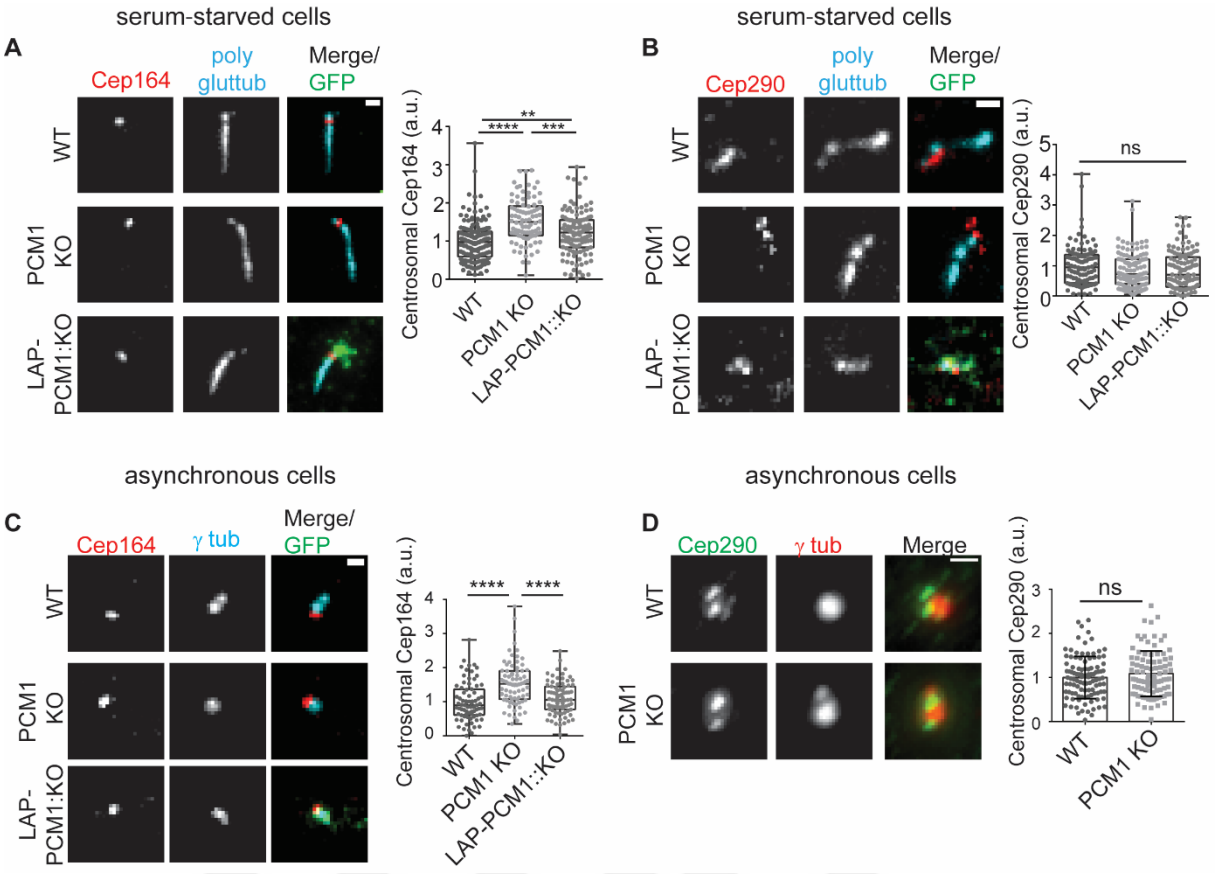

Figure 2.12 Effect of satellite loss on centrosomal abundance of Cep164 and Cep290 in serum-starved cells and asynchronous cells. Control, IMCD3 KO, and IMCD3 KO stably expressing LAP-PCM1 cells were fixed and stained with antibodies for the indicated proteins along with anti-GFP for marking LAP-PCM1 and anti-polyglutamylated tubulin or anti-gamma tubulin for marking centrosomes. DNA was stained with DAPI. Scale bar, 1 μm. Both ciliated and unciliated cells were quantified in a blinded manner. Images represent cells from the same coverslip taken with the same camera settings. The centrosomal fluorescence intensity of the indicated proteins was measured in a 3 μm^2 square area around the centrosome, and levels are normalized to 1. Results shown are the mean of two independent experiments ± SD (100 cells/experiment, *P < 0.5, **P < 0.01, ***P < 0.001, ns: not significant t-test). Error bars represent SD. Horizontal line represents mean value of each group. The boxes include data from the 25th to 75th percentiles in each group.

CP110 localizes to the distal ends of centrioles and is removed from the mother centrioles during ciliogenesis (Schmidt, Kleylein-Sohn et al. 2009). The centrosomal levels of CP110 were similar in control and IMCD3 PCM1 KO cells (Figure 2.13).

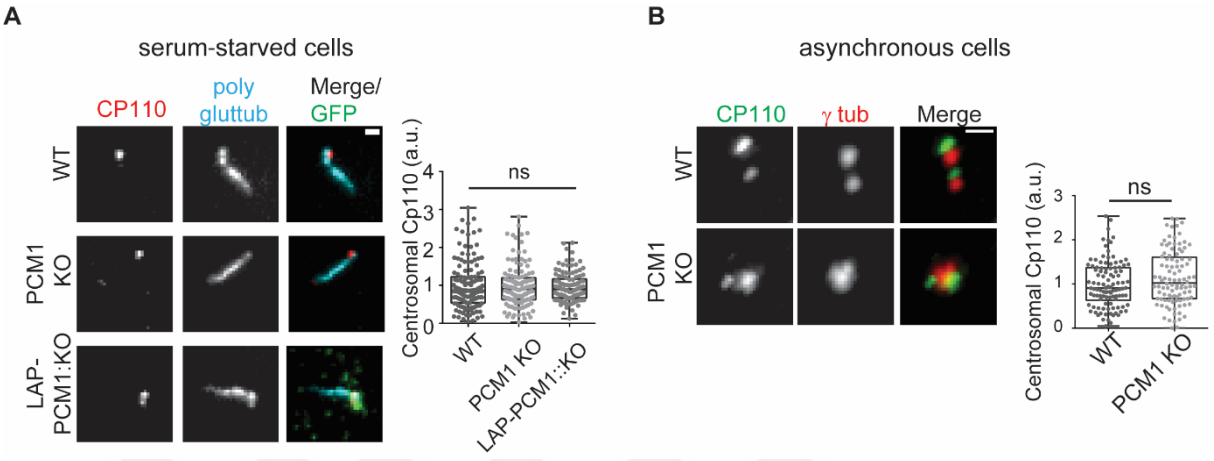

Figure 2.13 Effect of satellite loss on centrosomal abundance of Cp110 in serum-starved cells and asynchronous cells. Control, IMCD3 KO, and IMCD3 KO stably expressing LAP-PCM1 cells were fixed and stained with antibodies for the indicated proteins along with anti-GFP for marking LAP-PCM1 and anti-polyglutamylated tubulin or anti-gamma tubulin for marking centrosomes. DNA was stained with DAPI. Scale bar, 1 µm. Both ciliated and unciliated cells were quantified in a blinded manner. Images represent cells from the same coverslip taken with the same camera settings. The centrosomal fluorescence intensity of the indicated proteins was measured in a 3 μm^2 square area around the centrosome, and levels are normalized to 1. Results shown are the mean of two independent experiments ± SD (100 cells/experiment, *P < 0.5, **P < 0.01, ***P < 0.001, ns: not significant t-test). Error bars represent SD. Horizontal line represents mean value of each group. The boxes include data from the 25th to 75th percentiles in each group.

Importantly, IMCD3 PCM1 KO cells had a significant reduction in the basal body levels of IFT-B protein Ift88 in both asynchronous and serum-starved cells, which was rescued by stable expression of LAP-PCM1 (Figure 2.14). Given that the IFT-B machinery is required for the assembly of the ciliary axoneme, satellites might promote cilium assembly at a step upstream to the recruitment of the IFT machinery at the base of cilia (Pazour, Dickert et al. 2000, Pazour, Baker et al. 2002, Haycraft, Zhang et al. 2007, Bhogaraju, Cajanek et al. 2013).

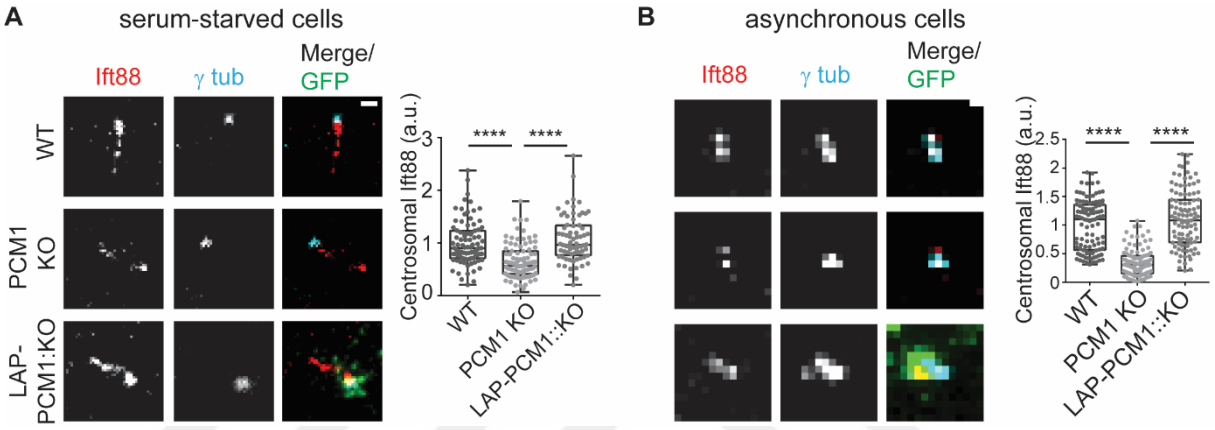

Figure 2.14 Effect of satellite loss on centrosomal abundance of Ift88 in serum-starved cells and asynchronous cells. Control, IMCD3 KO, and IMCD3 KO stably expressing LAP-PCM1 cells were fixed and stained with antibodies for the indicated proteins along with anti-GFP for marking LAP-PCM1 and anti-polyglutamylated tubulin or anti-gamma tubulin for marking centrosomes. DNA was stained with DAPI. Scale bar, 1 µm. Both ciliated and unciliated cells were quantified in a blinded manner. Images represent cells from the same coverslip taken with the same camera settings. The centrosomal fluorescence intensity of the indicated proteins was measured in a 3 μm^2 square area around the centrosome, and levels are normalized to 1. Results shown are the mean of two independent experiments ± SD (100 cells/experiment, *P < 0.5, **P < 0.01, ***P < 0.001, ns: not significant t-test). Error bars represent SD. Horizontal line represents mean value of each group. The boxes include data from the 25th to 75th percentiles in each group.

The inhibition of ciliogenesis in RPE1 PCM1 KO cells was shown to be a consequence of increased cellular and centrosomal levels of the E3 ubiquitin ligase Mib1, which led to a reduction in the centrosomal levels of the key ciliogenesis factor Talpid3/KIAA0586 through its destabilization (Wang, Lee et al. 2016). We investigated whether loss of satellites had similar molecular consequences in IMCD3 cells. Despite the significant 1.5 ± 0.26-fold increase in the cellular abundance of Mib1 in IMCD3 PCM1 KO cells (Figure 2.16-B), its centrosomal levels did not change in these cells relative to control cells (Figure 2.15-A and C). The centrosomal and cellular levels of Talpid3 in IMCD3 PCM1 KO cells were higher than those in control cells, which were rescued by stable LAP-PCM1 expression. (Figure 2.15-A, C and Figure 2.16-B). Thus, in contrast to RPE1 cells, Mib1 sequestration and consequent Talpid3 degradation at the centrosome were not induced in satellite-less IMCD3 cells despite their increased cellular levels. Collectively, these results identify differences in the efficiency of the centrosomal targeting of key ciliogenesis factors as a likely mechanism for the phenotypic variability of satellite-less IMCD3 and RPE1 cells during cilium formation.

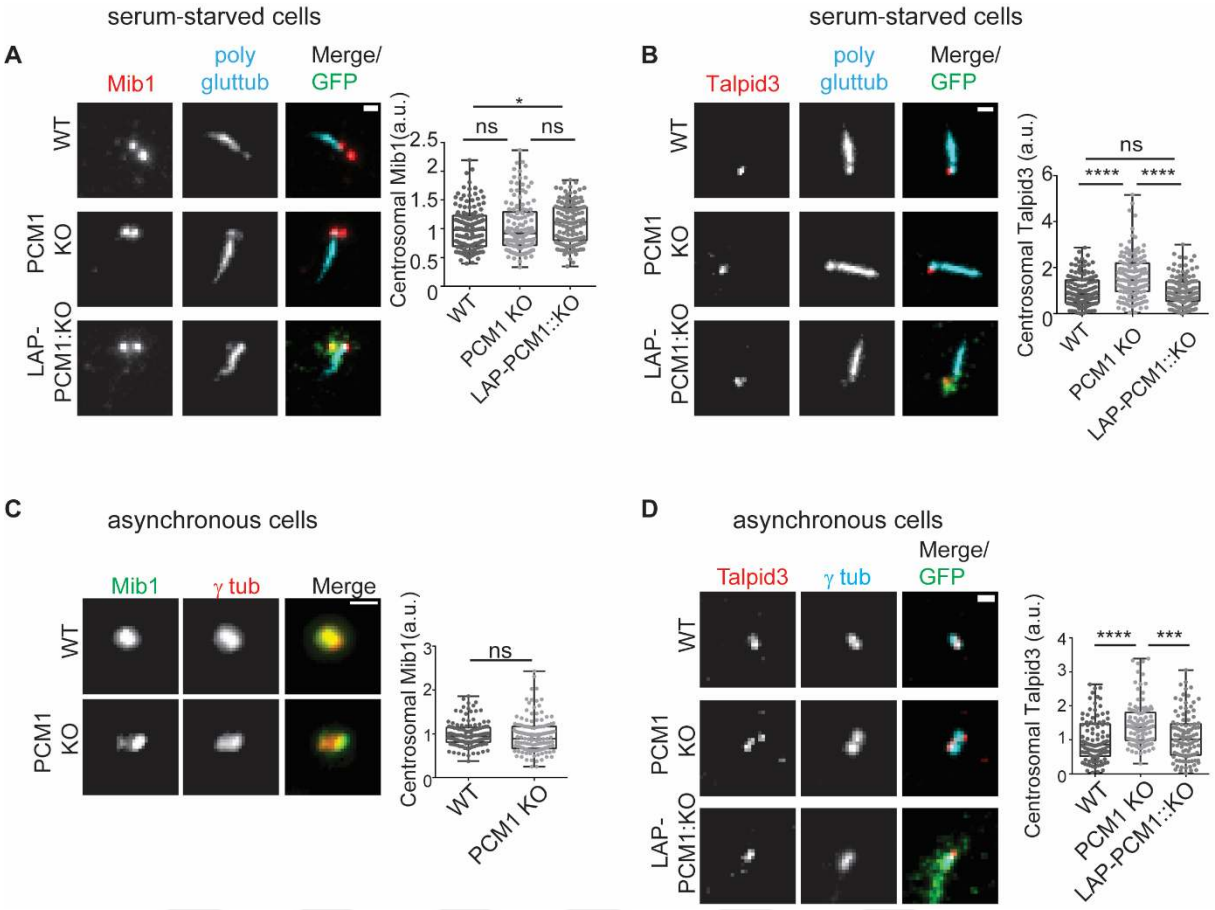

Figure 2.15 Effect of satellite loss on centrosomal abundance of Mib1 and Talpid3 in serum-starved cells and asynchronous cells. Control, IMCD3 KO, and IMCD3 KO stably expressing LAP-PCM1 cells were fixed and stained with antibodies for the indicated proteins along with anti-GFP for marking LAP-PCM1 and anti-polyglutamylated tubulin or anti-gamma tubulin for marking centrosomes. DNA was stained with DAPI. Scale bar, 1 μm. Both ciliated and unciliated cells were quantified in a blinded manner. Images represent cells from the same coverslip taken with the same camera settings. The centrosomal fluorescence intensity of the indicated proteins was measured in a 3 μm^2 square area around the centrosome, and levels are normalized to 1. Results shown are the mean of two independent experiments ± SD (100 cells/experiment, *P < 0.5, **P < 0.01, ***P < 0.001, ns: not significant t-test). Error bars represent SD. Horizontal line represents mean value of each group. The boxes include data from the 25th to 75th percentiles in each group.

We also performed immunoblot analysis of whole-cell lysates of asynchronous and serum-starved control and IMCD3 PCM1 KO cells to determine whether the cellular abundance of these proteins was affected. While there was an overall increase in the abundance of Mib1, Cep164, Cep131, and Ift88 and overall decrease in SLAIN2, the abundance of Bbs4, SSXIIP, Cep290, Cp110, Talpid3, and Arl13b was unaffected (Figure 2.16). Thus, loss of satellites has differential effects on the abundance of different centrosome and cilium proteins. Notably, except for Cep164, changes in abundance of these proteins were not reflected by similar changes in the recruitment of these proteins to the centrosome. For example, while Ift88 cellular levels increase significantly, its centrosomal levels had a significant reduction.

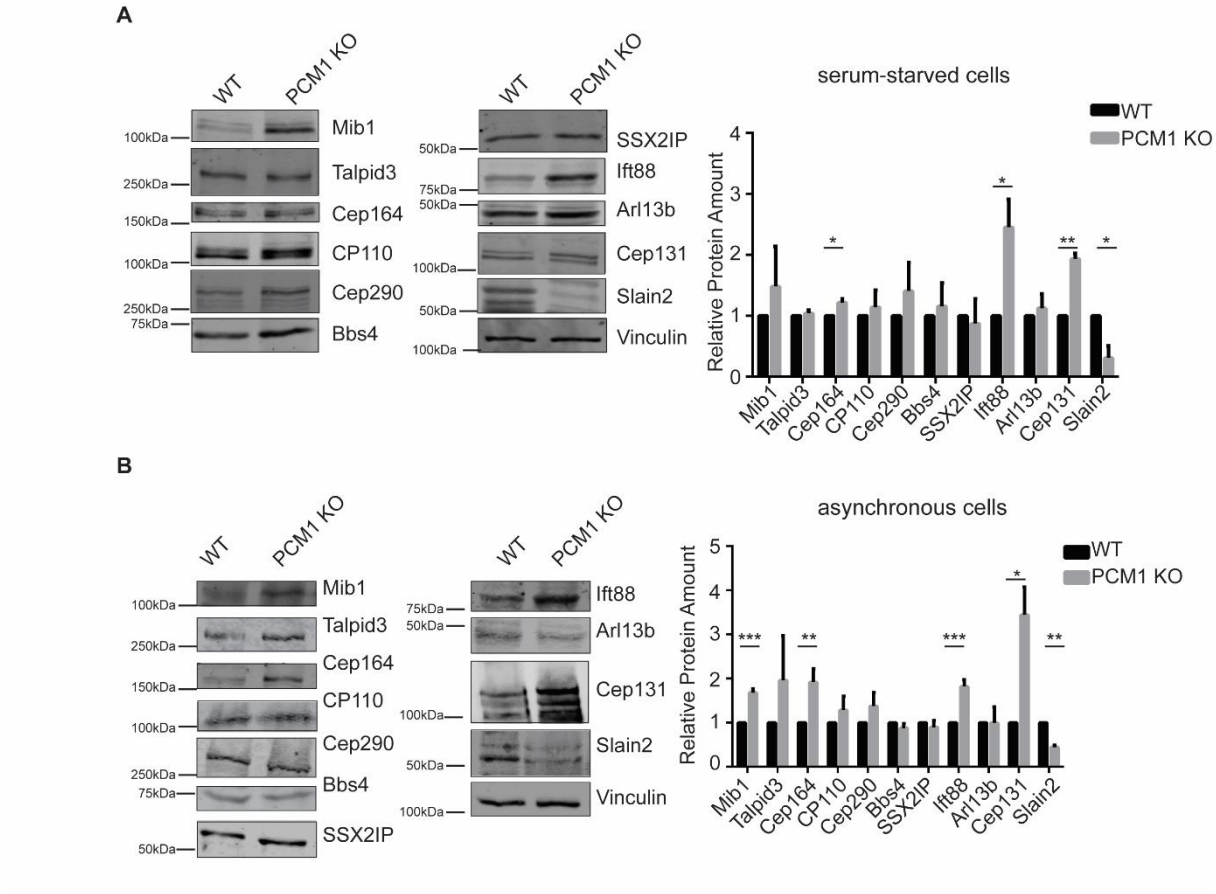

Figure 2.16 Effects of satellite loss on cellular abundance of centrosome proteins. Whole-cell lysates from control and IMCD3 PCM1 KO cells in asynchronous condition and serum-starved for 24 h were immunoblotted with the indicated antibodies. Vinculin was used as a loading control. Results shown are the mean of two independent experiments ± SD (*P < 0.5, **P < 0.01, t-test).

2.4.4 Satellites regulate ciliary protein content

Analogous to their function in regulating protein targeting to the centrosome, we hypothesized that satellites might also regulate ciliary recruitment of proteins. To test this, we examined the composition of the ciliary shaft and the ciliary membrane of control and IMCD3 PCM1 KO cells by determining the ciliary levels of various proteins using quantitative immunofluorescence. Control and IMCD3 PCM1 KO cells had similar levels of ciliary Arl13b, which associates with the ciliary membrane via palmitoylation (Figure 2.17-A) (Cevik, Hori et al. 2010). However, IMCD3 PCM1 KO cells had significantly reduced ciliary levels of the IFT-B protein Ift88, somatostatin receptor 3 (SSTR3-LAP), and the serotonin 6 receptor (HTR6-LAP) (Figure 2.17-B, C and D). The decrease in ciliary Ift88 in IMCD3 PCM1 KO cells was rescued by stable expression of LAP-PCM1 (Figure 2.17-D).

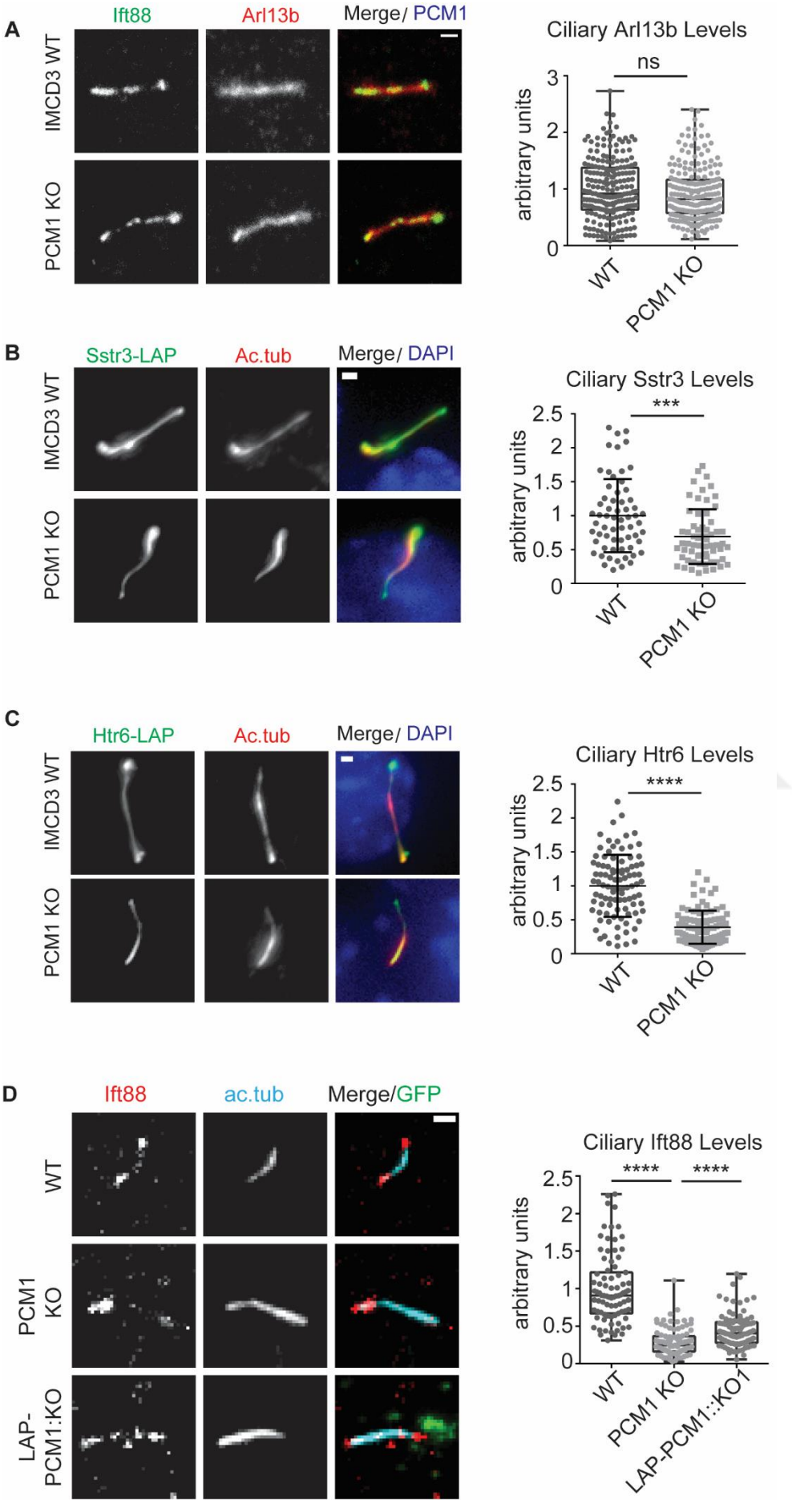
A
Ift88
Arl13b
Merge/ PCM1
IMCD3 WT
PCM1 KO
Ciliary Arl13b Levels
ns
arbitrary units
WT
PCM1 KO
B
Sstr3-LAP
Ac.tub
Merge/ DAPI
IMCD3 WT
PCM1 KO
Ciliary Sstr3 Levels
***
arbitrary units
WT
PCM1 KO
C
Htr6-LAP
Ac.tub
Merge/ DAPI
IMCD3 WT
PCM1 KO
Ciliary Htr6 Levels
****
arbitrary units
WT
PCM1 KO
D
Ift88
ac.tub
Merge/GFP
WT
PCM1 KO
LAP-PCM1:KO
Ciliary Ift88 Levels
****
****
arbitrary units
WT
PCM1 KO
LAP-PCM1::KO1

Figure 2.17 Satellites are required for regulating the ciliary content. Effects of satellite loss on the ciliary recruitment of ciliary membrane and shaft proteins. Control and IMCD3 PCM1 KO cells were serum-starved for 24 h, fixed and stained for the cilium with anti-acetylated tubulin (Ac. tub) or Arl13b, and (A) Ift88 with anti-Ift88 and Arl13b with anti-Arl13b (B) SSTR3-LAP with anti-GFP, (C) HTR6-LAP with anti-GFP. Effect of satellite loss on the ciliary abundance of Ift88 in control, IMCD3 PCM1 KO, and IMCD3 PCM1 KO::LAP-PCM1 cells serum-starved for 24 h. Cells were fixedand stained with Ift88, the ciliary marker acetylated tubulin. Scale bar, 1 μm. Images represent cells from the same coverslip taken with the same camera settings. Relative quantifications of the ciliary intensity of the indicated proteins are shown as the mean of two independent experiments ± SD (100 cells/experiment, **P < 0.01, ***P < 0.001, ****P < 0.0001, ns: not significant, t-test). The mean intensity of the control proteins was normalized to 1. Horizontal line represents the mean value of each group. The boxes include data from the 25th to 75th percentiles of each group.

To investigate the function of satellites in the dynamic recruitment of ciliary proteins, we performed half- and full-cilium fluorescence recovery after photobleaching (FRAP) to measure the dynamic behavior of HTR6-LAP and SSTR6-LAP in IMCD3 cells (Hu, Milenkovic et al. 2010). Both proteins did not recover in full-cilium FRAP experiments in control and PCM1 KO cells (Figure 2.18-A). Likewise, the half-time (LAP-SSTR3 in WT: 17.64 ± 3.41 s, PCM1 KO: 19.96 ± 4.31 s; LAP-HTR6 in WT: 43.24 ± 17.45 s, PCM1 KO: 53.87 ± 20.15 s) and percentage of their recovery (SSTR3-LAP in WT: 40.19 ± 6.73, in PCM1 KO: 35.85 ± 7.64 s; LAP HTR6 in WT: 45.36 ± 13.92, PCM1 KO: 42.57 ± 5.94) in half-cilium FRAP experiments were similar (Figure 2.18 B, C and D).

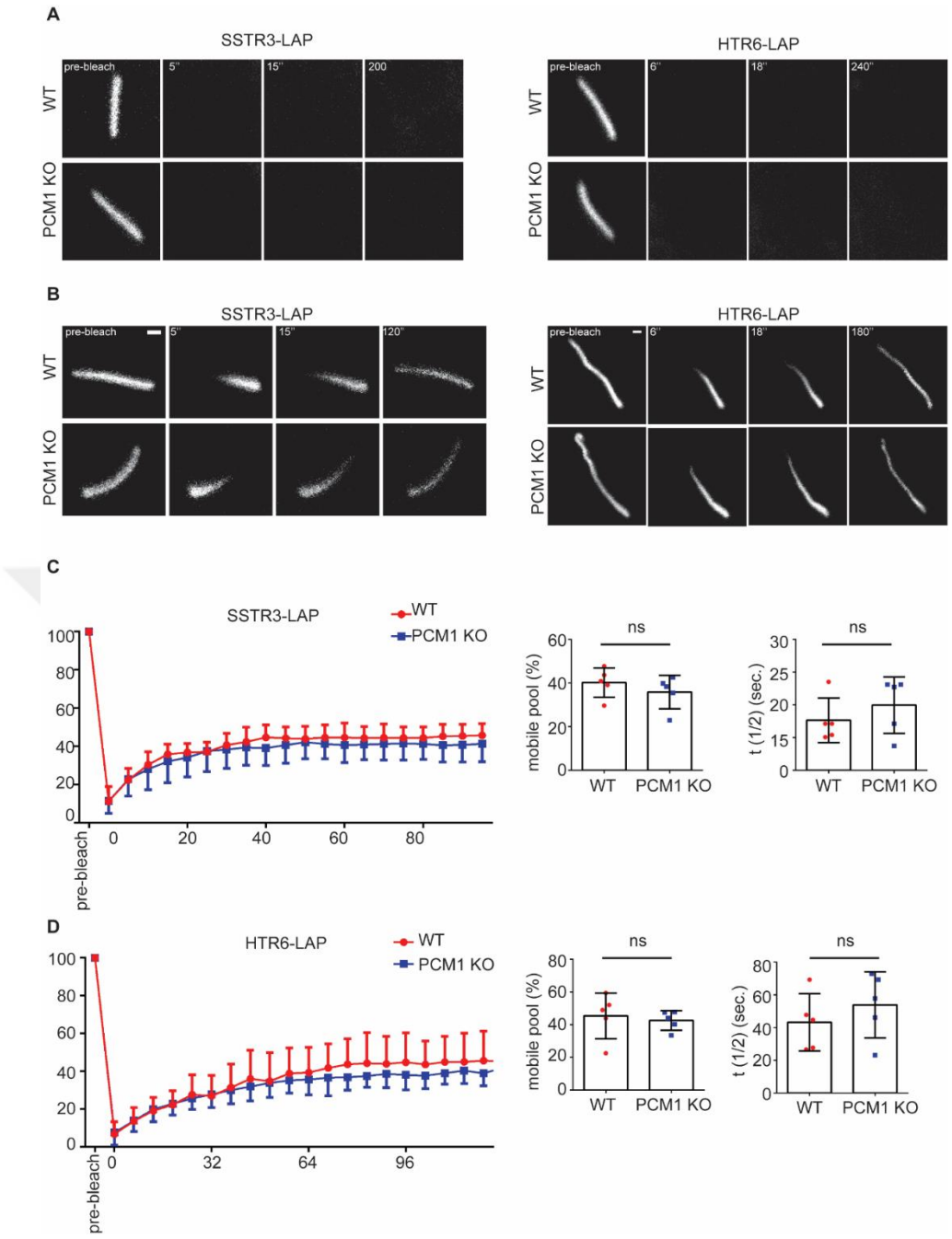

Figure 2.18 FRAP experiments in IMCD3 control and PCM1 KO cells expressing SSTR3-LAP and HTR6-LAP. Representative still images of FRAP in the (A) whole cilium and (B) half-cilium in IMCD3 24 h after serum starvation of IMCD3 cells stably expressing SSTR3-LAP and HTR6-LAP. Representative examples of different time points from each FRAP experiments were shown. Scale bar, 1 µm. (C, D) Quantification of half-cilium FRAP experiments for control and PCM1 KO cells expressing (C) SSTR3-LAP and (D) HTR6-LAP. Kinetics of average (±SD) fluorescence recovery of proteins photobleached in the half cilium, halftime of recovery t1/2 and percentage of recovery were quantified (n=5 cells).

The ciliary localization of some Hedgehog pathway components is dynamically regulated in response to pathway activation. To elucidate the function of satellites in this dynamic regulation and to investigate whether the cilia assembled in IMCD3 satellite-less cells can still respond to Hedgehog ligands, we quantified the ciliary recruitment of the seven-transmembrane protein Smo, which moves to cilia in response to Sonic Hedgehog (Shh) ligands (Corbit, Aanstad et al. 2005). To this end, we stimulated control and IMCD3 PCM1 KO cells with 200 nM Smoothened agonist (SAG) in a time course manner and quantified the percentage of cilia with Smo. A significant ($P < 0.01$) twofold reduction in the percentage of cilia with Smo was observed in PCM1 KO cells (40.1% ± 7.9 of total) relative to control cells (80.6% ± 6.9 of total) at 4 h, and 45.9% ± 18.2 of total in PCM1 KO cells relative to 75.5% ± 12.5 of total in control cells at 8 h (Figure 2.19). Notably, control and IMCD3 PCM1 KO cells had similar percentages of cilia with Smo after 12-h and 24-h SAG stimulation, indicating that lack of satellites directly or indirectly caused a delay in translocation of Smo to the cilium in response to SAG (Figure 2.19). Reduction in Smo relocalization phenotype was rescued by stable expression of LAP-tagged full-length human PCM1 at 4 and 8 h time points of SAG stimulation (Figure 2.19).

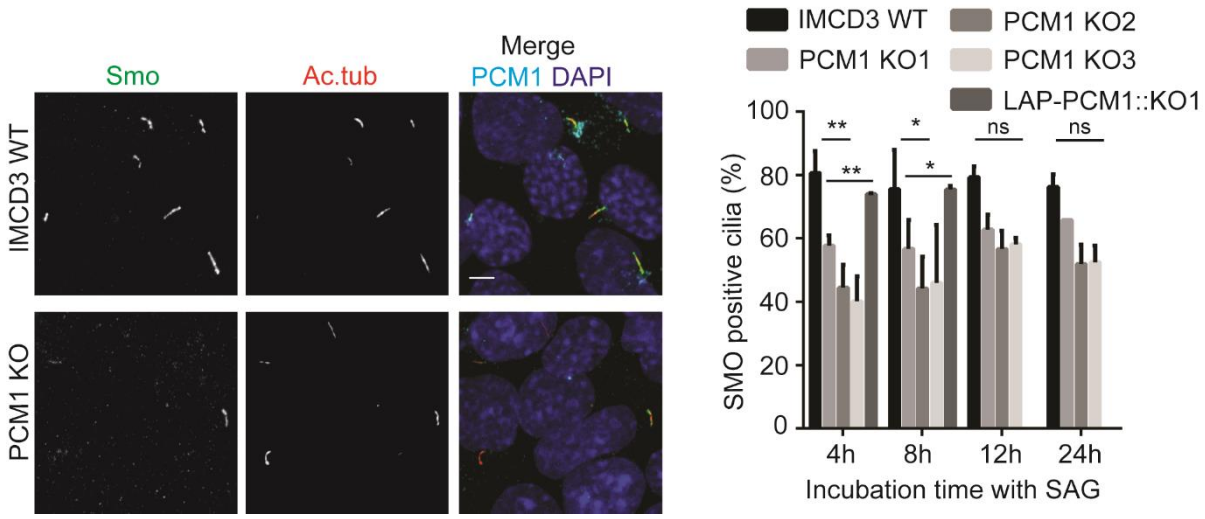

Figure 2.19 Effect of satellite loss on ciliary recruitment of Smo. Control, IMCD3 KO, and IMCD3 KO stably expressing LAP-PCM1 cells were serum-starved for 24 h, treated with 200 nM SAG for the indicated times, fixed and stained for Smo, acetylated tubulin (Ac. tub), and DAPI. Percentage of Smo-positive cilia was quantified. Scale bar, 4 µm. Results shown are the mean of three independent experiments ± SD (250 cells/experiment, $^{**}P < 0.01$, $^{*}P < 0.05$, t-test).

In the IMCD3 PCM1 KO and control cells that formed cilia, we determined ciliary Smo levels and concentrations, and found reduced localization in IMCD3 PCM1 KO cells relative to control cells. Ciliary SMO level in IMCD3 PCM1 KO cells decreased to 0.22 ± 0.16 compared to control cells, which is normalized to 1 after 4-h SAG treatment (Figure 2.20-A). Ciliary SMO concentration decreased to 0.19 ± 0.18 in IMCD3 PCM1 KO cells compared to control cells normalized to 1. This reduction was not due to changes in the cellular abundance of Smo (Figure 2.20-B).

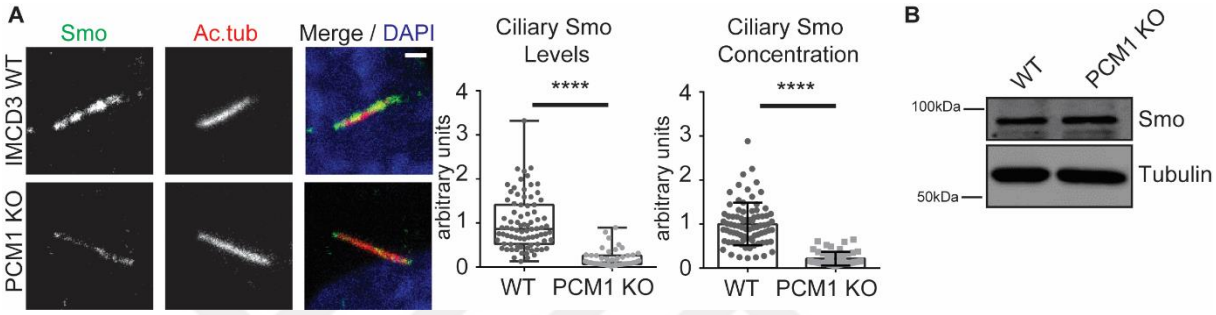

Figure 2.20 Effect of satellite loss on ciliary SMO levels. The ciliary intensity of SMO was quantified by staining 4 h SAG-treated cells for Smo and acetylated tubulin. DNA was stained with DAPI. Scale bar is 4 μm. Relative quantifications of the ciliary intensity and ciliary concentration of SMO are shown as the mean of two independent experiments ± SD (100 cells/experiment, ****P < 0.0001 t-test).

To assay the transcriptional response to Hedgehog pathway activation, we examined the expression of the Hedgehog target gene Gli1 in control and PCM1 KO cells. While wild-type cells had robust activation of Gli1 expression (normalized to 100%), PCM1 KO cells failed to upregulate Gli1 expression at 24 h (35% ± 25.6; Figure 2.21-A). There was a very small but significant decrease in Gli1 expression in PCM1 KO cells (89.46% ± 5.41) relative to control cells (100%) before SAG stimulation (Figure 2.21-B). Taken together, these results indicate that satellites are required for the localization of sufficient levels of Smo at cilia, and efficient activation of the Hedgehog pathway.

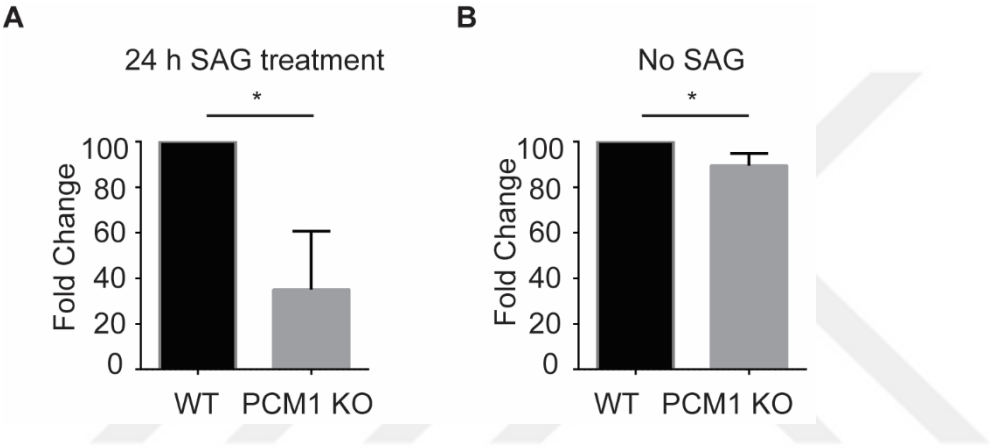

Figure 2.21 Effect of satellite loss on Gli1 transcriptional activation. (A) Gli1 mRNA was quantified by qPCR before SAG treatment and 24 h after SAG treatment, and its foldchange is normalized to control cells (=100). Results shown are the mean of two independent experiments ± SD (*P < 0.05, t-test). (B) Cellular abundance of Gli1 mRNA in control and PCM1 KO cells. Effect of satellite loss on Gli1 transcriptional activation. Gli2 mRNA was quantified by qPCR without any SAG treatment. Relative mRNA amount is normalized to control cells (=100). Results shown are the mean of two independent experiments ± SD (*P < 0.05, t-test).

2.4.5 Satellites are required for epithelial cell organization in 3D cultures

When grown in a three-dimensional gel matrix, epithelial cells organize into polarized, spheroid structures that reflect the in vivo organization of the epithelial tissues. Epithelial spheroids have been widely used to assay cilia dysfunction, because proper cilium assembly and ciliary signaling is essential for the establishment of the highly organized architecture and apicobasal polarity of epithelial cells in 3D (Delous, Hellman et al. 2009, Otto, Hurd et al. 2010, Mahjoub and Stearns 2012). To assay the consequences of ciliary defects associated with loss of satellites on tissue architecture, we used the 3D spheroid cultures of IMCD3 cells that mimic in vivo organization of the kidney collecting duct (Giles, Ajzenberg et al. 2014). Control and IMCD3 PCM1 KO cells were grown in Matrigel for 3 days, serum-starved for 2 days, and spheroid architecture was visualized by staining cells for markers for cilia, cell–cell contacts, and polarity. Control cells formed spheroids with prominent lumen, apical cilia oriented toward the lumen, and proper organization of apical and basal surfaces (ZO-1 and beta-catenin; Fig 2.22-A). However, PCM1 KO cells had a significant decrease in their ability to form proper spheroids relative to control cells, which was rescued by transient expression of myc-PCM1 (control: %70.75 ± 3.89; PCM1 KO: %46.45 ± 1.91; rescue: %59.80 ± 1.31; Fig 2.22-A and B). Instead, they formed cell clusters with no lumens that had misoriented cilia and disorganized apical and basolateral junctions (Figure 26A). Analogous to the ciliogenesis defects of 2D serum-starved cultures, ciliogenesis efficiency was significantly reduced in IMCD3 PCM1 KO cells grown in 3D cultures and this defect was rescued by transient expression of myc-PCM1 (control: %64.08 ± 19.19; PCM1 KO: %36.98 ± 21.28; rescue: %61.81 ± 17.25; Fig 2.22-A and C).

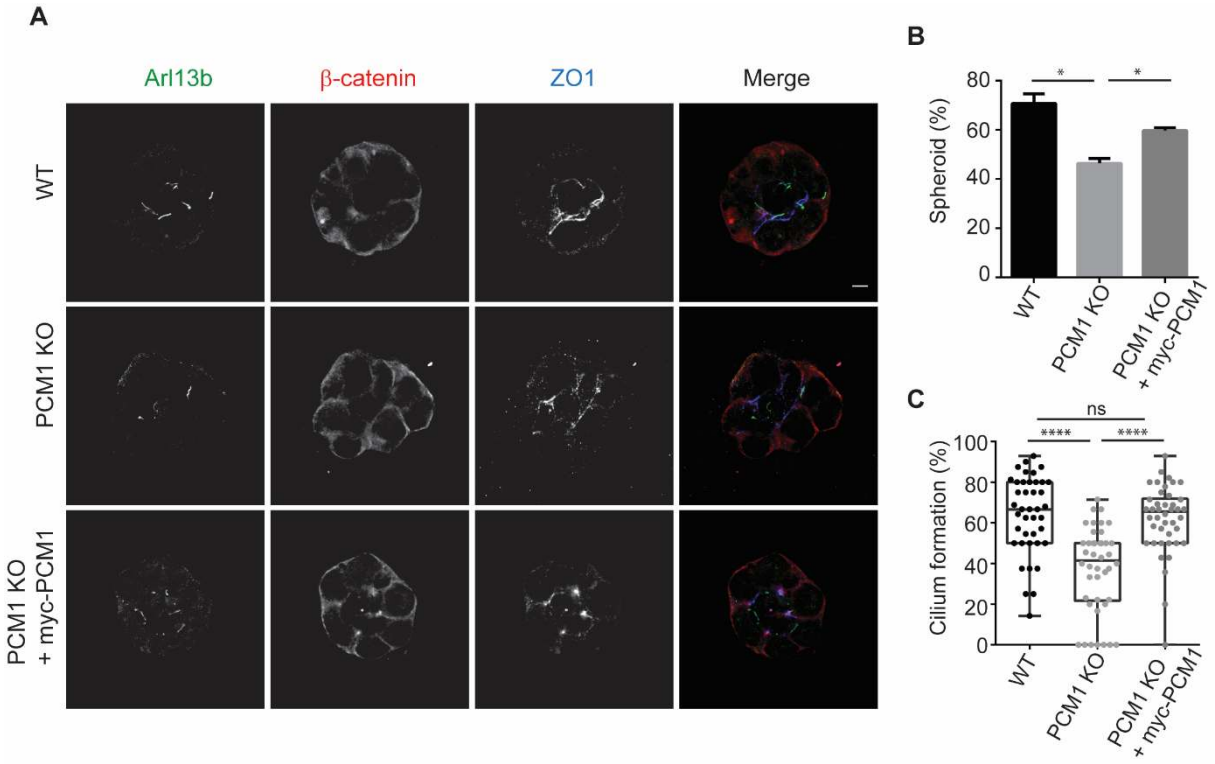

Figure 2.22 Satellites are required for epithelial cell organization in 3D spheroid cultures. Effects of satellite loss on epithelial cell organization. (A) IMCD3 cells were grown in matrigel for 3 days and serum-starved for 2 days. The spheroids were fixed and stained for apical junctions with anti-ZO1, cilia with anti-Arl13b, and basolateral surfaces with anti-beta-catenin. Scale bar, 5 μm. (B) Quantification of the frequency of spheroid formation in control, IMCD3 PCM1 KO cells, and IMCD3 PCM1 KO cells transfected with myc-PCM1. Results shown are the mean of three independent experiments ± SD (50 spheroids/experiment, *P < 0.05, t-test). (C) Quantification of the cilia formation in spheroids in control, IMCD3 PCM1 KO cells, and IMCD3 PCM1 KO cells transfected with myc-PCM1. Results shown are the mean of three independent experiments ± SD (50 spheroids/experiment, ****P < 0.00001, t-test). Error bars represent SD. Horizontal line represents the mean value of each group. The boxes include data from the 25th to 75th percentiles in each group.

Expression of myc PCM1 in rescue experiments was confirmed by immunofluorescence experiments (Figure 2.23). In agreement with the function of satellites in ciliogenesis and signaling, these results identify important roles for satellites in epithelial organization in this in vitro tissue model.

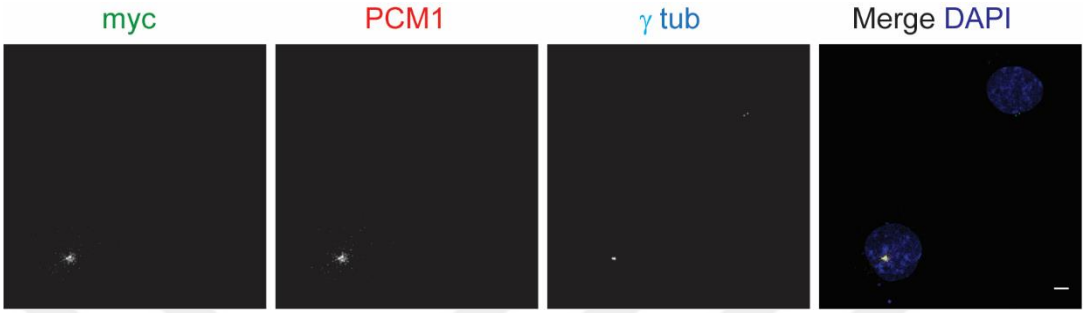

Figure 2.23 Expression of myc-PCM1 in IMCD3 PCM1 KO cells. Control and IMCD3 KO cells were transfected with myc-BirA*-PCM1, fixed and stained with antibodies against myc, PCM1, gamma-tubulin. DNA was stained with DAPI. Scale bar, 5 μm.

2.4.6 Loss of satellites leads to a rearrangement of the global proteome profile, but not the global transcriptome profile

Loss of satellites variably affected the cellular abundance of centrosome and cilium proteins in IMCD3 (Figures 2.12-2.16) and in RPE1 cells as reported previously (Wang, Lee et al. 2016). These data suggest functions for satellites in regulating the cellular abundance of proteins. However, whether these changes are a consequence of transcriptomic or proteomic modulation and which centrosome proteins are affected by these changes have not been investigated. To address this, we performed a systematic comparative analysis of the global transcriptomic and proteomic profile of IMCD3 PCM1 KO cells.

RNA sequencing (RNAseq) analysis of PCM1 KO and control IMCD3 cells revealed 8 genes, which were differentially regulated with log2 fold change > 1.5 and $P < 0.05$ (Table 2.1). Gene ontology and KEGG pathway functional analysis did not identify any functional clustering among these genes. Therefore, it seems unlikely that the differential expression of the identified genes is a direct result of the loss of satellites and the direct cause of the phenotypes observed in PCM1 KO cells. Together, these results show that loss of satellites does not induce a major stress response or compensation mechanism in these cells.

Gene Symbol	Gene Name	Function	Regulation	Fold Change
Pkrd1	protein kinase D1	Angiogenesis, Apoptosis, Differentiation	DR	Inf
Tsnax	translin-associated factor X	Differentiation, Spermatogenesis	DR	Inf
B4galt4	UDP-Gal:betaGlcNAc beta 1,4-galactosyltransferase, polypeptide 4	Protein glycosylation	DR	15.2
Fstl1	follistatin-like 1	Response to starvation	DR	12.7
Fat4	FAT atypical cadherin 4	Cell adhesion	DR	10.2
Mlf1	myeloid leukemia factor 1	Cell cycle, Differentiation	DR	9.4
Dmd	dystrophin, muscular dystrophy	Muscle cell cellular homeostasis	DR	6.1
Pcm1	pericentriolar material 1	Cilium biogenesis	DR	4.3
Gxylt2	glucoside xylosyltransferase 2	O-glycan processing	DR	3.7

Table 2.1 Genes significantly up- or down-regulated in IMCD3 PCM1 KO cells compared to WT controls (>1.5-fol, adj. P-value<0.05)

In contrast to the transcriptome analysis, tandem mass tag (TMT) labeling-based quantitative analysis of the global proteome of control and IMCD3 PCM1 KO cells showed that loss of satellites substantially altered the proteomics profile. A total of 6,956 proteins were identified with high confidence, 295 of which were upregulated, while 296 were downregulated (log2-transformed normalized ratios > 0.5) (Figure 2.24).

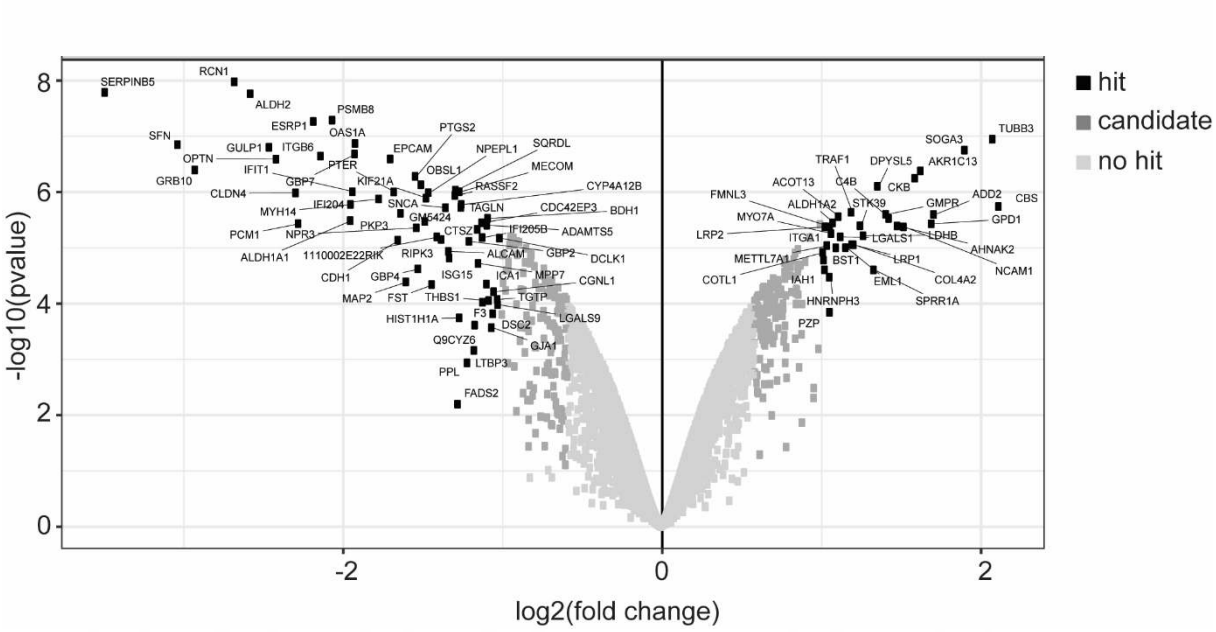

Figure 2.24 Quantitative proteomics profiling of IMCD3 PCM1 KO cells. Volcano plots illustrating that 591 proteins show a significant change in abundance. Data were derived from mass spectrometry analysis of three biological replicates of control and IMCD3 PCM1 KO cells. The x-axis corresponds to the log2 fold change value, and the y-axis displays the -log10 P-value. Proteins were classified into hits (indicated with black circles) if the FDR is smaller than 0.05 and a fold change of at least twofold is observed. Proteins were classified into candidates (indicated with medium gray circles) if the FDR is smaller than 0.2 and a fold change of at least 1.5-fold is observed.

GO-term analysis of the major biological processes and compartments enriched or depleted significantly in PCM1 KO cells identified categories related to “centrosome”, “cell proliferation”, and “microtubules” (Fisher's exact test, FDR < 0.05; Figure 2.25). This is in agreement with the function of satellites as regulators of the centrosome/cilium complex. Moreover, the GO terms actin cytoskeleton, cell migration and adhesion, endocytosis, neuronal processes, metabolic processes were among the most enriched and depleted compartments and processes in Figure 2.25-A and B, which was also illustrated as functional network clustering analysis in Figure 2.25-C and D. Together, this analysis suggests possible functions for satellites in these processes.

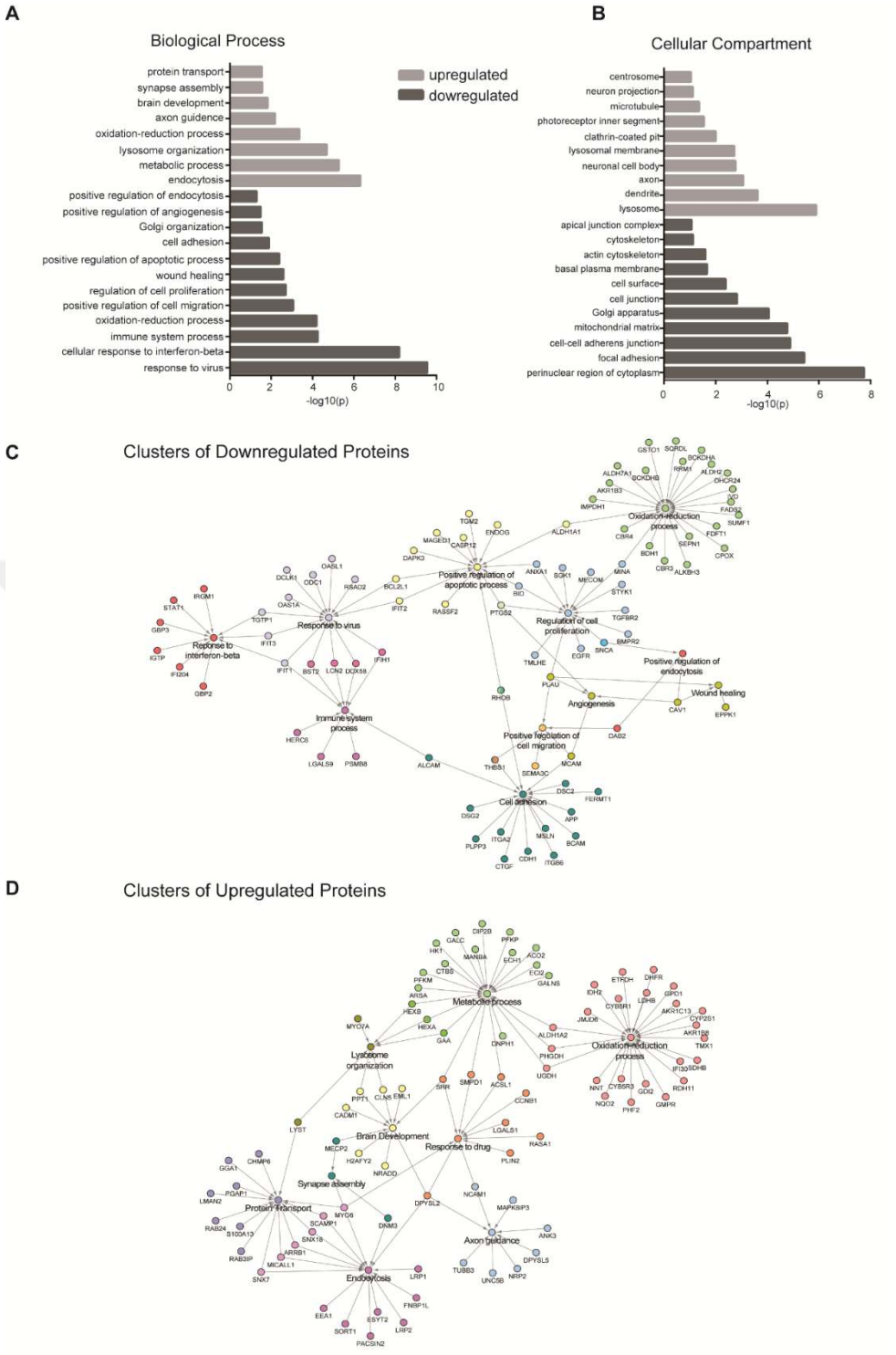

Figure 2.25 Interaction network and GO analysis of the upregulated and downregulated proteins in IMCD3 PCM1 KO cells. (A-B) GO-enrichment analysis for upregulated and downregulated proteins in satellite-less cells in (A) biological function and (B) cellular compartment categorizes. (C-D) Interaction network analysis for (C) downregulated and (D) upregulated proteins identified by GO-enrichment analysis revealed pathways enriched or depleted in satellite-less cells.

To specifically determine the consequences of satellite loss on the cellular abundance of centrosome proteins, we cross-correlated the global proteome dataset with the published centrosome proteome (Jakobsen, Vanselow et al. 2011). Unexpectedly, we found that majority of the 116 centrosome proteome identified remains in place, where only a few proteins including the satellite protein Cep131 and regulatory proteins Ran1Gap2 and Prkar2B were perturbed in the global proteome (Figure 2.26 A, B and C) (Sadrian, Cheng et al. 2012, Staples, Myers et al. 2012, Sha, Xue et al. 2017, Sha, Han et al. 2018). Consistent with the proteomics data, a significant increase in the cellular abundance of Cep131 and a significant decrease in SLAIN2 was detected using immunoblotting experiments (Figure 2.16-A). Due to the low abundant nature of centrosome proteins, we set a lower significance threshold (log2 > 0.3 for TMT labeling) for detecting changes in abundance, which identified 21 proteins in IMCD3 KO cells to be differentially expressed. The upregulated and downregulated centrosome proteins were implicated in a wide range of processes including suppressors and activators of ciliogenesis, centriole duplication, spindle formation, signaling, and microtubule cytoskeleton (Figure 2.25-A and B). The lack of functional clustering among these proteins shows that the regulatory roles of satellites on their resident proteins are specific to each protein and that phenotypic consequences of loss of satellites are likely combinatorial effects of these changes, instead of a specific pathway.

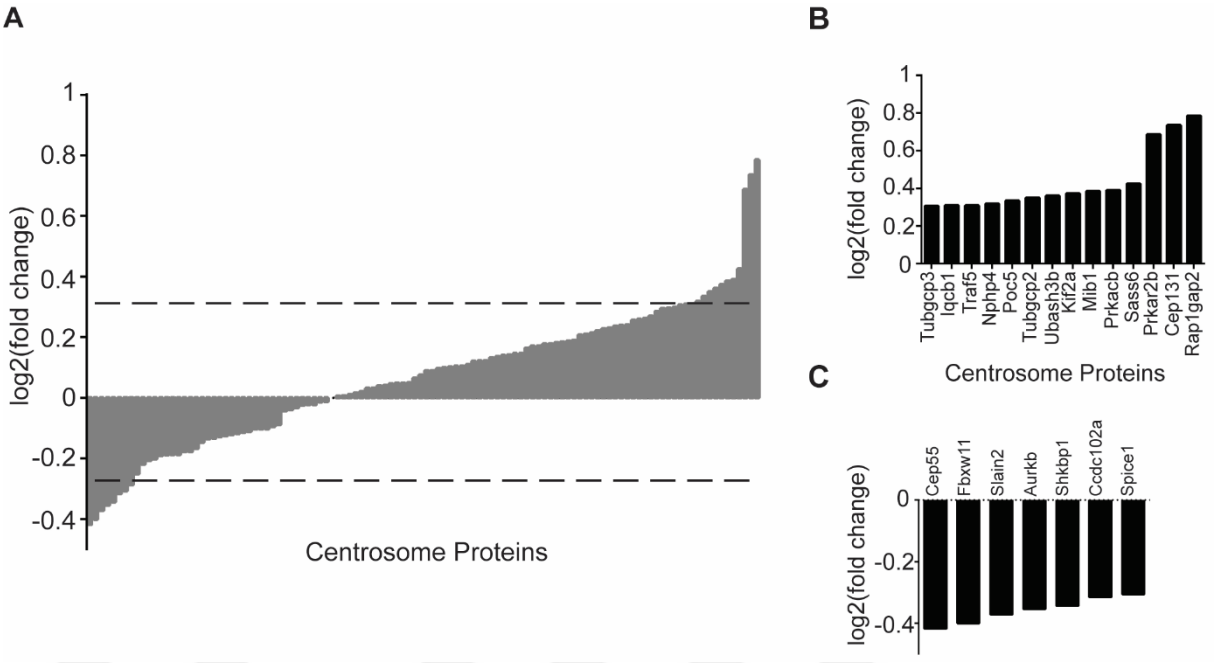

Figure 2.26 Comparison of the centrosome proteome with the IMCD3 PCM1 KO global proteome. 112 centrosome proteins identified in the global proteome (x-axis) were plotted against their log2-transformed ratios of fold changes (y-axis) between IMCD3 PCM1 KO and control samples. Dashed line indicates the threshold we determined for the significantly upregulated and downregulated proteins represented in (B and C). (B) Significantly upregulated centrosome proteins (log2 > 0.3). (C) Significantly downregulated centrosome proteins (log2 < -0.3).

2.5 Discussion

The results of our study reveal two specific roles of satellites in vertebrate cells. First, satellites are required for efficient ciliogenesis, regulation of the ciliary shaft and the ciliary membrane content, and epithelial cell organization in 3D cultures. In particular, satellites are required directly or indirectly for efficient response to Hedgehog pathway agonists. Second, satellites are regulators of the protein targeting and cellular proteostasis, not only for centrosome proteins but also for proteins from a diverse set of pathways. Given that mutations affecting various satellite components cause ciliopathies and loss of satellites in zebrafish leads to ciliopathy-related phenotypes, our findings suggest variable degrees of defects in cilium assembly, signaling, and tissue architecture linked to satellite mutations as mechanisms underlying diverse disease phenotypes of ciliopathies (Lopes, Prosser et al. 2011, Stowe, Wilkinson et al. 2012, Tollenaere, Mailand et al. 2015).

A variety of satellite-specific functions were reported through previous loss-of-function studies targeting PCM1. Transient depletion of PCM1 caused defects in organization of the interphase microtubule network in U2OS cells, cell cycle progression and cell proliferation in MRC-5 primary human fibroblasts and HeLa cells, and cilium formation in RPE1 cells (Dammermann and Merdes 2002, Srsen, Gnadt et al. 2006, Nachury, Loktev et al. 2007, Kim, Krishnaswami et al. 2008). Constitutive depletion of PCM1 from RPE1 and GBM cells caused inhibition of ciliogenesis (Hoang-Minh, Deleyrolle et al. 2016, Wang, Lee et al. 2016). We found that satellites are only required for cilium assembly and function, but not for cell proliferation, cell cycle progression, and centriole duplication in IMCD3 and RPE1 cells. This variation in phenotypes, except for the cilium-related ones, could be due to a functional compensation mechanism that rescues the defects caused by constitutive loss of satellites, previously reported for another satellite protein Azi1 (Hall, Keighren et al. 2013). Alternatively, the requirement for satellites in these processes may simply vary in different cell types, as we show for cilium-related processes in this study. We would like to highlight that loss-of-function studies of PCM1 also defined functions for satellites in autophagy, stress response and neuronal progenitor cell proliferation and migration which we have not focused on in this study (Ge, Frank et al. 2010, Villumsen, Danielsen et al. 2013, Insolera, Shao et al. 2014, Zhang, Kim et al. 2016, Joachim, Razi et al. 2017, Nielsen, Nordgaard et al. 2018).

Satellite loss in RPE1 cells caused an almost complete inhibition of ciliogenesis, identifying a direct and requisite role for satellites in cilium assembly in these cells (Wang, Lee et al. 2016). In contrast, satellite-less IMCD3 cells had a much weaker twofold reduction in their ability to ciliate. The variation in the phenotypes observed in IMCD3 and RPE1 cells might be due to differences in the species and tissues they are derived from, ciliogenesis mechanisms, and mechanism of transformation. IMCD3 cells that ciliated in the absence of satellites had cilia of similar length compared to control cells, which suggests that satellites in these cells are required to initiate assembly of the ciliary axoneme. While satellite-less cells proceeded normally through early steps of mother centriole maturation, they were defective in the recruitment of Ift88 to the basal body, suggesting that satellites promote ciliogenesis upstream of this stage during ciliogenesis. Supporting the relationship between IFT machinery and satellites, proteomics studies identified putative interactions of satellites with various IFT-A and IFT-B components, supporting the functional relationship between the IFT machinery and satellites (Gupta, Coyaud et al. 2015, Huttlin, Ting et al. 2015, Huttlin, Bruckner et al. 2017). Of note, we observed that centrosomal levels of Cep164 and Talpid3 increased in satellite-less cells and we do not know whether these changes have any functional consequences on ciliogenesis.

Satellites were shown to regulate the stability of the ciliogenesis factor Talpid3 and the Atg8 autophagy marker Gabarap through sequestration of Mib1, which suggested that they might mediate functions as regulators of protein degradation pathways (Wang, Lee et al. 2016, Joachim, Razi et al. 2017). However, the turnover of which centrosome proteins are regulated by satellites was not known. Global proteomics of IMCD3 cells showed that the majority of the centrosome proteome remained unaltered and that only the expression of a small subset of centrosome proteins were perturbed. Importantly, Mib1 was among upregulated centrosome proteins in IMCD3 satellite-less cells, corroborating the negative crosstalk between PCM1 and Mib1 stability (Akimov, Rigbolt et al. 2011, Villumsen, Danielsen et al. 2013, Wang, Lee et al. 2016, Joachim, Razi et al. 2017). It is important to note that the global proteome analysis is limited in identifying all the centrosome proteins and determining changes in their expression levels with high sensitivity, due to the low abundance levels of most centrosome proteins in cells (Bauer, Cubizolles et al. 2016).

In addition to regulating protein stability, satellites were shown to mediate their functions through targeting proteins to the centrosome or sequestering them to limit their centrosomal recruitment. In agreement, we detected changes in the centrosomal and ciliary levels of key ciliogenesis proteins, as well as ciliary membrane and shaft proteins. These results show functions for PCM1 in the ciliary recruitment of proteins for the first time and also suggest that these defects might be the underlying the satellite-related defects in vivo and in disease. Notably, for some proteins like Ift88 and Mib1, we showed that changes in the centrosomal levels of these proteins do not scale with changes in their cellular abundance. An attractive possibility for this discrepancy is that satellite-less cells compensate for functional defects through modulating the centrosomal recruitment of proteins. Because we performed this analysis only for a handful of proteins, future studies like identification of the centrosome and cilium proteome in satellite-less cells are required to elucidate the complete list of centrosome and cilium proteins regulated by PCM1.

Despite the unaltered abundance of the centrosome proteome, loss of satellites led to a significant rearrangement of the global proteome, suggesting that satellites regulate cellular proteostasis. Importantly, these global studies provided insight into previously uncharacterized satellite functions. Among the most enriched pathways were the ones related to the actin cytoskeleton such as cell migration, cell adhesion, and endocytosis. The possible functional connection of satellites to actin-related processes is noteworthy due to the function of centrosomes as actin-nucleating centers. In particular, satellites are required for centrosomal actin nucleation through targeting actin assembly factors to the centrosome (Farina, Gaillard et al. 2016, Obino, Farina et al. 2016). Satellites might also function in other actin-regulated ciliary processes, such as periciliary vesicle transport to the basal body and cilia length regulation (Kim, Lee et al. 2010, Kim, Jo et al. 2015, Kohli, Hohne et al. 2017, Wu, Chen et al. 2018). Moreover, we also found a markedly strong increase at the protein level in neurogenesis-linked pathways, such as neuronal body and extensions, postsynaptic membrane, and axon guidance. Consistently, mutations in PCM1 were associated with schizophrenia and PCM1, Hook3, DISC1, and SDCCAG8 were implicated in maintaining neural progenitor cells and neuronal migration during cortical development. Future studies on studying satellites in different contexts will be important to identify the full range of satellite

functions (Gurling, Critchley et al. 2006, Kamiya, Tan et al. 2008, Datta, McQuillin et al. 2010).

While phenotypic characterization of stable genetic knockout model for of satellite-less cells has led to important insights into satellite function and molecular mechanism, its disadvantage is the possible masking of some satellite phenotypes. Generation and maintenance of PCM1 KO lines using the CRISPR/Cas9 genome editing approach requires a long time frame where cells undergo many successive divisions without satellites and thus might have enough time to activate compensatory mechanisms that can mask satellite-specific phenotypes, specifically through proteomic modulation for satellite-less cells as their transcriptome scarcely change (Rossi, Kontarakis et al. 2015, El-Brolosy and Stainier 2017). Likewise, some of the changes we detected in global transcriptomics and proteomics might be specific to cell clones. Future studies using spatially and temporally controlled in vitro and in vivo experiments are required to overcome these limitations.

In summary, our findings identify a more complex molecular and functional relationship between satellites and the centrosome/cilium complex. We suggest that satellites are among the additional regulatory mechanisms vertebrates acquired during evolution in order to prevent defects in the biogenesis and function of the centrosome/cilium complex and thereby associated diseases. Future studies are required to elucidate the functions of satellites in different cell types and tissues and to investigate how defects in these functions are associated with different disease states.

CHAPTER 3: COMPARASION OF PCM1 INTERACTOME IN CYCLING AND CILIATED CELLS BY MINITURBO LABELING METHOD

3.1 Introduction

The centrosome / cilium complex is a structure that functions essential for cells, including cell division, cell movement, and the transmission of signaling pathways (Nigg and Raff 2009). The centrosome / cilium complex in mammals consists of three different structures: centrosome, primary cilium and centriolar satellites (Odabasi, Batman et al. 2020, Prosser and Pelletier 2020). Although the structure and functions of centrosomes and cilia have been examined in detail by studies in the literature, there are many unanswered questions about centriolar satellites. Centriolar satellites are granular structures of 70-100 nm in size that are arranged around the centrosome and are organized by microtubules nucleated from the centrosomes (Hori and Toda 2017, Odabasi, Batman et al. 2020). Recent studies have shown that centriolar satellites act as controllers in many cellular activities such as centrosome duplication, primary cilium formation, cell division (Firat-Karalar, Rauniyar et al. 2014, Tollenaere, Mailand et al. 2015, Wang, Lee et al. 2016, Odabasi, Gul et al. 2019, Aydin, Taflan et al. 2020). More importantly, the structural and functional defects of centriolar satellites associate with neurocognitive disorders including schizophrenia and ciliopathies characterized by retinal degeneration, polydactyly, kidney cysts, obesity and diabetes (Kamiya, Tan et al. 2008, Tabares-Seisdedos and Rubenstein 2009, Stowe, Wilkinson et al. 2012, Conkar, Culfa et al. 2017). The controlling functions of centriolar satellites in cells and their relationship with genetic diseases show the importance of these structures at the cell and organism level. The main purpose of this study is to define the molecular mechanism under roles of centriolar satellites during primary cilium formation. In line with this aim, we determined proteome of centriolar satellites in ciliated cells using the proximity based labeling method, miniTurbo to dissect the mechanism underline ciliogenesis control by centriolar satellites.

3.2 Literature Review

3.2.1 Structures and Functions of Centrosome / Cilium Complex

Centrosome is the membrane-less organelle which functions as main microtubule organizing center (MTOC) in the cells (Luders and Stearns 2007, Nachury and Mick 2019). Centrosome plays an important role in many different biological functions from cell division to cilia and flagella formation (Nigg and Raff 2009, Bettencourt-Dias, Hildebrandt et al. 2011). In the center of the centrosome, there are two centrioles in which nine sets of three microtubules are organized in a radially symmetrical fashion. The pericentriolar material surrounding the centrioles contains gamma tubulin and related proteins involved in the nucleation and regulation of microtubules (Azimzadeh and Marshall 2010). Centrosome plays an important role in cell division due to its functions in the formation of mitotic spindles and the assembly of signal proteins involved in cell division (Chavali, Putz et al. 2014).

The most important function of centrioles is their function as “basal bodies” during the formation of cilia and flagella, which play a role in cell movement, intracellular and intercellular signal transmission (Marshall 2007, Hoyer-Fender 2010). Primary cilium is a microtubule-based organelle which is found in almost all cells in the human body. It acts as an antenna to receive and transmit important signaling pathways such as Hedgehog and Wnt signaling pathways (Nachury and Mick 2019). Considering their important functions at the cell and organism level, it is not surprising that centrosome and primary cilium structure and function disorders cause very different diseases in humans. These diseases include cancer, primary microcephaly, ciliopathies, dwarfism (Bettencourt-Dias, Hildebrandt et al. 2011). The most common type of disease shown to be caused by mutations associated with ciliary genes is human genetic diseases known as ciliopathy (Braun and Hildebrandt 2017). Ciliopathies are multisystemic genetic diseases that occur as a result of structural and functional disorders in primary cilium and centrosome such as retinal degeneration, polydactyly, kidney cyst, obesity, diabetes, and neurocognitive disorders (Nigg and Raff 2009, Bettencourt-Dias, Hildebrandt et al. 2011, Braun and Hildebrandt 2017). Determination of the mechanisms that control the formation and functions of centrosome and primary cilium will provide an understanding of the molecular basis of these diseases and will therefore guide the diagnosis and treatment studies of these diseases.

In order to understand the mechanism underlying ciliopathies, it is important to understand how centrosome/cilium complex is regulated in time and space. Centriolar satellites structure is the recently identified as third component of this complex (Odabasi, Batman et al. 2020). Centriolar satellites are formed by granules localized around centrosome and move along microtubules. The size of the granules is about 70-100 nm. PCM1 protein is scaffolding protein for these granules. Other than PCM1, centriolar satellites have many other resident protein including centrosomal and ciliary proteins (Gheiratmand, Coyaud et al. 2019, Quarantotti, Chen et al. 2019). Recent studies show that depletion of PCM1 inhibits the formation of centriolar satellite structure and results establishing cells without satellite (Hoang-Minh, Deleyrolle et al. 2016, Wang, Lee et al. 2016, Odabasi, Gul et al. 2019). The characterization of satellite-less cells shows that primary cilium formation is affected in the absence of centriolar satellites (Wang, Lee et al. 2016, Odabasi, Gul et al. 2019). Moreover, content and the function of the primary cilia in satellite-less cells are affected. Cells without satellites give late response to Hedgehog signaling pathway activation (Odabasi, Gul et al. 2019). These observations show that centriolar satellites have role in ciliogenesis and regulation of ciliary content and function. However, the mechanism of this regulation is not known.

3.2.2 miniTurbo Proximity Labeling Method

Cellular events are carried out and controlled by the interaction of proteins with each other. Therefore, in order to understand the function of a protein, it is important to know which proteins it binds to and which proteins it interacts with. There are different methods used to determine protein-protein interaction. Yeast or mammalian double-hybrid systems, immunoprecipitation or pull-down analysis, cross-linking analysis can be given as examples of methods used to determine protein-protein interactions that have been used for a long time (Miura 2018). While these methods are effective, they can only identify proteins to which the relevant proteins are physically bound. During dynamic cellular functions, proteins can dynamically interact not only with the proteins to which they are physically bound, but also with other proteins in their proximity. The methods mentioned above are insufficient to identify these proteins. Rous et al. has developed a new method for studying protein-protein interactions. This method is known as BioID (biotin identification) proximity marking method. BioID interactions are based on combining the protein of interset with the mutant E. coli biotin ligase

BirA*. BirA* biotin ligase activates the labeling reaction of this ligase by biotinylating all proteins (proximal proteins) with a diameter of 10 nM in the presence of biotin. Marked proteins are determined by mass spectrometry analysis (Roux, Kim et al. 2012). The BioID technique has been used extensively since 2014 to determine the proximity interactions of centrosome and centriolar satellite proteins(Firat-Karalar, Rauniyar et al. 2014, Gupta, Coyaud et al. 2015, Conkar, Culfa et al. 2017, Gheiratmand, Coyaud et al. 2019). Although this technique is very useful for molecular and functional characterization of centrosome proteins, the major drawback of this method is that the biotinylation time is 18-24 hours. Due to this long biotinylation time, the BioID method has two disadvantages: First one is that long biotinylation time is not suitable for determining cellular events that occur in a short times. Second one is that active biotinylating radicals "biotinoyl-5'-AMP" in the cell cause non-specific biotinylation during prolonged biotinylation.

Since 2012, studies have been continuing to improve the BioID method. Some of these are studies to improve biotinylation efficiency and biotinylation diameter such as BioID2, split-BioID (Kim, Jensen et al. 2016, De Munter, Gornemann et al. 2017). miniTurbo and TurboID proximity marking enzymes were developed by Alice Ting and her team in 2018 as a result of creating new point mutations on the biotin ligase (BirA) enzyme. One of the most important advantages of miniTurbo and TurboID enzymes is that the biotinylation time, which is 18-24 hours in the BioID method, is reduced to 10 minutes (Branon, Bosch et al. 2018). The miniTurbo enzyme is 28 kDA and the TurboID enzyme is 35 kDa. MiniTurbo and TurboID enzymes, which provide short-term biotinylation, are a promising technique that can be used to study short-term cellular events. In addition, since they provide biotinylation in a shorter time, they enable more specific proximity maps to be created, as non-specific biotinylation reactions are reduced. TurboID and miniTurbo methods are more suitable for determining proximal proteins of proteins involved in cellular events that occur rapidly in less than 18 hours in the cell cycle and to develop more specific proximity maps.

The goal of this study, determining the interaction of PCM1 which is scaffolding protein of centriolar satellites in ciliated cells using miniTurbo labeling method. For this purpose, we developed cells lines expressing Flag-miniTurbo-PCM1 and performed miniTurbo labeling in asynronous and ciliated cells. We created the proteins in the proximity to PCM1 in ciliated cells by comparing proximity lists in asynronous and

ciliated cells. With this approach, we aim to enlighten mechanism under regulation of ciliogenesis by centriolar satellites.

3.3 Materials and Methods

3.3.1 Cell Culture and Transfection

IMCD3::Flippin cells (gift from Max Nachury, UCSF, CA) were grown in DMEM/F12 50/50 (Life Technologies) supplemented with 10% fetal bovine serum (FBS; Life Technologies). Cells were cultured at 37°C and 5% CO2. IMCD3 cells were transfected with the plasmids using Lipofectamine LTX according to the manufacturer's instructions (Life Technologies). IMCD3 cells stably expressing miniTurbo and miniTurbo-PCM1. were generated by cotransfecting IMCD3 Flip-in cells with pcDNA5 FRT/TO expression vectors and pOG44 at a ratio of 1:7 using Lipofectamine LTX. After incubating cells with the transfection mix for 6 h, medium was replaced with complete medium for 24 h, which was followed by selection with 200 lg/ml hygromycin B (Sigma-Aldrich) for 1 week. Colonies formed within 10–14 days, individual colonies were picked after selection and screened by immunofluorescence for expression of Flag and streptavidin. For cilium-related experiments, cells were incubated in low-serum medium (0.5% serum) for 48 h.

3.3.2 Immunofluorescence and microscopy

For immunofluorescence experiments, cells were grown on coverslips and fixed in either methanol for 5 min or 4% PFA for 15 min in PBS for indirect immunofluorescence. After rehydration in PBS, cells were blocked in 3% BSA (Sigma-Aldrich) in PBS + 0.1% Triton X-100 for 30 min. Coverslips were incubated in primary antibodies diluted in blocking solution for 1 h at room temperature and Alexa Fluor 488-, 594-, or 680-conjugated secondary antibodies for 1 h at room temperature. Samples were mounted using Mowiol mounting medium containing N-propyl gallate (Sigma-Aldrich). Coverslips of cells were imaged using LAS X software (Premium; Leica) on a scanning confocal microscope (SP8; Leica Microsystems) with Plan Apofluar 63 × 1.4 NA objective or a fluorescent microscope (DMi8; Leica Microsystems) with Plan Apofluar 63 × 1.4 NA objective using a digital CMOS camera (Hamamatsu Orca Flash 4.0 V2 Camera). Images were processed using Photoshop (Adobe) or ImageJ (National Institutes of Health, Bethesda, MD).

3.3.3 miniTurbo Labeling, Cell Lysis, Streptavidin Pulldown and Immunoblotting

For preparation of cell extracts, cells were trypsinized off the plate, washed in PBS, and lysed in lysis buffer 50 mM Tris pH 8, 150 mM NaCl, 0.1% SDS, 0.5% sodium deoxycholate, 1% Triton X-100, 1× protease inhibitor cocktail (Sigma-Aldrich), and 1 mM PMSF) for 30 min. Lysates were sonicated 30% amplitude for 30 sec in pulses then 40% amplitude for 30 s in pulses. Lysate was clarified by centrifugation at 10,000 r.p.m. for 15 min at 4 °C. The protein concentration of cell lysate was determined with the Bradford solution (Bio-Rad Laboratories, CA, USA).

For immunoblotting, equivalent amount of total protein for each cell extract were first resolved on SDS–PAGE gels, transferred onto nitrocellulose membranes, blocked in TBS-T (Tris-buffered saline with 0.1% Tween-20) with 5% milk, blotted with primary antibodies overnight at 4°C and secondary antibodies for 1 h at room temperature. Visualization of the blots was carried out with the LI-COR Odyssey Infrared Imaging System and software at 169 lm (LI-COR Biosciences).

3.3.4 Mass Spectrometry

After on-bead tryptic digest of biotinylated proteins, peptides were analyzed by online C18 nanoflow reversed-phase nano liquid chromatography (Dionex Ultimate 3000 RS LC, Thermo Scientific, Waltham, MA) combined with orbitrap mass spectrometer (Q Exactive Orbitrap, Thermo Scientific, Waltham, MA). Samples were separated in an in-house packed 75 μm i.d. 23-cm C18 column (Reprosil-Gold C18, 3 μm, 200 Å, Dr. Maisch) using 75-minute linear gradients from 5%–25%, 25%–40%, 40%–95% acetonitrile in 0.1% formic acid with 300 nL/minute flow in 90 minutes of total run time. The scan sequence began with an MS1 spectrum (Orbitrap analysis; resolution 70,000; mass range 400–1,500 m/z; automatic gain control [AGC] target 1 × 106 ; maximum injection time, 32 ms). Up to 15 of the most intense ions per cycle were fragmented and analyzed in the orbitrap with data-dependent acquisition (DDA). MS2 analysis consisted of collision-induced dissociation (higher-energy collisional dissociation [HCD]) (resolution 17,500; AGC 1 × 106 ; normalized collision energy [NCE] 26; maximum injection time, 85 ms). The isolation window for MS/MS was 2.0 m/z. Raw files were processed with Thermo Proteome Discoverer 1.4.Carbamidomethylation of cysteine was used as fixed modification, and acetylation (protein N termini) and oxidation of methionine were used as variable modifications. Maximal two missed cleavages were allowed for the tryptic peptides. The precursor

mass tolerance was set to 10 ppm, and both peptide and protein false discovery rates (FDRs) were set to 0.01. The database search was performed against the human Uniprot database (release 2016).

3.3.5 Analysis of Mass Spectrometry

Mass spectrometry data for each sample were derived from two biological and two technical replicates. Spectral counts of identified proteins were used to calculate the BFDR and probability of possible protein–protein interaction by SAINTexpress v.3.6.3 with -L option [50]. Proteins were filtered out according to SAINTscore (>0.5) and BFDR (<0.05). The cutoffs for enrichment (>1.25-fold relative to control) and depletion (0.75-fold relative to control) of proteins in cells with peripheral clusters were determined empirically by assessing which range in the comparative analysis include proteins we validated using immunofluorescence as part of peripheral clusters or previously implicated in cilium biogenesis. Interaction maps were drawn using Cytoscape. GO-enrichment analysis was done using EnrichR. The significantly altered GO categories (biological process and cellular compartment) were selected with a Bonferroni-adjusted cutoff p-value of 0.05.

3.3 Results

3.3.1 miniTurbo-PCM1 forms satellites in satelliteless cells and induces biotinylation

To identify the PCM1 proximity interactome, we applied miniTurbo approach to mouse Inner Medullary Collecting Duct-3 (IMCD3) cells. Cell lines stably expressing miniTurbo and miniTurbo PCM1 is established to PCM1 null IMCD3 cells which was characterized before in our studies (Odabasi, Gul et al. 2019). To generate stable cells with expression low levels of the fusion protein, we cloned an N-terminal fusion of PCM1 into a pcDNA5/TO expression vector designed for use with the T-REx System. Using FlpIn system, we generated IMCD3 cells that stably express Flag-miniTurbo and Flag-miniTurbo-PCM1. We then assessed the expression of Flag-miniTurbo-PCM1 and biotinylation of its proximal interactors by immunostaining and immunoblotting for Flag to detect the fusion protein, streptavidin to detect biotinylated proteins and/or gamma-tubulin to mark the centrosome (Figure 3.1-3.3). Flag-miniTurbo-PCM1 localized around the centrosome in interphase cells. Streptavidin signal shows biotinylated proteins in satellites in the presence of biotin (Figure 3.1).

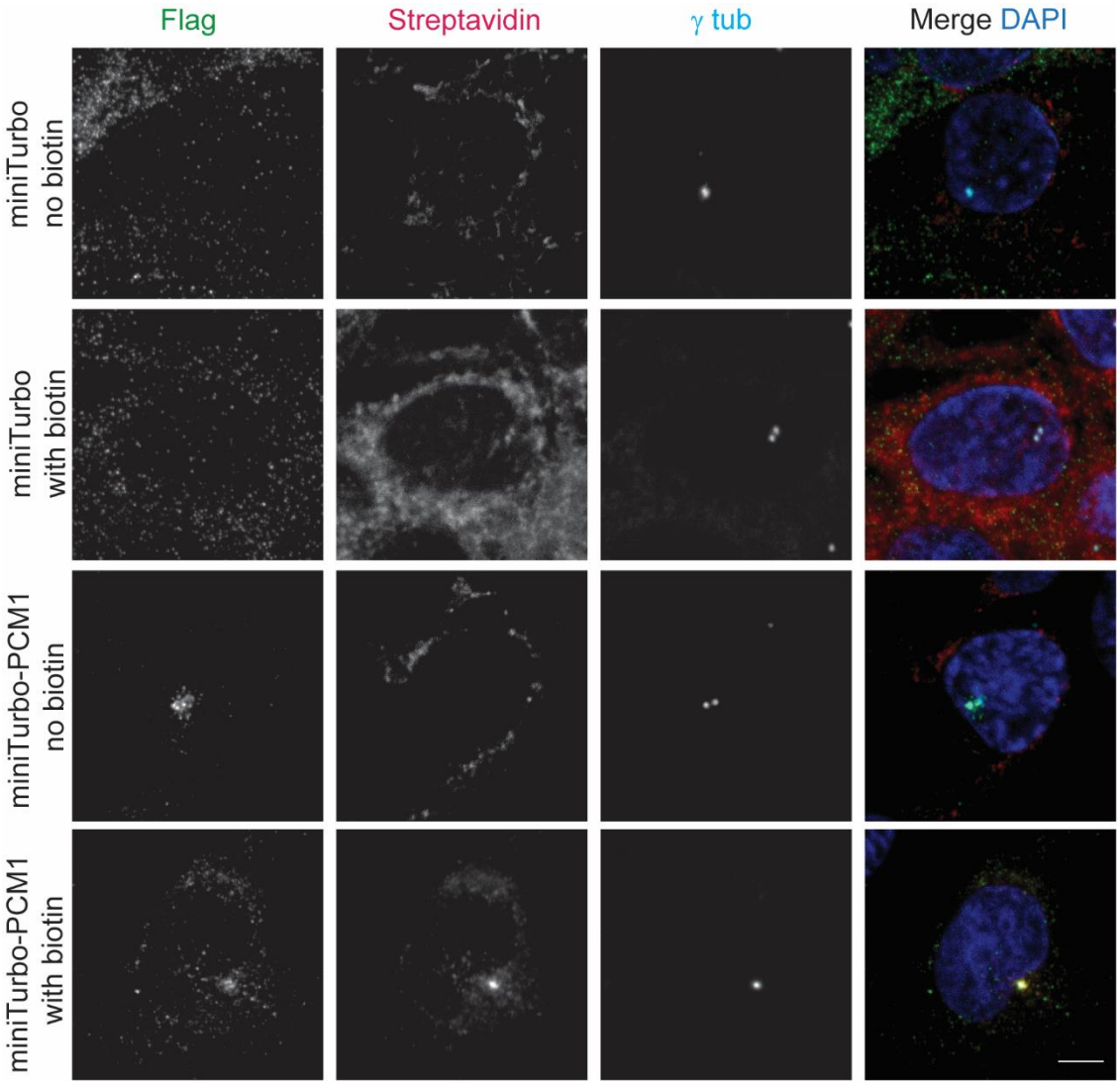

Figure 3.1 Localization of miniTurbo and miniTurbo-PCM1 in presence and absence of biotin. Flag antibody labels miniTurbo and miniTurbo PCM1 fusion proteins. Streptavidin labels biotinylated proteins. Scale bar is 5 μm.

PCM1 staining shows that Flag-miniTurbo-PCM1 forms the satellites in IMCD3 PCM1 KO cells. On the other hand, cells expressing Flag-miniTurbo do not have the satellite structure (Figure 3.2).

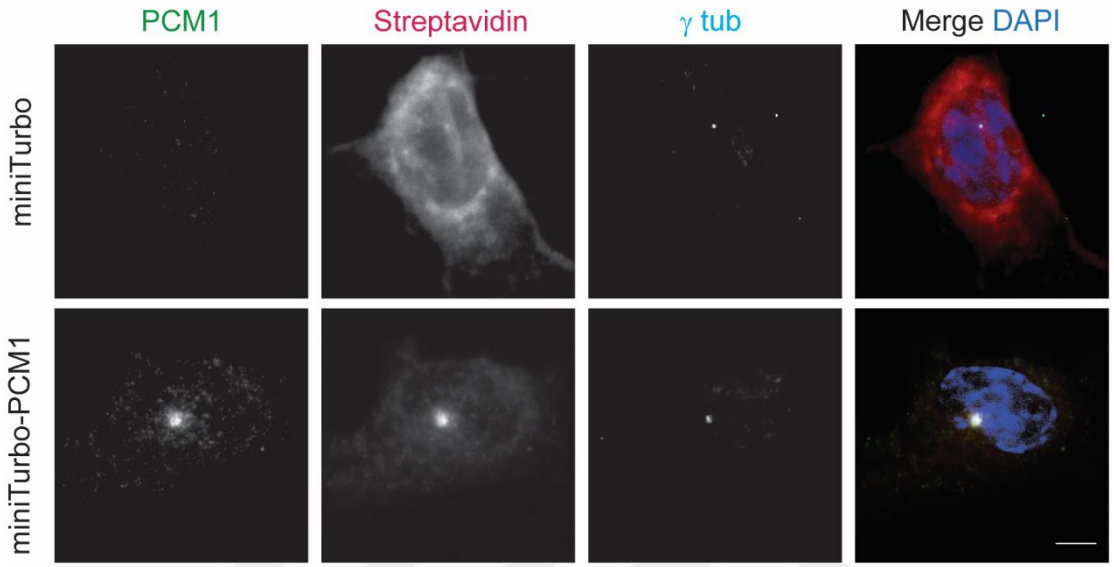

Figure 3.2 Localization of miniTurbo and miniTurbo-PCM1 in IMCD3 PCM1 KO cells. Scale bar is 5 μm.

Immunoblotting of lysates from cells stably expressing Flag-miniTurbo and Flag-miniTurbo-PCM1 confirmed their expression with Flag antibody. Streptavidin signal shows that the levels of biotinylated proteins in lysates from Flag-miniTurbo and and Flag-miniTurbo-PCM1 cells treated with biotin was substantially higher relative to no biotin control (Figure 3.3).

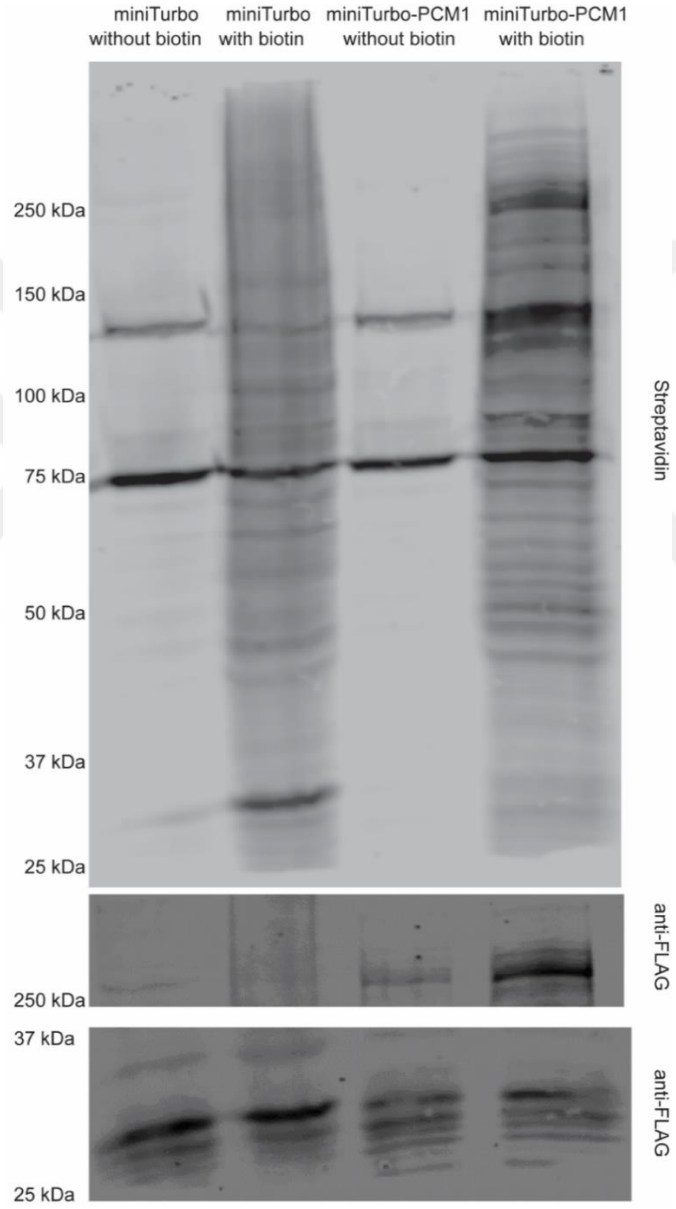

Figure 3.3 Expression and biotinylation of Flag-miniTurbo and Flag-miniTurbo-PCM1 in stable cells lines in IMCD3 PCM1 KO cells. Control and biotin-treated IMCD3 PCM1 KO cells stably expressing Flag-miniTurbo and Flag-miniTurbo-PCM1 were lysed. biotinylated proteins were detected with Streptavidin.

3.3.2 Identification and validation of the PCM1 proximity interactome in asynchronous and ciliated cells.

We performed label-free quantitative proteomics to generate the PCM1 proximity interactome in asynchronous and ciliated. For large-scale pulldowns, asynchronous cells stably expressing Flag-miniTurbo-PCM1 were grown in 10x15 cm plates. Five of the 15cm plates are serum starved for 24h to generate interactome in ciliated cells. All cells were incubated with 500 μM biotin for 10 min. Following denaturing lysis of cells, biotinylated proteins were captured by streptavidin beads and analyzed by mass spectrometry. Cells expressing Flag-miniTurbo were processed as controls. Pulldowns are confirmed with streptavidin and Flag blots (Figure 3.4). Two biological replicates for Flag-miniTurbo and Flag-miniTurbo-PCM1 were processed for mass spectrometry analysis.

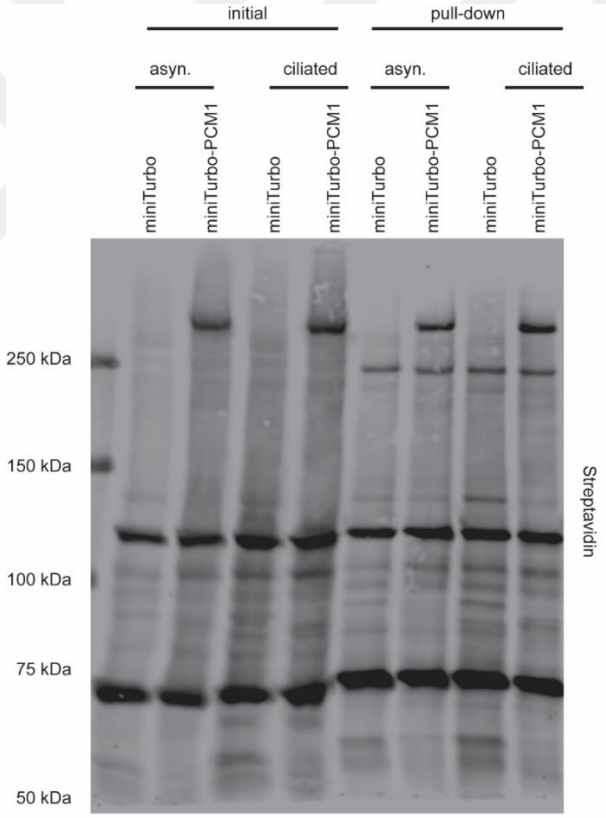

Figure 3.4 Pulldown of biotiylated proteins in IMCD3 PCM1 KO cells stably expressing Flag-miniTurbo and Flag-miniTurbo PCM1. Asynchronous (asyn.) and ciliated biotin-treated IMCD3 PCM1 KO cells stably expressing Flag-miniTurbo and Flag-miniTurbo-PCM1 were lysed and biotinylated proteins were precipitated by streptavidin beads. The initial sample (initial) and captured biotinylated proteins (pulldown) were run on a SDS gel and immunoblotted with the fluorescent streptavidin.

In order to define the high-confidence proximity interactome of PCM1 in asynchronous and ciliated IMCD3 cells, we performed significance analysis of interactome (SAINT) analysis. We used CRAPome and REPRINT online resources for SAINTexpress analysis. We determined the BDFR cutoff of <0.2 to determine high confidence PCM1 proximity interactors. We identified centrosome and centriolar satellites proteins in list of asynchronous and ciliated IMCD3 cells (Figure 3.5 and 3.6). This shows the success of the miniTurbo experiments.

Proximity partners of PCM1 in asynchronous cells identified centrosome, centriolar satellite proteins and kinetochore proteins. Gene Ontology (GO) analysis for cellular localization identifies centrosome, centriolar satellite, ciliary basal body, spindle and chromosome kinetochore categories (Figure 3.5-B). GO analysis for biological process identifies the protein at the following categories: protein localization to centrosome, cilium morphogenesis, metaphase plate congression and cell cycle (Figure 3.5-C).

Proximity partners of PCM1 in ciliated cells identified centrosome, centriolar satellite proteins with kinetochore proteins. GO analysis for cellular localization identifies centrosome, centriolar satellite, microtubule, ciliary basal body and kinetochore categories (Figure 3.6-B). GO analysis for biological process reveals protein localization to centrosome, cilium morphogenesis, cell cycle and attachment of spindle microtubules to kinetochore categories (Figure 3.6-C).

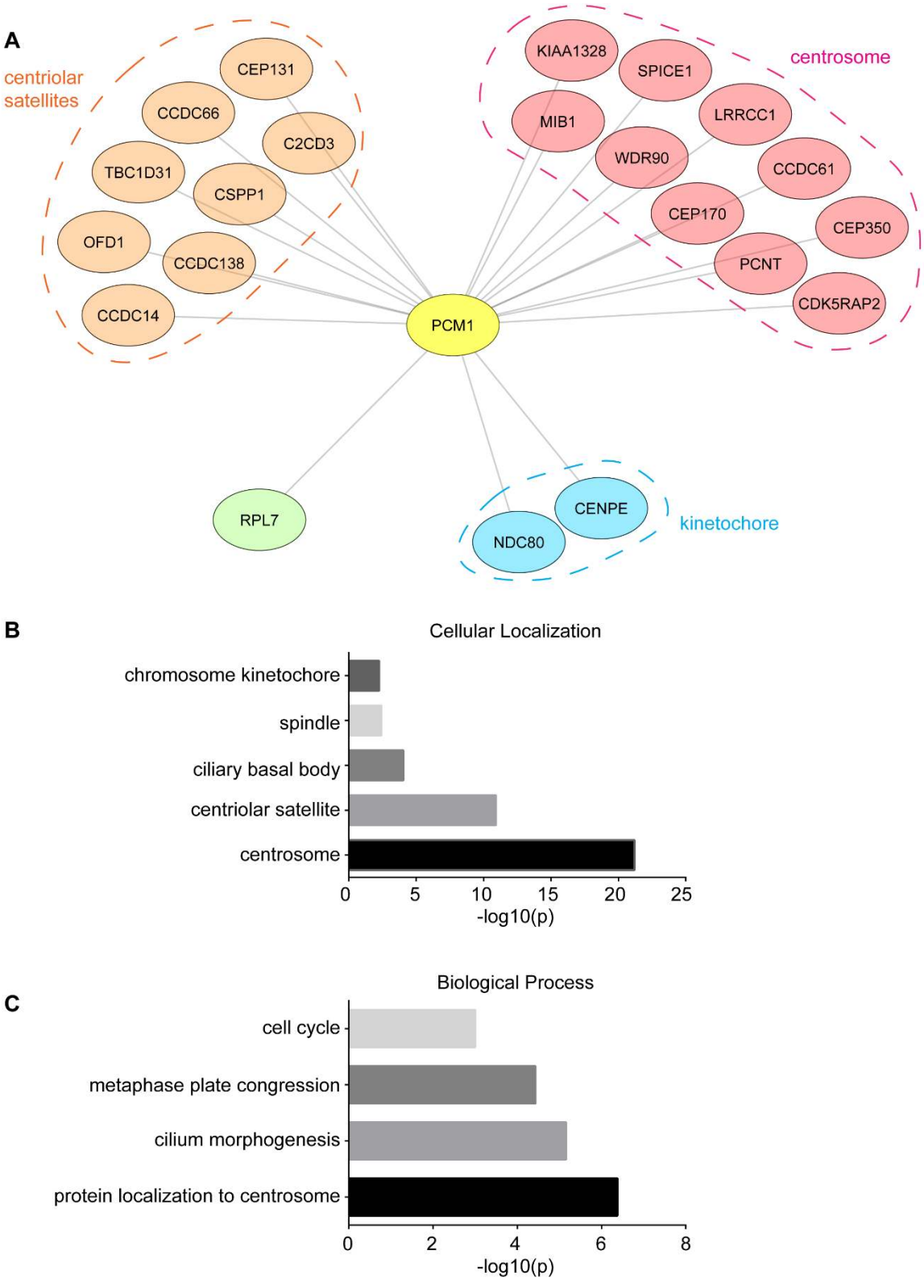

Figure 3.5 Interactome of PCM1 in asynchronous IMCD3 cells (A) Proximity map of PCM1 cells in asynchronous cells. (B) GO analysis for cellular localization (C) GO analysis for biological process.

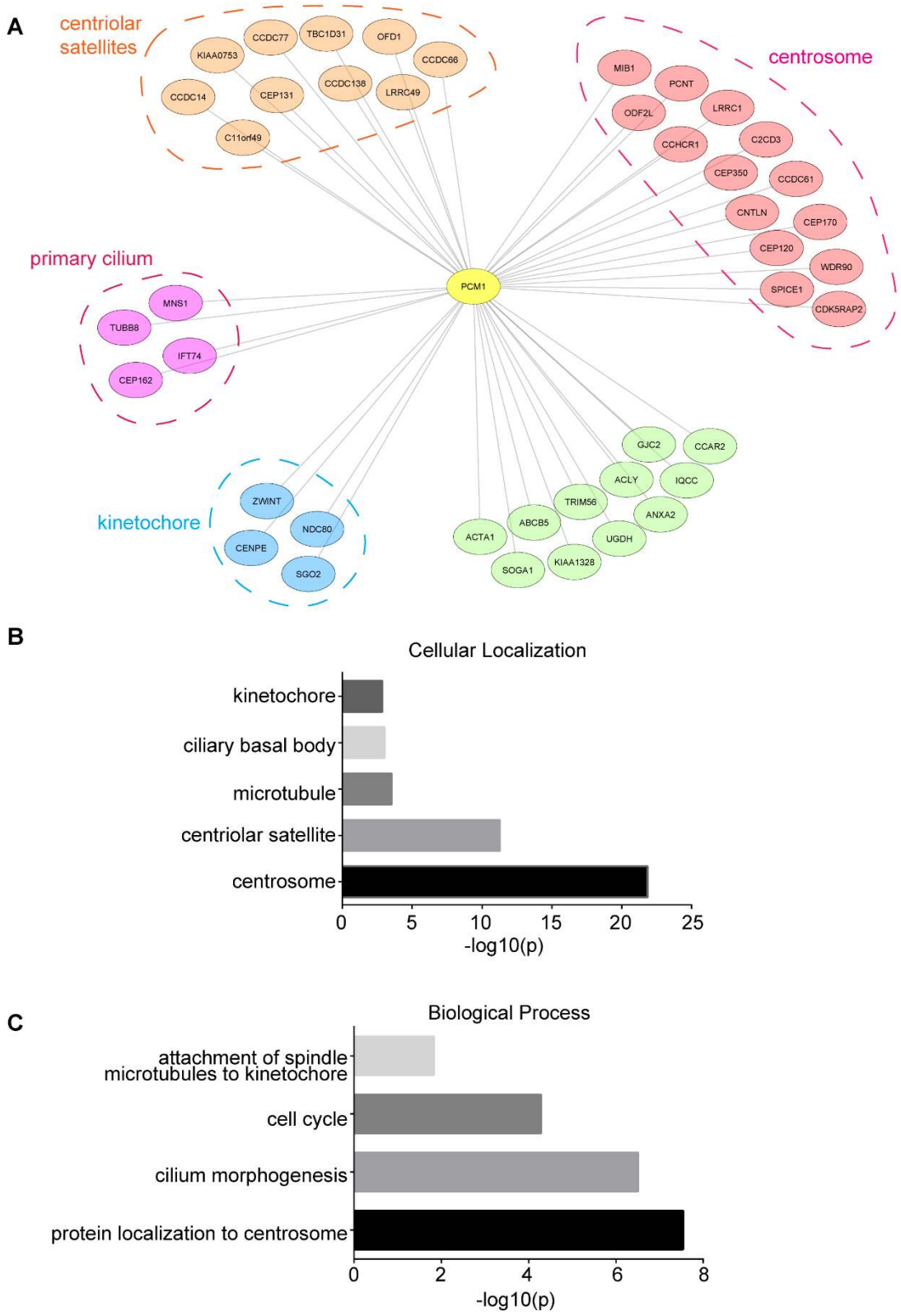

Figure 3.6 Interactome of PCM1 in ciliated IMCD3 cells (A) Proximity map of PCM1 cells in ciliated cells. (B) GO analysis for cellular localization (C) GO analysis for biological process.

3.3.3 Comparison of PCM1 interactome in asynronous and ciliated cells.

In order to identify specific interaction partners of PCM1 in ciliated cells, we compared the interaction partners in asynronous and ciliated cells (Figure 3.7). Protein list specific to ciliated cells includes proteins involved in different stages of primary cilium formation, such as CEP162, CEP120, and IFT74. In addition, novel centriolar satellite proteins such as LRRC49 and CCDC77 are present in this list. Although these proteins were identified as centriolar satellite protein in recent centriolar satellite proteome lists, their roles in primary cilium formation are unknown (Gupta, Coyaud et al. 2015, Gheiratmand, Coyaud et al. 2019). To better understand the role of centriolar satellites in primary cilium formation, the roles of these proteins need be studied.

In the common proteins between asynronous and ciliated cells, there are proteins that their roles are known in ciliogenesis such as CCDC66, OFD1 and MIB1 (Tang, Lin et al. 2013, Wang, Lee et al. 2016, Conkar, Culfa et al. 2017). More peptides of these proteins were identified in ciliated cells than asynronous cells with miniTurbo experiments so interaction between of these proteins and PCM1 enrich in ciliated cells. These interactions might contribute the roles of these proteins in ciliogenesis.

TBC1D31 is also present in both asynronous and ciliated cells proximity lists of PCM1. This protein was identified as centriolar satellite protein by BioID experiments (Gheiratmand, Coyaud et al. 2019). However, it's role is not clear for ciliogenesis. There are more TBC1D31 peptides identified in proximity list in ciliated cells. This might show that TBC1D31 protein has role in ciliogenesis with centriolar satellites. To investigate the function of TBC1D31 protein, we performed localization and the loss of function experiments.

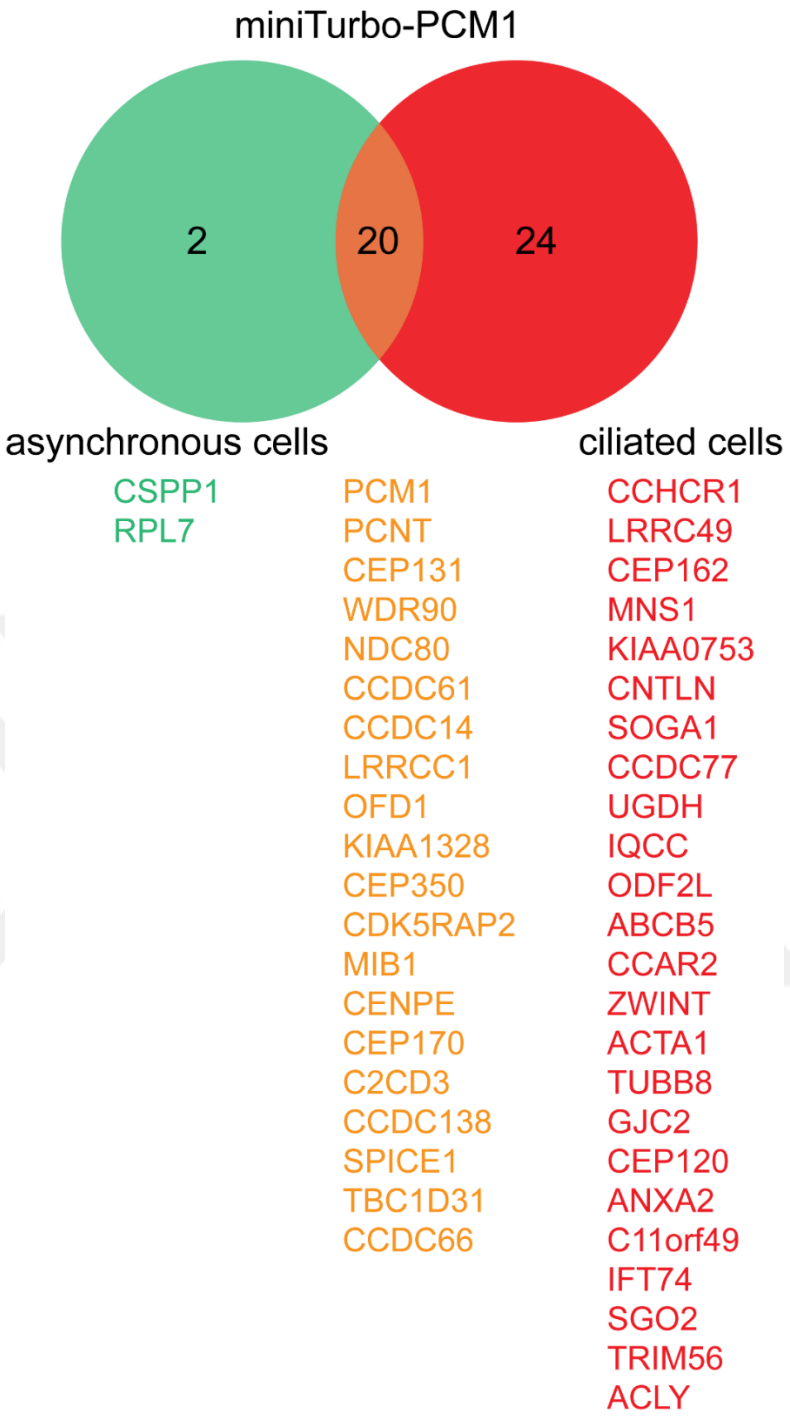

Figure 3.7 Comparison of PCM1 interactome in asynronous and ciliated cells

3.3.4 TBC1D31 is a novel TBC1D31 centriolar satellite protein

TBC1D31 is previously reported as centrosome and centriolar satellite protein by proximity-dependent biotin identification (Gheiratmand, Coyaud et al. 2019). To define the localization of the endogenous protein, we used polyclonal TBC1D31 antibody along with different centrosome markers. Immunofluorescence analysis confirmed that TBC1D31 localized to centrosome. We used markers for distal and proximal parts of the centrosome. TBC1D31 is proximal to CEP164 which localizes to distal appendages of the mother centriole (Figure 3.8-A). Moreover, TBC1D31 is distal C-NAP1 which localizes to proximal part of the centrosome (Figure 3.8-B).

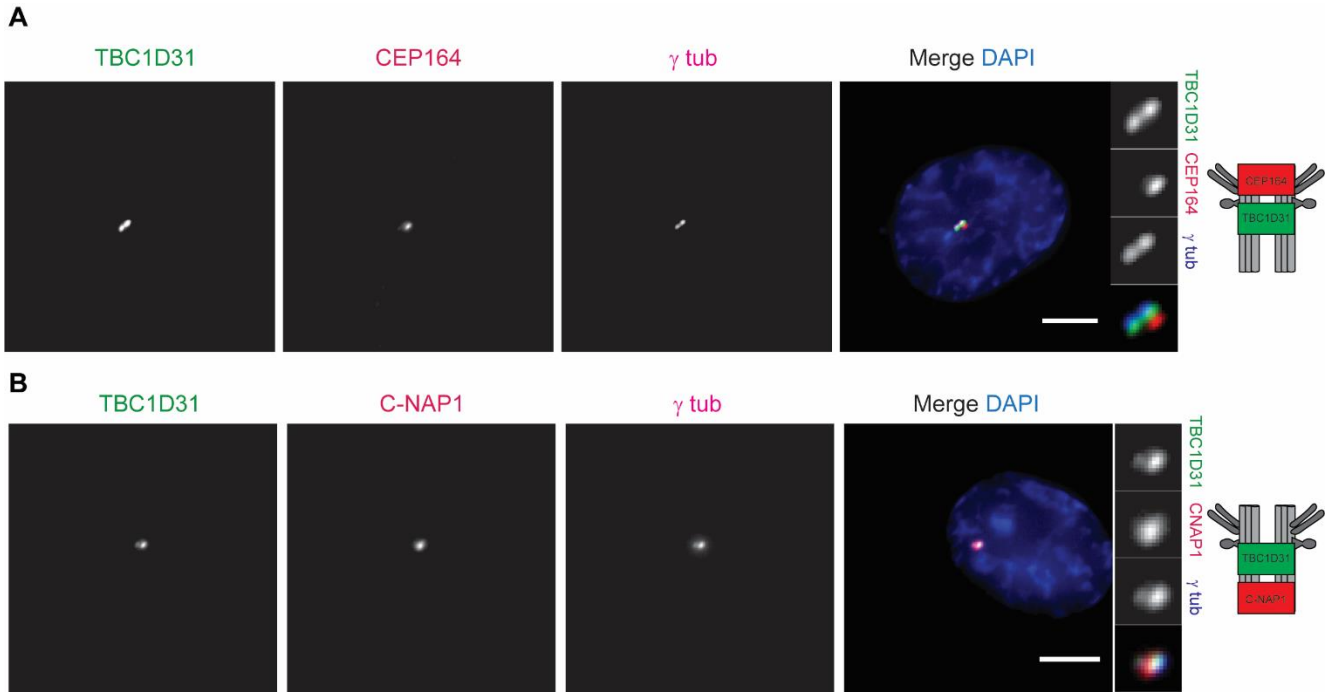

Figure 3.8 Localization of TBC1D31. (A) Cells were fixed and stained for TBC1D31 antibody along with distal marker of centrosome, CEP164, and centrosome marker gamma tubulin. (B) Cells were fixed and stained for TBC1D31 antibody along with proximal marker of centrosome, C-NAP1, and centrosome marker gamma tubulin.

3.3.5 TBC1D31 has role in ciliogenesis

In order to understand role of TBC1D31 in primary cilium formation, TBC1D31 gene is depleted using siRNA. Depletion of TBC1D31 is confirmed by qPCR (Figure 3.9-A). Expression of TBC1D31 was decreased to 12% ± 3.8 with siTBC1D31-1. Expression of TBC1D31 was decreased to 22.5% ± 3.5 with siTBC1D31-2 (Figure 3.9-A). Depletion of TBC1D31 with both siRNAs results in defect in ciliogenesis (siControl: 71.42% ± 1.24; siTBC1D31-1: 51.16% ± 7.8; siTBC1D31-2: 56.01 ± 5.29) (Figure 3.9-B). Moreover, depletion of TBC1D31 with siRNA1 leads to significantly shorter cilia. On the other hand, depletion of TBC1D31 with siRNA2 does not affect cilia length (siControl: 2.83 ± 0,93µm; siTBC1D31-1: 51.16% ± 7.8µm; siTBC1D31-2: 2.72 ± 0.95µm) (Figure 3.8-C). The reason could be that depletion with siRNA2 is less efficient than depletion with siRNA1.

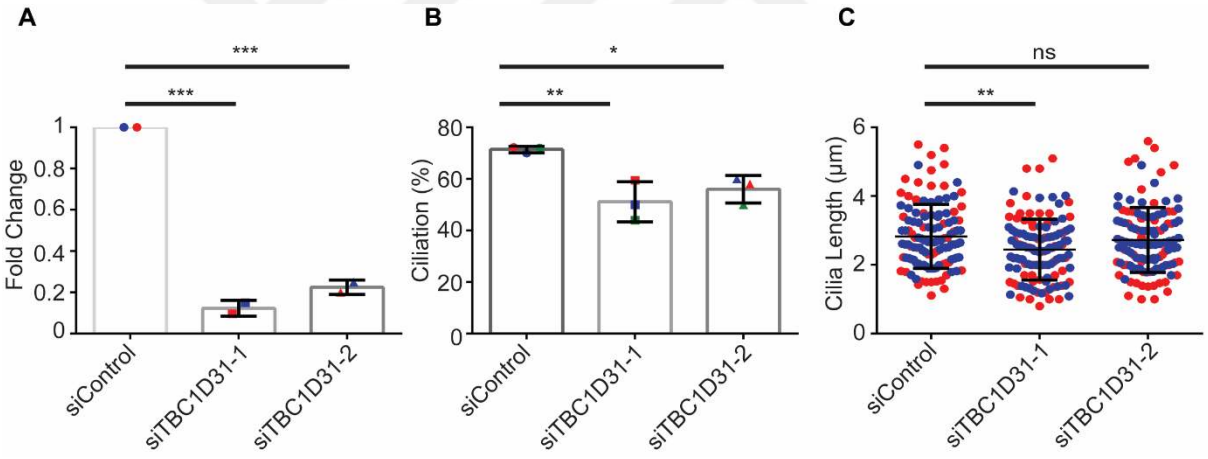

Figure 3.9 Depletion of TBC1D31 results in ciliogenesis defect. (A) TBC1D31 mRNA was quantified by qPCR in control and depleted cells. Fold change is normalized to control cells (=1). Results shown are the mean of two independent experiments ± SD (***P < 0.001, t-test). (B) Quantification of ciliogenesis experiments. Results shown are the mean of three independent experiments ± SD (100 cells/experiment, *P < 0.05 **P < 0.01, t-test). (C) Effect of TBC1D31 depletion on cilium length. Quantification of cilium length was done from three independent experiments with an average of 100 cilia measured per experiment (ns P >0.05, *P < 0.05, t-test). Error bars represent SD. Horizontal line represents the mean value of each group.

3.4 Discussion and Future Directions

Proximity dependent labeling methods is used to identify interaction and proximity partners of the protein of interest. One of these methods, BioID is utilized in the fields of centrosome/cilia and centriolar satellites to identify protein composition of these compartments. (Arslanhan, Gulensoy et al. 2020). Researchers continue to enhance and develop new biotin dependent proximity labeling methods which one of them is miniTurbo. miniTurbo is E. coli biotin ligase which is shorter than BirA* of BioID (Branon, Bosch et al. 2018). The major advantage of this method over to BioID is the biotinylation time. Biotinlation takes 18-24 hours in BioID. This long biotinylation time accumulates unspecific proteins starting from translation of the protein to degradation of the protein. Biotinlation time can be minimized to 10 minutes with miniTurbo. Short biotinlation time eliminates the background and gives the more specific interactions. This gives an opportunity to tackle specific interaction during specific biological process such as cilium formation.

We identified centrosome and centriolar satellite proteins with miniTurbo in the proximity of PCM1 and most of them were already identified in the interactome of PCM1 with BioID (Gupta, Coyaud et al. 2015, Gheiratmand, Coyaud et al. 2019). However, we identified less protein than BioID list because biotinylation time is much shorter than BioID. In order to improve peptide list and peptide number biotinylation time and biotin amount can be optimized.

In our previous study, we reported that PCM1 has a role in regulation of Hedgehog signaling pathway activation (Odabasi, Gul et al. 2019). In order to understand how PCM1 regulates Hedgehog signaling pathway, similar strategy of miniTurbo for PCM1 can be applied in the future. With this way, we can determine the interaction partners of PCM1 during activation of Hedgehog signaling pathway.

TBC1D31 is recently identified as centriolar satellite protein with BioID studies (Gheiratmand, Coyaud et al. 2019). Before it is identified as centriolar satellite protein, evolutionary study from Azimzadeh et. al. reported that loss of TBC1D31 causes decrease in ciliogenesis in RPE1 cells (Azimzadeh, Wong et al. 2012). We also confirmed decrease in ciliogenesis in the TBC1D31 depleted RPE1 cells by siRNA. We also observed decrease in cilium length in the depletion of TBC1D31 with one of the siRNAs. These observations indicate that TBC1D31 has a role not just in ciliogenesis

but also in cilium length control. Since TBC1D31 is a centriolar satellite protein and interaction between PCM1 and TBC1D31 increases in ciliated cells, centriolar satellites might control ciliogenesis in a pathway which includes TBC1D31. This relationship needs to be investigated with more details in future studies.

BIBLIOGRAPHY

Akimov, V., K. T. Rigbolt, M. M. Nielsen and B. Blagoev (2011). "Characterization of ubiquitination dependent dynamics in growth factor receptor signaling by quantitative proteomics." Mol Biosyst **7**(12): 3223-3233.

Arslanhan, M. D., D. Gulensoy and E. N. Firat-Karalar (2020). "A Proximity Mapping Journey into the Biology of the Mammalian Centrosome/Cilium Complex." Cells **9**(6).

Aydin, O. Z., S. O. Taflan, C. Gurkaslar and E. N. Firat-Karalar (2020). "Acute inhibition of centriolar satellite function and positioning reveals their functions at the primary cilium." PLoS Biol **18**(6): e3000679.

Azimzadeh, J. and W. F. Marshall (2010). "Building the centriole." Curr Biol **20**(18): R816-825.

Azimzadeh, J., M. L. Wong, D. M. Downhour, A. Sanchez Alvarado and W. F. Marshall (2012). "Centrosome loss in the evolution of planarians." Science **335**(6067): 461-463.

Banani, S. F., H. O. Lee, A. A. Hyman and M. K. Rosen (2017). "Biomolecular condensates: organizers of cellular biochemistry." Nat Rev Mol Cell Biol **18**(5): 285-298.

Barenz, F., D. Mayilo and O. J. Gruss (2011). "Centriolar satellites: busy orbits around the centrosome." Eur J Cell Biol **90**(12): 983-989.

Bauer, M., F. Cubizolles, A. Schmidt and E. A. Nigg (2016). "Quantitative analysis of human centrosome architecture by targeted proteomics and fluorescence imaging." EMBO J **35**(19): 2152-2166.

Bernhard W, d. H. E. (1960). L'ultrastructure du centriole et d'autres éléments de l'appareril achromatique. 4th International Conference on Electron Microscopy. Berlin, Springer-Verlag**:** 218–227.

Bettencourt-Dias, M., F. Hildebrandt, D. Pellman, G. Woods and S. A. Godinho (2011). "Centrosomes and cilia in human disease." Trends Genet **27**(8): 307-315.

Bhogaraju, S., L. Cajanek, C. Fort, T. Blisnick, K. Weber, M. Taschner, N. Mizuno, S. Lamla, P. Bastin, E. A. Nigg and E. Lorentzen (2013). "Molecular basis of tubulin transport within the cilium by IFT74 and IFT81." Science **341**(6149): 1009-1012.

Bradshaw, N. J. and D. J. Porteous (2012). "DISC1-binding proteins in neural development, signalling and schizophrenia." Neuropharmacology **62**(3): 1230-1241.

Branon, T. C., J. A. Bosch, A. D. Sanchez, N. D. Udeshi, T. Svinkina, S. A. Carr, J. L. Feldman, N. Perrimon and A. Y. Ting (2018). "Efficient proximity labeling in living cells and organisms with TurboID." Nat Biotechnol **36**(9): 880-887.

Braun, D. A. and F. Hildebrandt (2017). "Ciliopathies." Cold Spring Harb Perspect Biol **9**(3).

Carvalho-Santos, Z., J. Azimzadeh, J. B. Pereira-Leal and M. Bettencourt-Dias (2011). "Evolution: Tracing the origins of centrioles, cilia, and flagella." J Cell Biol **194**(2): 165-175.

Cevik, S., Y. Hori, O. I. Kaplan, K. Kida, T. Toivenon, C. Foley-Fisher, D. Cottell, T. Katada, K. Kontani and O. E. Blacque (2010). "Joubert syndrome Arl13b functions at ciliary membranes and stabilizes protein transport in Caenorhabditis elegans." J Cell Biol **188**(6): 953-969.

Chavali, P. L., M. Putz and F. Gergely (2014). "Small organelle, big responsibility: the role of centrosomes in development and disease." Philos Trans R Soc Lond B Biol Sci **369**(1650).

Conkar, D., H. Bayraktar and E. N. Firat-Karalar (2019). "Centrosomal and ciliary targeting of CCDC66 requires cooperative action of centriolar satellites, microtubules and molecular motors." Sci Rep **9**(1): 14250.

Conkar, D., E. Culfa, E. Odabasi, N. Rauniyar, J. R. Yates, 3rd and E. N. Firat-Karalar (2017). "The centriolar satellite protein CCDC66 interacts with CEP290 and functions in cilium formation and trafficking." J Cell Sci **130**(8): 1450-1462.

Corbit, K. C., P. Aanstad, V. Singla, A. R. Norman, D. Y. Stainier and J. F. Reiter (2005). "Vertebrate Smoothened functions at the primary cilium." Nature **437**(7061): 1018-1021.

Dammermann, A. and A. Merdes (2002). "Assembly of centrosomal proteins and microtubule organization depends on PCM-1." J Cell Biol **159**(2): 255-266.

Datta, S. R., A. McQuillin, M. Rizig, E. Blaveri, S. Thirumalai, G. Kalsi, J. Lawrence, N. J. Bass, V. Puri, K. Choudhury, J. Pimm, C. Crombie, G. Fraser, N. Walker, D. Curtis, M. Zvelebil, A. Pereira, R. Kandaswamy, D. St Clair and H. M. Gurling (2010). "A threonine to isoleucine missense mutation in the pericentriolar material 1 gene is strongly associated with schizophrenia." Mol Psychiatry **15**(6): 615-628.

De Munter, S., J. Gornemann, R. Derua, B. Lesage, J. Qian, E. Heroes, E. Waelkens, A. Van Eynde, M. Beullens and M. Bollen (2017). "Split-BioID: a proximity biotinylation assay for dimerization-dependent protein interactions." FEBS Lett **591**(2): 415-424.

Delous, M., N. E. Hellman, H. M. Gaude, F. Silbermann, A. Le Bivic, R. Salomon, C. Antignac and S. Saunier (2009). "Nephrocystin-1 and nephrocystin-4 are required for epithelial morphogenesis and associate with PALS1/PATJ and Par6." Hum Mol Genet **18**(24): 4711-4723.

deThé (1964). "Cytoplasmic microtubules in different animals." J Cell Biol: 265–275.
El-Brolosy, M. A. and D. Y. R. Stainier (2017). "Genetic compensation: A phenomenon in search of mechanisms." PLoS Genet **13**(7): e1006780.

Espigat-Georger, A., V. Dyachuk, C. Chemin, L. Emorine and A. Merdes (2016). "Nuclear alignment in myotubes requires centrosome proteins recruited by nesprin-1." J Cell Sci **129**(22): 4227-4237.

Farina, F., J. Gaillard, C. Guerin, Y. Coute, J. Sillibourne, L. Blanchoin and M. Thery (2016). "The centrosome is an actin-organizing centre." Nat Cell Biol **18**(1): 65-75.

Firat-Karalar, E. N., N. Rauniyar, J. R. Yates, 3rd and T. Stearns (2014). "Proximity interactions among centrosome components identify regulators of centriole duplication." Curr Biol **24**(6): 664-670.

Franken, H., T. Mathieson, D. Childs, G. M. Sweetman, T. Werner, I. Togel, C. Doce, S. Gade, M. Bantscheff, G. Drewes, F. B. Reinhard, W. Huber and M. M. Savitski (2015). "Thermal proteome profiling for unbiased identification of direct and indirect drug targets using multiplexed quantitative mass spectrometry." Nat Protoc **10**(10): 1567-1593.

Ge, X., C. L. Frank, F. Calderon de Anda and L. H. Tsai (2010). "Hook3 interacts with PCM1 to regulate pericentriolar material assembly and the timing of neurogenesis." Neuron **65**(2): 191-203.

Gheiratmand, L., E. Coyaud, G. D. Gupta, E. M. Laurent, M. Hasegan, S. L. Prosser, J. Goncalves, B. Raught and L. Pelletier (2019). "Spatial and proteomic profiling reveals centrosome-independent features of centriolar satellites." EMBO J **38**(14): e101109.

Giles, R. H., H. Ajzenberg and P. K. Jackson (2014). "3D spheroid model of mIMCD3 cells for studying ciliopathies and renal epithelial disorders." Nat Protoc **9**(12): 2725-2731.

Gimpel P, L. Y., Sobota RM, Calvi A, Koullourou V, Patel R, Mamchaoui K, Nedelec F, Shackleton S, Schmoranzer J (2017). "Nesprin-1α-dependent microtubule nucleation from the nuclear envelope via Akap450 is necessary for nuclear positioning in muscle cells." Curr Biol: 2999–3009.

Gupta, G. D., E. Coyaud, J. Goncalves, B. A. Mojarad, Y. Liu, Q. Wu, L. Gheiratmand, D. Comartin, J. M. Tkach, S. W. Cheung, M. Bashkurov, M. Hasegan, J. D. Knight, Z. Y. Lin, M. Schueler, F. Hildebrandt, J. Moffat, A. C. Gingras, B. Raught and L. Pelletier (2015). "A Dynamic Protein Interaction Landscape of the Human Centrosome-Cilium Interface." Cell **163**(6): 1484-1499.

Gurling, H. M., H. Critchley, S. R. Datta, A. McQuillin, E. Blaveri, S. Thirumalai, J. Pimm, R. Krasucki, G. Kalsi, D. Quested, J. Lawrence, N. Bass, K. Choudhury, V. Puri, O. O'Daly, D. Curtis, D. Blackwood, W. Muir, A. K. Malhotra, R. W. Buchanan, C. D. Good, R. S. Frackowiak and R. J. Dolan (2006). "Genetic association and brain morphology studies and the chromosome 8p22 pericentriolar material 1 (PCM1) gene in susceptibility to schizophrenia." Arch Gen Psychiatry **63**(8): 844-854.

Hall, E. A., M. Keighren, M. J. Ford, T. Davey, A. P. Jarman, L. B. Smith, I. J. Jackson and P. Mill (2013). "Acute versus chronic loss of mammalian Azi1/Cep131 results in distinct ciliary phenotypes." PLoS Genet **9**(12): e1003928.

Haycraft, C. J., Q. Zhang, B. Song, W. S. Jackson, P. J. Detloff, R. Serra and B. K. Yoder (2007). "Intraflagellar transport is essential for endochondral bone formation." Development **134**(2): 307-316.

Hoang-Minh, L. B., L. P. Deleyrolle, N. S. Nakamura, A. K. Parker, R. T. Martuscello, B. A. Reynolds and M. R. Sarkisian (2016). "PCM1 Depletion Inhibits Glioblastoma Cell Ciliogenesis and Increases Cell Death and Sensitivity to Temozolomide." Transl Oncol **9**(5): 392-402.

Hodges, M. E., N. Scheumann, B. Wickstead, J. A. Langdale and K. Gull (2010). "Reconstructing the evolutionary history of the centriole from protein components." J Cell Sci **123**(Pt 9): 1407-1413.

Holdgaard, S. G., V. Cianfanelli, E. Pupo, M. Lambrughi, M. Lubas, J. C. Nielsen, S. Eibes, E. Maiani, L. M. Harder, N. Wesch, M. M. Foged, K. Maeda, F. Nazio, L. R. de la Ballina, V. Dotsch, A. Brech, L. B. Frankel, M. Jaattela, F. Locatelli, M. Barisic, J. S. Andersen, S. Bekker-Jensen, A. H. Lund, V. V. Rogov, E. Papaleo, L. Lanzetti, D. De Zio and F. Cecconi (2019). "Selective autophagy maintains centrosome integrity and accurate mitosis by turnover of centriolar satellites." Nat Commun **10**(1): 4176.

Hori, A. and T. Toda (2017). "Regulation of centriolar satellite integrity and its physiology." Cell Mol Life Sci **74**(2): 213-229.

Hoyer-Fender, S. (2010). "Centriole maturation and transformation to basal body." Semin Cell Dev Biol **21**(2): 142-147.

Hu, Q., L. Milenkovic, H. Jin, M. P. Scott, M. V. Nachury, E. T. Spiliotis and W. J. Nelson (2010). "A septin diffusion barrier at the base of the primary cilium maintains ciliary membrane protein distribution." Science **329**(5990): 436-439.

Huang da, W., B. T. Sherman and R. A. Lempicki (2009). "Bioinformatics enrichment tools: paths toward the comprehensive functional analysis of large gene lists." Nucleic Acids Res **37**(1): 1-13.

Hughes, C. S., S. Foehr, D. A. Garfield, E. E. Furlong, L. M. Steinmetz and J. Krijgsveld (2014). "Ultrasensitive proteome analysis using paramagnetic bead technology." Mol Syst Biol **10**: 757.

Huttlin, E. L., R. J. Bruckner, J. A. Paulo, J. R. Cannon, L. Ting, K. Baltier, G. Colby, F. Gebreab, M. P. Gygi, H. Parzen, J. Szpyt, S. Tam, G. Zarraga, L. Pontano-Vaites, S. Swarup, A. E. White, D. K. Schweppe, R. Rad, B. K. Erickson, R. A. Obar, K. G. Guruharsha, K. Li, S. Artavanis-Tsakonas, S. P. Gygi and J. W. Harper (2017). "Architecture of the human interactome defines protein communities and disease networks." Nature **545**(7655): 505-509.

Huttlin, E. L., L. Ting, R. J. Bruckner, F. Gebreab, M. P. Gygi, J. Szpyt, S. Tam, G. Zarraga, G. Colby, K. Baltier, R. Dong, V. Guarani, L. P. Vaites, A. Ordureau, R. Rad, B. K. Erickson, M. Wuhr, J. Chick, B. Zhai, D. Kolippakkam, J. Mintseris, R. A. Obar, T. Harris, S. Artavanis-Tsakonas, M. E. Sowa, P. De Camilli, J. A. Paulo, J. W. Harper

and S. P. Gygi (2015). "The BioPlex Network: A Systematic Exploration of the Human Interactome." Cell **162**(2): 425-440.

Insolera, R., W. Shao, R. Airik, F. Hildebrandt and S. H. Shi (2014). "SDCCAG8 regulates pericentriolar material recruitment and neuronal migration in the developing cortex." Neuron **83**(4): 805-822.

Jain, S., J. R. Wheeler, R. W. Walters, A. Agrawal, A. Barsic and R. Parker (2016). "ATPase-Modulated Stress Granules Contain a Diverse Proteome and Substructure." Cell **164**(3): 487-498.

Jakobsen, L., K. Vanselow, M. Skogs, Y. Toyoda, E. Lundberg, I. Poser, L. G. Falkenby, M. Bennetzen, J. Westendorf, E. A. Nigg, M. Uhlen, A. A. Hyman and J. S. Andersen (2011). "Novel asymmetrically localizing components of human centrosomes identified by complementary proteomics methods." EMBO J **30**(8): 1520-1535.
Joachim, J., M. Razi, D. Judith, M. Wirth, E. Calamita, V. Encheva, B. D. Dynlacht, A. P. Snijders, N. O'Reilly, H. B. J. Jefferies and S. A. Tooze (2017). "Centriolar Satellites Control GABARAP Ubiquitination and GABARAP-Mediated Autophagy." Curr Biol **27**(14): 2123-2136 e2127.

Joachim, J. and S. A. Tooze (2018). "Control of GABARAP-mediated autophagy by the Golgi complex, centrosome and centriolar satellites." Biol Cell **110**(1): 1-5.
K, K., L. K and R. K (2012). "CEP90 is required for the assembly and centrosomal accumulation of centriolar satellites, which is essential for primary cilia formation." PLoS One **7**.

Kamiya, A., P. L. Tan, K. Kubo, C. Engelhard, K. Ishizuka, A. Kubo, S. Tsukita, A. E. Pulver, K. Nakajima, N. G. Cascella, N. Katsanis and A. Sawa (2008). "Recruitment of PCM1 to the centrosome by the cooperative action of DISC1 and BBS4: a candidate for psychiatric illnesses." Arch Gen Psychiatry **65**(9): 996-1006.

Kim, D. I., S. C. Jensen, K. A. Noble, B. Kc, K. H. Roux, K. Motamedchaboki and K. J. Roux (2016). "An improved smaller biotin ligase for BioID proximity labeling." Mol Biol Cell **27**(8): 1188-1196.

Kim, J., H. Jo, H. Hong, M. H. Kim, J. M. Kim, J. K. Lee, W. D. Heo and J. Kim (2015). "Actin remodelling factors control ciliogenesis by regulating YAP/TAZ activity and vesicle trafficking." Nat Commun **6**: 6781.

Kim, J., S. R. Krishnaswami and J. G. Gleeson (2008). "CEP290 interacts with the centriolar satellite component PCM-1 and is required for Rab8 localization to the primary cilium." Hum Mol Genet **17**(23): 3796-3805.

Kim, J., J. E. Lee, S. Heynen-Genel, E. Suyama, K. Ono, K. Lee, T. Ideker, P. Aza-Blanc and J. G. Gleeson (2010). "Functional genomic screen for modulators of ciliogenesis and cilium length." Nature **464**(7291): 1048-1051.

Kodani, A., T. W. Yu, J. R. Johnson, D. Jayaraman, T. L. Johnson, L. Al-Gazali, L. Sztriha, J. N. Partlow, H. Kim, A. L. Krup, A. Dammermann, N. J. Krogan, C. A.

Walsh and J. F. Reiter (2015). "Centriolar satellites assemble centrosomal microcephaly proteins to recruit CDK2 and promote centriole duplication." Elife **4**.

Kohli P, H. M., Jungst C, Bertsch S, Ebert LK, Schauss AC, Benzing T, Rinschen MM, Schermer B. (2017). "The ciliary membrane-associated proteome reveals actin-binding proteins as key components of cilia." EMBO Rep: 1521–1535.

Kohli, P., M. Hohne, C. Jungst, S. Bertsch, L. K. Ebert, A. C. Schauss, T. Benzing, M. M. Rinschen and B. Schermer (2017). "The ciliary membrane-associated proteome reveals actin-binding proteins as key components of cilia." EMBO Rep **18**(9): 1521-1535.

Kubo, A., H. Sasaki, A. Yuba-Kubo, S. Tsukita and N. Shiina (1999). "Centriolar satellites: molecular characterization, ATP-dependent movement toward centrioles and possible involvement in ciliogenesis." J Cell Biol **147**(5): 969-980.

Kubo, A. and S. Tsukita (2003). "Non-membranous granular organelle consisting of PCM-1: subcellular distribution and cell-cycle-dependent assembly/disassembly." J Cell Sci **116**(Pt 5): 919-928.

Lambert, J. P., M. Tucholska, C. Go, J. D. Knight and A. C. Gingras (2015). "Proximity biotinylation and affinity purification are complementary approaches for the interactome mapping of chromatin-associated protein complexes." J Proteomics **118**: 81-94.

Lopes, C. A., S. L. Prosser, L. Romio, R. A. Hirst, C. O'Callaghan, A. S. Woolf and A. M. Fry (2011). "Centriolar satellites are assembly points for proteins implicated in human ciliopathies, including oral-facial-digital syndrome 1." J Cell Sci **124**(Pt 4): 600-612.

Luders, J. (2012). "The amorphous pericentriolar cloud takes shape." Nat Cell Biol **14**(11): 1126-1128.

Luders, J. and T. Stearns (2007). "Microtubule-organizing centres: a re-evaluation." Nat Rev Mol Cell Biol **8**(2): 161-167.

Mahjoub, M. R. and T. Stearns (2012). "Supernumerary centrosomes nucleate extra cilia and compromise primary cilium signaling." Curr Biol **22**(17): 1628-1634.

Mahjoub, M. R., Z. Xie and T. Stearns (2010). "Cep120 is asymmetrically localized to the daughter centriole and is essential for centriole assembly." J Cell Biol **191**(2): 331-346.

Marshall, W. F. (2007). "What is the function of centrioles?" J Cell Biochem **100**(4): 916-922.

Mick, D. U., R. B. Rodrigues, R. D. Leib, C. M. Adams, A. S. Chien, S. P. Gygi and M. V. Nachury (2015). "Proteomics of Primary Cilia by Proximity Labeling." Dev Cell **35**(4): 497-512.

Mirvis, M., T. Stearns and W. James Nelson (2018). "Cilium structure, assembly, and disassembly regulated by the cytoskeleton." Biochem J **475**(14): 2329-2353.
Miura, K. (2018). "An Overview of Current Methods to Confirm Protein-Protein Interactions." Protein Pept Lett **25**(8): 728-733.

Moggridge, S., P. H. Sorensen, G. B. Morin and C. S. Hughes (2018). "Extending the Compatibility of the SP3 Paramagnetic Bead Processing Approach for Proteomics." J Proteome Res **17**(4): 1730-1740.

Nachury, M. V. (2014). "How do cilia organize signalling cascades?" Philos Trans R Soc Lond B Biol Sci **369**(1650).

Nachury, M. V., A. V. Loktev, Q. Zhang, C. J. Westlake, J. Peranen, A. Merdes, D. C. Slusarski, R. H. Scheller, J. F. Bazan, V. C. Sheffield and P. K. Jackson (2007). "A core complex of BBS proteins cooperates with the GTPase Rab8 to promote ciliary membrane biogenesis." Cell **129**(6): 1201-1213.

Nachury, M. V. and D. U. Mick (2019). "Establishing and regulating the composition of cilia for signal transduction." Nat Rev Mol Cell Biol **20**(7): 389-405.

Nielsen, J. C., C. Nordgaard, M. A. X. Tollenaere and S. Bekker-Jensen (2018). "Osmotic Stress Blocks Mobility and Dynamic Regulation of Centriolar Satellites." Cells **7**(7).

Nigg, E. A., L. Cajanek and C. Arquint (2014). "The centrosome duplication cycle in health and disease." FEBS Lett **588**(15): 2366-2372.

Nigg, E. A. and A. J. Holland (2018). "Once and only once: mechanisms of centriole duplication and their deregulation in disease." Nat Rev Mol Cell Biol **19**(5): 297-312.

Nigg, E. A. and J. W. Raff (2009). "Centrioles, centrosomes, and cilia in health and disease." Cell **139**(4): 663-678.

Obino, D., F. Farina, O. Malbec, P. J. Saez, M. Maurin, J. Gaillard, F. Dingli, D. Loew, A. Gautreau, M. I. Yuseff, L. Blanchoin, M. Thery and A. M. Lennon-Dumenil (2016). "Actin nucleation at the centrosome controls lymphocyte polarity." Nat Commun **7**: 10969.

Odabasi, E., U. Batman and E. N. Firat-Karalar (2020). "Unraveling the mysteries of centriolar satellites: time to rewrite the textbooks about the centrosome/cilium complex." Mol Biol Cell **31**(9): 866-872.

Odabasi, E., S. Gul, I. H. Kavakli and E. N. Firat-Karalar (2019). "Centriolar satellites are required for efficient ciliogenesis and ciliary content regulation." EMBO Rep **20**(6).

Otto, E. A., T. W. Hurd, R. Airik, M. Chaki, W. Zhou, C. Stoetzel, S. B. Patil, S. Levy, A. K. Ghosh, C. A. Murga-Zamalloa, J. van Reeuwijk, S. J. Letteboer, L. Sang, R. H. Giles, Q. Liu, K. L. Coene, A. Estrada-Cuzcano, R. W. Collin, H. M. McLaughlin, S. Held, J. M. Kasanuki, G. Ramaswami, J. Conte, I. Lopez, J. Washburn, J. Macdonald, J. Hu, Y. Yamashita, E. R. Maher, L. M. Guay-Woodford, H. P. Neumann, N.

Obermuller, R. K. Koenekoop, C. Bergmann, X. Bei, R. A. Lewis, N. Katsanis, V. Lopes, D. S. Williams, R. H. Lyons, C. V. Dang, D. A. Brito, M. B. Dias, X. Zhang, J. D. Cavalcoli, G. Nurnberg, P. Nurnberg, E. A. Pierce, P. K. Jackson, C. Antignac, S. Saunier, R. Roepman, H. Dollfus, H. Khanna and F. Hildebrandt (2010). "Candidate exome capture identifies mutation of SDCCAG8 as the cause of a retinal-renal ciliopathy." Nat Genet **42**(10): 840-850.

Pampliega, O., I. Orhon, B. Patel, S. Sridhar, A. Diaz-Carretero, I. Beau, P. Codogno, B. H. Satir, P. Satir and A. M. Cuervo (2013). "Functional interaction between autophagy and ciliogenesis." Nature **502**(7470): 194-200.

Paz, J. and J. Luders (2018). "Microtubule-Organizing Centers: Towards a Minimal Parts List." Trends Cell Biol **28**(3): 176-187.

Pazour, G. J., S. A. Baker, J. A. Deane, D. G. Cole, B. L. Dickert, J. L. Rosenbaum, G. B. Witman and J. C. Besharse (2002). "The intraflagellar transport protein, IFT88, is essential for vertebrate photoreceptor assembly and maintenance." J Cell Biol **157**(1): 103-113.

Pazour, G. J., B. L. Dickert, Y. Vucica, E. S. Seeley, J. L. Rosenbaum, G. B. Witman and D. G. Cole (2000). "Chlamydomonas IFT88 and its mouse homologue, polycystic kidney disease gene tg737, are required for assembly of cilia and flagella." J Cell Biol **151**(3): 709-718.

Prosser, S. L. and L. Pelletier (2020). "Centriolar satellite biogenesis and function in vertebrate cells." J Cell Sci **133**(1).

Quarantotti, V., J. X. Chen, J. Tischer, C. Gonzalez Tejedo, E. K. Papachristou, C. S. D'Santos, J. V. Kilmartin, M. L. Miller and F. Gergely (2019). "Centriolar satellites are acentriolar assemblies of centrosomal proteins." EMBO J **38**(14): e101082.

Rai, A. K., J. X. Chen, M. Selbach and L. Pelkmans (2018). "Kinase-controlled phase transition of membraneless organelles in mitosis." Nature **559**(7713): 211-216.

Reiter, J. F. and M. R. Leroux (2017). "Genes and molecular pathways underpinning ciliopathies." Nat Rev Mol Cell Biol **18**(9): 533-547.

Rossi, A., Z. Kontarakis, C. Gerri, H. Nolte, S. Holper, M. Kruger and D. Y. Stainier (2015). "Genetic compensation induced by deleterious mutations but not gene knockdowns." Nature **524**(7564): 230-233.

Roux, K. J., D. I. Kim, M. Raida and B. Burke (2012). "A promiscuous biotin ligase fusion protein identifies proximal and interacting proteins in mammalian cells." J Cell Biol **196**(6): 801-810.

Sadrian, B., T. W. Cheng, O. Shull and Q. Gong (2012). "Rap1gap2 regulates axon outgrowth in olfactory sensory neurons." Mol Cell Neurosci **50**(3-4): 272-282.

Sanchez, A. D. and J. L. Feldman (2017). "Microtubule-organizing centers: from the centrosome to non-centrosomal sites." Curr Opin Cell Biol **44**: 93-101.

Savitski, M. M., M. Wilhelm, H. Hahne, B. Kuster and M. Bantscheff (2015). "A Scalable Approach for Protein False Discovery Rate Estimation in Large Proteomic Data Sets." Mol Cell Proteomics **14**(9): 2394-2404.

Schmidt, T. I., J. Kleylein-Sohn, J. Westendorf, M. Le Clech, S. B. Lavoie, Y. D. Stierhof and E. A. Nigg (2009). "Control of centriole length by CPAP and CP110." Curr Biol **19**(12): 1005-1011.

Sha, J., Q. Han, C. Chi, Y. Zhu, J. Pan, B. Dong, Y. Huang, W. Xia and W. Xue (2018). "PRKAR2B promotes prostate cancer metastasis by activating Wnt/beta-catenin and inducing epithelial-mesenchymal transition." J Cell Biochem **119**(9): 7319-7327.

Sha, J., W. Xue, B. Dong, J. Pan, X. Wu, D. Li, D. Liu and Y. Huang (2017). "PRKAR2B plays an oncogenic role in the castration-resistant prostate cancer." Oncotarget **8**(4): 6114-6129.

Silva, E., E. Betleja, E. John, P. Spear, J. J. Moresco, S. Zhang, J. R. Yates, 3rd, B. J. Mitchell and M. R. Mahjoub (2016). "Ccdc11 is a novel centriolar satellite protein essential for ciliogenesis and establishment of left-right asymmetry." Mol Biol Cell **27**(1): 48-63.

Sorokin, S. (1962). "Centrioles and the formation of rudimentary cilia by fibroblasts and smooth muscle cells." J Cell Biol **15**: 363-377.

Sorokin, S. P. (1968). "Reconstructions of centriole formation and ciliogenesis in mammalian lungs." J Cell Sci **3**(2): 207-230.

Sprague, B. L., R. L. Pego, D. A. Stavreva and J. G. McNally (2004). "Analysis of binding reactions by fluorescence recovery after photobleaching." Biophys J **86**(6): 3473-3495.

Srsen, V., X. Fant, R. Heald, C. Rabouille and A. Merdes (2009). "Centrosome proteins form an insoluble perinuclear matrix during muscle cell differentiation." BMC Cell Biol **10**: 28.

Srsen, V., N. Gnadt, A. Dammermann and A. Merdes (2006). "Inhibition of centrosome protein assembly leads to p53-dependent exit from the cell cycle." J Cell Biol **174**(5): 625-630.

Staples, C. J., K. N. Myers, R. D. Beveridge, A. A. Patil, A. J. Lee, C. Swanton, M. Howell, S. J. Boulton and S. J. Collis (2012). "The centriolar satellite protein Cep131 is important for genome stability." J Cell Sci **125**(Pt 20): 4770-4779.

Stowe, T. R., C. J. Wilkinson, A. Iqbal and T. Stearns (2012). "The centriolar satellite proteins Cep72 and Cep290 interact and are required for recruitment of BBS proteins to the cilium." Mol Biol Cell **23**(17): 3322-3335.

Tabares-Seisdedos, R. and J. L. Rubenstein (2009). "Chromosome 8p as a potential hub for developmental neuropsychiatric disorders: implications for schizophrenia, autism and cancer." Mol Psychiatry **14**(6): 563-589.

Tang, Z., M. G. Lin, T. R. Stowe, S. Chen, M. Zhu, T. Stearns, B. Franco and Q. Zhong (2013). "Autophagy promotes primary ciliogenesis by removing OFD1 from centriolar satellites." Nature **502**(7470): 254-257.

Tollenaere, M. A., N. Mailand and S. Bekker-Jensen (2015). "Centriolar satellites: key mediators of centrosome functions." Cell Mol Life Sci **72**(1): 11-23.

Tollenaere, M. A. X., B. H. Villumsen, M. Blasius, J. C. Nielsen, S. A. Wagner, J. Bartek, P. Beli, N. Mailand and S. Bekker-Jensen (2015). "p38- and MK2-dependent signalling promotes stress-induced centriolar satellite remodelling via 14-3-3-dependent sequestration of CEP131/AZI1." Nat Commun **6**: 10075.

Villumsen, B. H., J. R. Danielsen, L. Povlsen, K. B. Sylvestersen, A. Merdes, P. Beli, Y. G. Yang, C. Choudhary, M. L. Nielsen, N. Mailand and S. Bekker-Jensen (2013). "A new cellular stress response that triggers centriolar satellite reorganization and ciliogenesis." EMBO J **32**(23): 3029-3040.

Vladar, E. K. and T. Stearns (2007). "Molecular characterization of centriole assembly in ciliated epithelial cells." J Cell Biol **178**(1): 31-42.

Wang, L. and B. D. Dynlacht (2018). "The regulation of cilium assembly and disassembly in development and disease." Development **145**(18).

Wang, L., K. Lee, R. Malonis, I. Sanchez and B. D. Dynlacht (2016). "Tethering of an E3 ligase by PCM1 regulates the abundance of centrosomal KIAA0586/Talpid3 and promotes ciliogenesis." Elife **5**.

Werner, T., G. Sweetman, M. F. Savitski, T. Mathieson, M. Bantscheff and M. M. Savitski (2014). "Ion coalescence of neutron encoded TMT 10-plex reporter ions." Anal Chem **86**(7): 3594-3601.

Wu, C. T., H. Y. Chen and T. K. Tang (2018). "Myosin-Va is required for preciliary vesicle transportation to the mother centriole during ciliogenesis." Nat Cell Biol **20**(2): 175-185.

Zhang, W., P. J. Kim, Z. Chen, H. Lokman, L. Qiu, K. Zhang, S. G. Rozen, E. K. Tan, H. S. Je and L. Zeng (2016). "MiRNA-128 regulates the proliferation and neurogenesis of neural precursors by targeting PCM1 in the developing cortex." Elife **5**.

APPENDIX

Antibodies used for immunofluorescence		
rabbit anti-PCM1	19856-1-AP; Proteintech	1:1000
goat anti-PCM1	E-5, sc50164; Santa Cruz Biotechnology	1:1000
Mouse anti-GFP	3e6,11120; Sigma-Aldrich	1:750
mouse anti-gamma tubulin	GTU-88,T6557; Sigma-Aldrich	1:4000
mouse anti-acetylated tubulin	6-11-B; Sigma-Aldrich	1:10000
mouse anti-polyglutamylated tubulin	GT335, Adipogen	1:500
mouse anti-Arl13b	75-287; Neuromab	1:500
mouse anti-Smo	D-19, sc166685; Santa Cruz Biotechnology	1:500
rabbit anti-IFT88	13967-1-AP; Proteintech	1:500
mouse anti-MIB1	M5948; Sigma-Aldrich	1:500
rabbit anti-CP110	12780-1-AP; Proteintech	1:5000
mouse anti-Cep164	E9, sc515403; Santa Cruz Biotechnology	1:500
rabbit anti-Talpid3	24421-1-AP; Proteintech	1:500
rabbit anti-CEP290	ab84870; Abcam	1:500
rat anti-ZO1	sc33725; Santa Cruz Biotechnology	1:200
rabbit anti-beta-catenin	51062-2-AP; Proteintech	1:500
rabbit TBC1D31	HPA023710; Sigma-Aldrich	1:1000
rabbit C-NAP1	F7, sc 390540; Santa Cruz Biotechnology	1:250
All secondary antibodies are AlexaFluor 488-, 568- or 633-coupled.		1:2000
Antibodies used for western blotting		
rabbit anti-PCM1	19856-1-AP; Proteintech	1:500
mouse anti-gamma tubulin	GTU-88,T6557; Sigma-Aldrich	1:4000
mouse anti-acetylated tubulin	6-11-B; Sigma-Aldrich	1:10000
mouse anti-polyglutamylated tubulin	GT335, Adipogen	1:500
mouse anti-Arl13b	75-287; Neuromab	1:500

mouse anti-Smo	D-19, sc166685; Santa Cruz Biotechnology	1:500
rabbit anti-IFT88	13967-1-AP; Proteintech	1:500
mouse anti-MIB1	M5948; Sigma-Aldrich	1:500
Rabbit anti-BBS4	12766-1-AP; Proteintech	1:500
rabbit anti-CP110	12780-1-AP; Proteintech	1:5000
rabbit anti-Cep164	22227-1-AP; Proteintech	1:500
rabbit anti-Talpid3	24421-1-AP; Proteintech	1:500
rabbit anti-CEP290	22490-1-AP; Proteintech	1:500
mouse anti-vinculin	H-10, sc25336; Santa Cruz Biotechnology	1:1000
All secondary antibodies are IRDye 680- and IRDye 800- coupled.	LI-COR Biosciences	1:15000

VITA

Ezgi Odabaşı Kurtuluş received her B.Sc. degree in Molecular Biology and Genetics from Bilkent University, Ankara in 2015. From September 2015 to June 2021, she worked as a teaching and research assistant in Koç University, Istanbul and performed her Ph.D. studies in the Cytoskeleton Laboratory under the supervision of Dr. Elif Nur Firat-Karalar. Her Ph.D. research was on "Centriolar satellites are required for efficient ciliogenesis and ciliary content regulation".

Publications

Odabasi E, Batman U, Firat-Karalar EN. (2020) Unraveling the mysteries of centriolar satellites: time to rewrite the textbooks about the centrosome/cilium complex. *Mol Biol Cell.*

Muratcioglu S, Aydin C, **Odabasi E**, Ozdemir ES, Firat-Karalar EN, Jang H, Tsai CJ, Nussinov R, Kavakli IH, Gursoy A, Keskin O. (2020) Oncogenic K-Ras4B Dimerization Enhances Downstream Mitogen-activated Protein Kinase Signaling. *J Mol Biol.*

Odabasi E., Gul S., Kavakli I. H., & Firat-Karalar E. N. (2019) Centriolar satellites are required for efficient ciliogenesis and ciliary content regulation. *EMBO reports*

Conkar D**,** Culfa E, **Odabasi E**, Rauniyar N, Yates JR 3rd, Firat-Karalar EN. (2017) The centriolar satellite protein CCDC66 interacts with CEP290 and functions in cilium formation and trafficking. *Journal of Cell Science.*